A Compact Defected-Ground UWB Antenna for Breast Tumor Detection Using SAR Analysis

Thesis

Submitted to the

G.B. Pant University of Agriculture & Technology
Pantnagar-263145, Uttarakhand, India

By

Rekha Kandpal
Id. No. 55621

IN PARTIAL FULFILLMENT OF THE REQUIREMENTS FOR THE DEGREE OF

Master of Technology
(Electronics and Communication Engineering)

February, 2022

ACKNOWLEDGEMENT

It is a humbling experience to acknowledge those people who have helped me along the journey of my degree programme. I would like to express my deepest sense of gratitude to the almighty "GOD" for blessing me with enough patience, endurance & strength to overcome all the hurdles that crossed my path. Accomplishment of this thesis is the result of benevolence of omnipotent almighty and blesssing of my teachers.

Firstly, my family deserves endless gratitude I dedicate this dissertation to my father Mr. Lalit Mohan Kandpal, mother Mrs. Bimla Kandpal, my uncle Mr. Shankar Dutt Upreti, aunt Mrs. Deepa Upreti whose efforts during their life made it possible for me to study in a better place and become an educated person so that I can add meaning to my life and help others too.

I would like to express my gratitude and respect to my advisor and chairman of advisory committee, ***Dr. Paras,*** *Associate Professor, Department of Electronics and Communication, for all I have learned from him and his invaluable motivation, sincere guidance, encouragement and support in all stages of this thesis.*

I express my deep sense of gratitude to members of my Advisory Committee, ***Dr. Sanjay Mathur,*** *Head, Department of Electronics and Communication,* ***Dr. Abhishek Tomar,*** *Associate Professor, Department of Electronics and Communication and* ***Dr. Reeta Verma,*** *Assistant Professor, Department of Electronics and Communication, for giving me the valuable suggestions and help during the thesis work.*

I also owe great thanks to Dean, PGS, and Dean, COT for providing necessary facilities during the pursuit of my research work. I would like to acknowledge all the teachers I learned from since my childhood, I would not have been here without their guidance, blessing and support.

I am highly obliged and grateful to all the staff members of Department of Electronics and Communication for their help, co-operation and encouragement. I am very grateful to my respected seniors Mr. Abhay Singh, Mr. Brij Bharti, Ms. Suchitra

Tiwari, Mr. Mitesh Upreti of Department of Electronics and Communication for their guidance, encouragement and help.

I wish to extend my sincere thanks to all my Professors, Librarian, teaching and non-teaching staffs, Information Technology for supporting and giving useful suggestions during the course of work.

Thanks a lot to my supportive friends, Kavita, Nipun Pande, Lavi Tyagi, Abhishek Joshi who made the friendly environment for working. Company of these friends make all time joyful during course of research. I am also grateful to all my loving brothers, Himanshu, Deepanshu, Mayank and sister, Mansi for their active help. I sincerely admire the contribution of my special friends Pawan, Hemant, Swati, Bhawna, Komal and Neha. Thank you for always inspiring me and providing me the mental support during this course of time.

I feel the limitation of my diction to truly reflect my feelings of gratitude. Hence, I have chosen this simple way of acknowledging the help received. I wish to thank all well wishers whose blessing propelled me to achieve my dreams and could not find a separate mention due to lack of space.

Pantnagar
February, 2022

(Rekha Kandpal)
Authoress

CERTIFICATE-I

This is to certify that the thesis entitled "**A Compact Defected-Ground UWB Antenna for Breast Tumor Detection Using SAR Analysis"** submitted in partial fulfillment of the requirements for the degree of **Masters of Technology** with major in **Electronics and Communication Engineering** of the College of Post-Graduate Studies, G.B. Pant University of Agriculture and Technology, Pantnagar, is a record of bona-fide research carried out by **Ms. Rekha Kandpal, Id. No. 55621** under my supervision and no part of the thesis has been submitted for any other degree or diploma.

The assistance and help received during the course of this investigation have been acknowledged.

(Paras)
Chairman
Advisory Committee

Pantnagar
February, 2022

CERTIFICATE -II

We, the undersigned, member of the Advisory Committee of **Ms. Rekha Kandpal, Id. No. 55621** a candidate for the degree of **Masters of Technology** with major in **Electronics and Communication Engineering,** with major in **Electronics and Communication Engineering,** agree that the thesis entitled **"A Compact Defected-Ground UWB Antenna for Breast Tumor Detection Using SAR Analysis"** may be submitted in partial fulfillment of the requirements for the degree.

09/02/2022

(Paras)
Chairman
Advisory Committee

(Sanjay Mathur)
Member

(Abhishek Tomar)
Member

(Reeta Verma)
Member

TABLE OF CONTENTS

LIST OF TABLES

LIST OF FIGURES

LIST OF ABBREVIATIONS

Abbreviations	Extended full forms
EM	Electromagnetic
TW	Thin wire
VNA	Vector Network Analyzer
PCB	Printed circuit board
VSWR	Voltage standing ratio
UWB	Ultra wide band
DGS	Defected ground structure
IEEE	Institute of electrical and electronics engineering
WLAN	Wireless local area network
Wi-MAX	World interoperability of microwave access
PMA	Printed monopole antenna
PCMA	Printed circular monopole antenna
PET	Positron Emission Tomography
MRI	Magnetic Resonance Imaging
MWI	Microwave imaging
SAR	Specific absorption rate
HFSS	High frequency structure simulator
MRS-UWB	Multi ring slots ultra wide band
TEM	Transverse electromagnetic

Introduction

Chapter 1 INTRODUCTION

Breast cancer is one of the most common cancers among women and one of the most dangerous diseases worldwide. As a result of breast cancer/tumor, the death rate of women has increased significantly. During the years 2006-2010, it is estimated that there were 123.8 cases of breast cancer deaths for every 100,000 women. This problem can be solved by detecting a tumor at an early stage. Detection technologies such as X-Ray Mammography, Ultrasonic sensor, Magnetic Resonance Imaging (MRI), Microwave Imaging, and others have been used in several studies **(Wang *et al.* 2015, Alshehri *et al.* 2009, Sill *et al*. 2005, Shao *et al.* 2005, Huynh *et al*. 1998).**

According to the American Cancer Society, breast cancer is the leading cause of disease in many young women around the world (2019). X-ray mammography, Positron Emission Tomography (PET), Ultrasound imaging, and Magnetic Resonance Imaging (MRI) are some of the earliest cancer detection modalities available in the medical world. Because it uses low-energy radiation, X-ray mammography is a popular tool for early cancer detection, but it has a number of drawbacks. According to several studies, women under the age of 40 are more likely to be harmed during routine screening than older women. Mammography screening necessitates the compression of the breast in order to achieve precise imaging. Patients experience pain as a result of this procedure, and it is difficult to discern between cancerous and healthy tissue on a mammography scan since both tissues appear white. In addition to cancer detection, MRI is a non-invasive screening technology. Under the excitation of strong magnetic fields and radio waves, the quantity of energy absorbed by two different bodily tissues is measured. In order to obtain better images when using MRI for soft tissues like the breast, contrast liquid must be injected. Because an MRI scan is not cost effective, it is usually recommended just before a surgical procedure. PET, unlike MRI and X-ray, can detect cancer tissue at an early stage, although the images are low-resolution. These limitations in the existing breast cancer detection techniques motivate to the development of an alternative imaging methodology.

1.1 STATISTICS OF BREAST CANCER

The American Cancer Society's Surveillance and Health Services Research department evaluated breast cancer statistics (2019). According to this research, in the United States, there were approximately 268,600 new cases of invasive breast cancer and 41,760 estimated breast cancer deaths. Fig 1.1 shows the likelihood of having invasive cancer from 2013 to 2015, according to the American Cancer Society 2019.

Breast cancer is the most frequent malignancy among Indian women in a number of cities. An estimated 70,218 women died of breast cancer in India for the year 2012 the highest in the world for that year most of which is among the age group 30-50. Almost 1,62,468 new cases of breast cancer have been reported, with an 87,090 death rate by the year 2018 **(Ferlay, 2018).** Breast cancer is becoming more common in India as people reach their early thirties, peaking between the ages of 50 and 64.

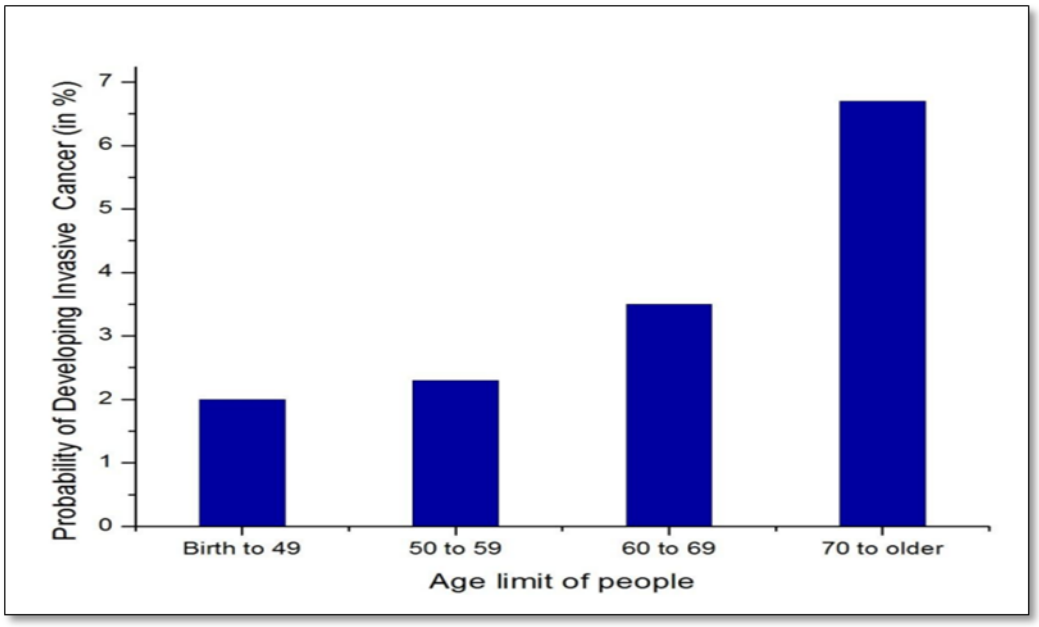

Fig 1.1 Report on Probability of developing invasive cancer for selected age (American Cancer Society 2019)

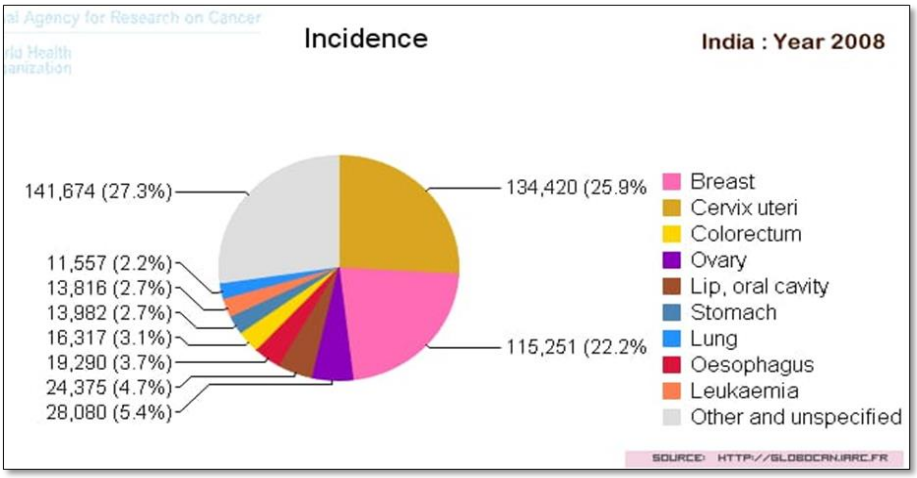

(a)

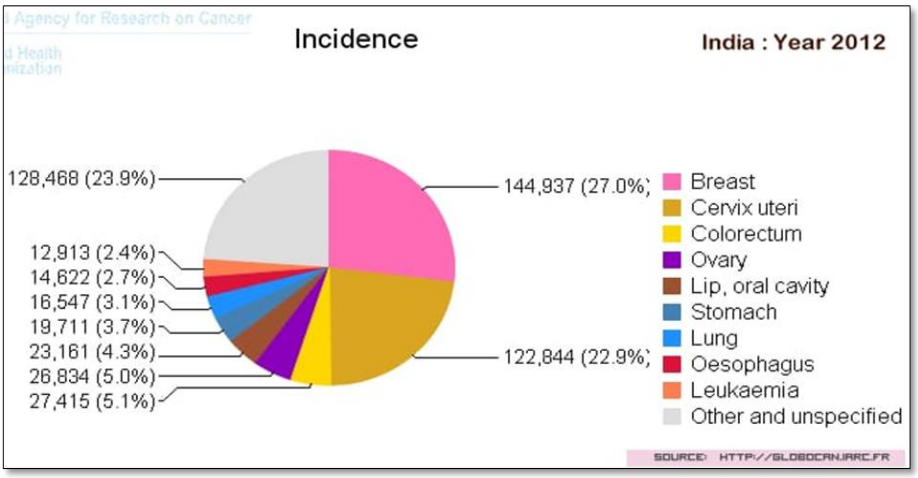

(b)

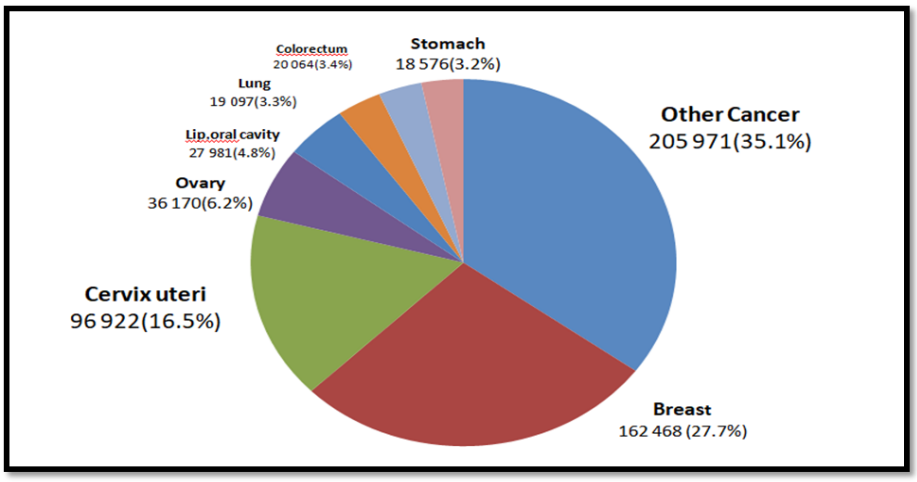

(c)

Fig 1.2 Estimated Number of new cases in (a) 2008, (b) 2012, (c) 2018 in India, females, all ages

The X-Ray mammography imaging technology is commonly used to detect tumors, however it is expensive and difficult to pinpoint the specific position of the tumor. Furthermore, it has the potential to damage the healthiest breast tissue when it is surrounded by cancerous cells (**Alshehri & Khatun 2009)**. Because of the risk, X-rays cannot be repeated, especially in women under the age of 40. **(wang *et al.* 2015, Shao.W *et al.* 2005)**.

The standard tool for detecting symptoms or indicators of breast cancer with a size of a few mm is ultrasound. It's very useful for distinguishing beginning cysts from cysts, solid tumors, or suspicions of malignancy. Despite its widespread availability and low cost, it is difficult to discern between benign and malignant tumors, and it commonly misses micro calcifications due to the speckle **(Huo *et al*., 2003).**

Another option is magnetic resonance imaging (MRI), which is more effective and sensitive than mammography in detecting tumors in women who have a hereditary risk of breast cancer **(Mieke Kriege *et al.* 2004)**. The MRI is used to discover suspicious objects such as benign and malignant breast lesions, but it has a high false positive rate **(Wang *et al*. 2015 and Shao *et al*. 2005)** and is costly and complicated. Using UWB Microwave imaging, these constraints can be overcome **(Lai *et al*. 2011, Bindu *et al*. 2006 and Adnan *et al.* 2010).**

Positron Emission Tomography is another imaging technique that can detect the presence of cancer tissues at an early stage. The testing procedure is by injecting a radioactive material along with glucose to the patient before going for examination. The infected cancer cells have the characteristics to grow faster than the other cells. Injected material shows a significant difference in tissue characteristic between the healthy tissue and cancer tissue after injecting the chemical compound. PET scanner cannot detect small sized cancer cells in the dense breast tissue. Further, the image resolution is too low in it. Usually, PET scans are utilized along with CT scan and also in any other detecting methodology to create high resolution images.

Because microwave imaging and depth of penetration in tissue are non-ionizing, non-invasive, and safe for patients, several researchers have been directed to use microwave for the detection of breast cancer, particularly in the UWB frequency region for microwave imaging and depth of penetration in tissue **(Lai *et al.* 2011, Shao *et al.* 2011, Xiao *et al.* 2008 and Banu *et al.* 2013)** As shown in Figure 1.2, the MWI system comprises of an array of antennas that operate as a transmitter and receiver of electromagnetic signals on the human breast. Fig 1.3 depicts the basic principle of microwave imaging, in which microwave radiation is shined on the breast and the reflected energy is detected (a). Fig 1.3 shows how the difference in the energy levels of transmitted and reflected waves is used to detect the existence of a tumor (b).

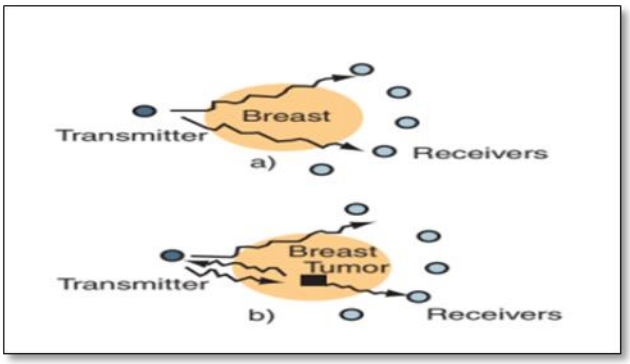

Fig 1.3 Basic concept of microwave imaging: a) without tumor and b) with tumor

When breast tumor tissue is subjected to a UWB signal, it emits electrical properties that are completely different from those of typical healthy breast tissue. The tumor size, location, form, and electrical properties are all collected by the scattering parameter of normal and malignant tissue, which varies greatly. When a tumor affects a normal tissue, the tumor's permittivity increases, and it is proportional to the electrical energy stored in the tissue **(Bindu *et al.* 2006)**.

It is necessary to understand the electrical properties of breast tissue in order to understand how electromagnetic waves interact with it **(Adnan *et al.* 2010**). For example, using the dielectric permittivity and conductivity of normal and malignant tissue, we can easily identify the tumor by transmitting three ultra wideband signals to the affected area of the breast **(Banu *et al.* 2013).**

Broadband antennas were widely utilized in the beginning, especially in the receiving sector. UWB commercial systems meet the requirements of standard broadband antennas, allowing the entire design approach to be rented. Nonetheless, the US Federal Communication Commission (FCC) suggested the UWB concept in 2002, with a frequency range of 3.1 to 10.6 GHz, which is different from typical wideband. UWB is popular because of its qualities, which include high data transmission rates in wireless medium, high security, low profile, simple construction, and low fabrication cost. UWB antennas can be square, rectangular, triangular, circular, elliptical, pentagonal, hexagonal, and other shapes **(Gautam *et al.*, 2013, Mondal *et al.*, 2013, Mazhar *et al.*, 2013, Mandal *et al.*, 2012, Yang *et al.*, 2012, Kasi *et al.*, 2011).**

A micro-strip patch antenna consists of a very thin metallic patch, a dielectric substrate, and a large metallic ground plane. The radiating patch is normally supported by the dielectric substrate material. There are two sides to the dielectric substrate material, one with a radiating patch and the other with a ground plane. Although a high dielectric constant combined with a thin substrate reduces undesired radiation in microwave electronics, the increased loss, which results in decreased efficiency and bandwidth, is not desirable.

By varying the thickness of the substrate, the antenna's gain and efficiency can be altered. It has been noticed that the thicker the dielectric substrate, the greater the gain, up to a point. Due to growth of dielectric substrate thickness whose dielectric constant is lower may lead to unwanted consequence like surface wave excitation. The antenna efficiency is reduced by surface waves, which disturb the radiation pattern. As a result, choosing the best relative permittivity (r) and thickness of dielectric substrate material is critical.

The range of relative permittivity is usually between 2.2 and 12. Ansoft HFSS, a 3-D electromagnetic full wave simulation software based on the Finite Element Method (FEM) that is more precise due to its solving technique, can be used to analyse such antenna designs.

1.2 UWB ANTENNAS

As in the case in conventional wireless communication systems, an antenna also plays a very crucial role in UWB systems. However, there are more challenges in designing a UWB antenna than a narrow band one. A suitable UWB antenna should be capable of operating over an ultra wide bandwidth as allocated by the FCC. At the same time the Federal Communication Commission (FCC) has assigned license free bandwidth of 7.5GHz (from 3.1GHz to 10.6GHz) for ultra wideband (UWB) wireless communications, UWB is rapidly advancing as a high data rate wireless communication systems like according to IEEE 802 standard ,2.4-2.48 GHz is assigned for WLAN ,Wi-Fi , and Bluetooth are works in this range,3.3-3.7 GHz Wi - MAX, 3.7-4.2 GHz C-band satellite communication channels, 5.15-5.825 GHz WLAN (IEEE 802.11a and HIPERLAN/2), 7.25-7.75 GHz X-band satellite communication channels and the 8.02-8.4GHz ITU (International telecommunication union),these band may cause interference with the UWB wireless communication systems so it is required to lower the interference effects originated by the mentioned earlier narrow bands within the UWB band shown in the fig-1.4.

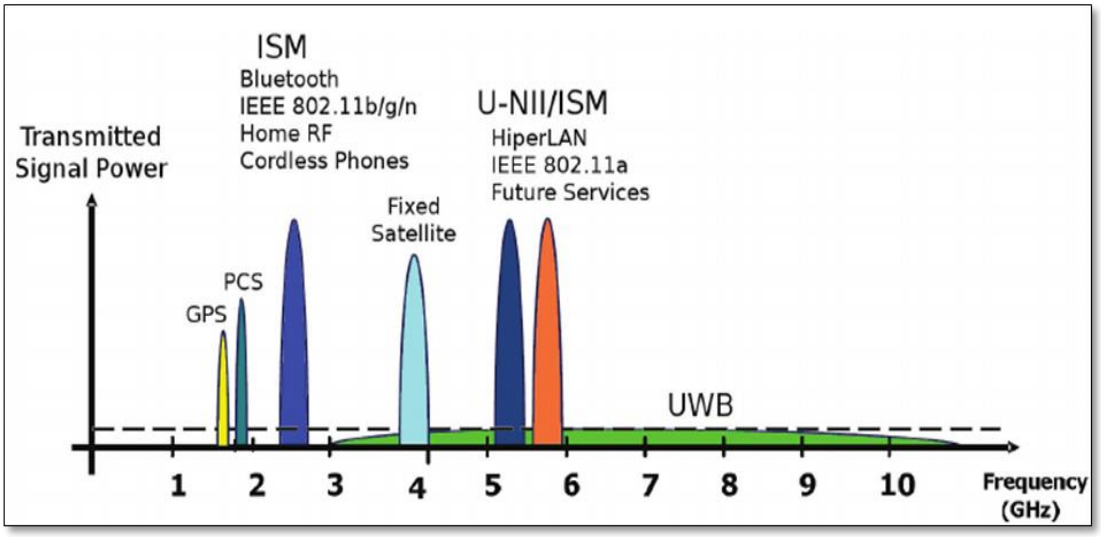

Fig 1.4: different narrow bands which make interference with UWB system

In some applications, the UWB antenna include filters to cut-off these interference bands. Certainly, the use of filters increases the complications of the UWB antennas which may increase system cost and space. But still, for PCS

(Personal Communication System) application and other handheld devices, miniaturization of the system is of foremost importance. The limitations of the UWB antenna with multi band notched are the mutual coupling of elements used for different bands notching, the limited space within the compact UWB antenna and the inclusion of a part of the frequency band of the UWB application in the rejected interference band. Hence it is required to cover sharp frequency band rejection method in the antenna design for interfering band.

There are different techniques have been proposed in various research articles to design band notched antennas. Adding parasitic elements, modified ground plane, etching slots and insertion of slits into the patch are simple and most commonly used approaches reject the desired band from the UWB antennas. The defected Ground Structure (DGS) is one of the important techniques for improving the antenna gain and bandwidth which is usefull in wide band applications. Various cuts in ground plane help in the distribution of current in the ground plane as well as patch in controlled manner. By using DGS, current in the ground plane as well as patch in controlled manner. By using DGS, current distribution can change the electromagnetic behavior resulting in an improved performance of microstrip patch antenna (MSA).

1.2.1 Properties of UWB

- Unintentional users have a hard time detecting it.
- Extremely safe.
- It does not interfere with other communication systems.
- Transmitting energy is really low (less than 1mW)
- Extremely high bandwidth in a small area (200Mbps within 10m)
- Line-of-sight and non-line-of-sight operations are both possible to implement.
- Has the ability to pass through solid objects, such as walls and doors.
- High resistance to several paths.

- Low-cost frequency diversity.
- Communication, radar, and positioning architectures are all the same.
- Low-cost, low-power, almost entirely digital, single-chip architecture.

1.3 SPECIFIC ABSORPTION RATE

The current basic safety limitations for wireless devices are specified in terms of specific absorption rate (SAR), which is defined as the rate at which a person absorbs Electromagnetic radiation per unit mass; SAR can be expressed by X-g SAR when averaged over X gram of tissue. The SAR in a biological body subjected to an RF field is determined by a variety of parameters, including tissue shape and dielectric characteristics, as well as the body's orientation relative to the source **(Chou et al. 1996).**

There exist three different limits defined by:

1. Whole-body average SAR
2. Local peak SAR
3. Specific absorption (SA)

Short pulses' power is limited as a result of this. 1 and 2 must be averaged over a specific time period. Absorption occurs only in regions of the body that are close to the device while using wireless devices with frequencies above 300 MHz. As a result, the local peak SAR limit is the most essential value. The IEEE/ANSI/FCC recommends an upper safety limit of 2.0 W/kg for localised SAR averaged over 10-g and 1g of tissue, i.e. peak 10-g SAR and peak 1-g SAR not exceeding 2.0 W/kg and 1.6 W/kg, respectively **(Mahmud et al. 2013).**

The SAR, or specific absorption rate, is a measurement of how much RF radiation is absorbed by human tissue. SAR is a function of electrical conductivity (measured in Siemens / meter), induced E-field from radiated energy (measured in volts/ meter), and tissue mass density (measured in kilogram /cubic meter). The SAR is determined by averaging (or integrating) across a specified volume (usually 1 gram or 10 gram area).

$$\mathrm{SAR} = \int_{\mathrm{sample}} \frac{\sigma(\mathbf{r})|\mathbf{E}(\mathbf{r})|^2}{\rho(\mathbf{r})} d\mathbf{r} \tag{1.1}$$

The units of SAR are W/kg or mW/g, respectively. In the United States, the SAR limit for cell phones is 1.6 W/kg, averaged across 1 gram of tissue. SAR limits in Europe are 2.0 W/kg averaged over 10 gram of tissue.

1.4 Main objectives of the thesis:-

The idea behind the work to design and create an antenna which encompasses the whole of the UWB range with considerable gain, SAR, current density and electric field distribution properties as well as used for the detection of the tumor tissues in the breast phantom. Thus, following point should be followed while designing an antenna:-

1. To Design of Microstrip antenna that can identify tumor cells with a radius less than 4 milli-metre (mm).
2. SAR Analysis (Specific Absorption Rate) analysis will be applied for early detection of malignant tissues.
3. The analysis based on current density and electric field distribution on the antenna as these parameters can be used to distinguish between normal skin, tumor cells and the fatty tissues.
4. To fabricate the UWB antenna for the proposed work in order to achieve better results and to compare simulation and measured results like return loss (S_{11}), gain radiation pattern, VSWR with the results in literature with the help of HFSS software.

To achieve the objectives listed above, following work are carried out

1. To conduct a comprehensive literature study on breast cancer detection.
2. To study previous research work done in UWB antenna for biomedical applications.
3. To study the DGS techniques and their effects on antenna performance.

4. To design the UWB antenna for this proposed work and also find the areas of improvement, if any,
5. The proposed design allows the easy detection of the tumor cells.
6. To study and analyse the SAR (Specific absorption rate), current density, electric field distribution using HFSS software.
7. To simulate the proposed UWB antenna using high frequency structure simulator (HFSS) and to achieve desired results with optimization technique.
8. The comparison between the results of with tumor models and those without tumor models are measured for better results.
9. To investigate the effects of SAR and current density on different values of tumor cells as well as on different locations of tumor cells for the same value of tumor.
10. To compare the simulated results of proposed antenna with reference paper results and with early advances in breast tumor detection techniques, VSWR, gain, radiation pattern and cost of the antenna.

The dimensions of patch of the proposed MSA at the beginning calculated with the help of transmission line mode (TLM) and further optimization have done on patch, ground, feed dimensions and their location to get FCC assigned UWB frequency ranges from (3.1GHz to 10.6 GHz) for wireless applications. But did not get the desired wide band, the proposed antenna is then miniaturized by cutting the patch and ground-plane, it was very useful in enhancing the bandwidth and gain. Then the T-shaped slot and rectangular slot are loaded in the patch and ground respectively. All the parametric study and simulation works are being done in HFSSv19 software.

HFSS is a finite element method (FEM) software which is used to design, simulate and visualize 3D Electromagnetic (EM) problems. Different antenna parameters such as S_{11}, radiation patterns, radiation efficiency, antenna parameter and VSWR can be simulated with this software.

1.5 Outline of the Thesis

Chapter 1: This chapter gives the introduction of breast cancer, breast cancer detection techniques, UWB antenna, SAR analysis, biomedical applications and also the steps to meet the desired objective set for my research work in a brief.

Chapter 2: In this, review of literature about earlier reported work performed in the field of UWB antenna, breast tumor detection, SAR and current density analysis has been discussed.

Chapter 3: In this all the materials and methods is described which is used for carrying out this whole research work, this chapter also contains the steps which are used for the development of the proposed UWB antenna for breast tumor detection using SAR analysis.

Chapter 4: In this, simulated results of various antenna parameter i.e. reflection coefficient, peak gain, VSWR and radiation patterns are presented and analyzed with the help of design and plots. The SAR, current density and electric field distribution plot are analyzed to define the tumor values i.e. size and location.

Chapter 5: In this chapter conclusion and future scope of research work is described.

Review of Literature

Chapter 2 REVIEW OF LITERATURE

To meet the objective to design, simulate, fabricate and measure the proposed antenna it it essential to understand the research work behind breast tumor detection using UWB antennas. Here, the important work has been studied for further research in UWB antenna for medical application field.

Lindenblad *et al.* (1941) have presented an antenna capable of transmitting a wide range of frequencies. It's a practical radiator with a horizontally polarised wave and a low factor of reflection across the whole frequency range. An antenna with one or more conductors whose length is a significant percentage of the working wave's length. For example, conductors with a diameter ranging from 15 cm (maximum diameter of one component) to 26 cm (maximum diameter of the extra component) have been employed in accordance with this invention. The diameter of the antenna, as a whole, is configured to decrease with increasing distance from the antenna's neutral voltage planes in a few modified versions of this invention.

Shanwar (2000) proposed a UWB micro-strip antenna with polimide as substrate and Cu as conductors. This antenna radiates at tera-hertz. Unique features of terahertz it is sensitive to polar substances such as water & hydrogen state. Hence good for soft tissues than X-Rays.

Fear and Stuchly (2000) This research describes a microwave system for breast tumor identification that employs previously developed confocal microwave imaging techniques. To detect malignancies, an ultra-wide band pulse is utilised to illuminate the breast, and a synthetic scan of the focal point is used; however, the geometric configuration and algorithms are different from those previously used. The feasibility of detecting tumors using tiny antennas is studied. The effectiveness of skin subtraction algorithms designed to mitigate the dominating reflection from the skin is demonstrated, and signal processing techniques developed to mitigate the dominant reflection from the skin are presented. With varying numbers of antennae, images of homogeneous and heterogeneous breast models are recreated. The impact of antenna

spacing as well as the applicability of simplified models for system evaluation are also investigated.

Kornguth, *et al.* (2000) The pain experienced during mammography in women who were treated conservatively for breast cancer was investigated in this study. It looked at the relationship between pain severity and a variety of demographic, medical, and pain coping characteristics, as well as objective breast compression measurements. Breasts that had been treated and those that had not been treated were rated independently and compared to a group of 125 women who had never had breast cancer. Women reported much more pain in the breast that had been treated (41 percent greater than the untreated breast and 32 percent greater than the control group). There was no clear link between mammography pain and pain management. The most accurate predictor of pain in both breasts was the average level of discomfort at the previous mammography. During mammography of the treated breast, women who have been treated conservatively for breast cancer feel much more pain. By inquiring about the discomfort experienced during the previous mammography, radiologists and technicians can identify women who are at risk for an unpleasant mammogram.

Kuo *et al.* (2003) For the 2.4 GHz and 5.2 GHz frequency bands, they have developed a stacked or double T shaped monopole antenna. The lower frequency band is controlled by a larger T-shaped monopole, while the higher frequency band is controlled by a lower horizontal strip and a portion of the vertical strip, resulting in dual band functioning. This antenna is made of FR4 epoxy with a dielectric constant of 4.4, a loss tangent of 0.02, and a thickness of 0.8 mm, with a dimension of 5075 mm^2. For equivalent resonant frequencies of 2.4 GHz and 5.2 GHz, impedance bandwidths of 540 MHz and 210 MHz were achieved. For the corresponding resonant frequencies, peak gain is found to be 1.8dBi and 1.5dBi. The desired outcomes are attained by following the steps below. The desired results are acquired through a parametric evaluation of the stacked T shaped patch's dimensions

Schantz (2004) paper shows an historical summary of ultra-wideband antennas offering key improvements at the root of modern design.

Chen *et al.* (2006) has examined broadband antennas for UWB applications and identified the key challenges in broadband antenna design for UWB applications. Planar monopoles with fixed ground planes are investigated. After that, we'll talk about roll antennas with better radiation performance. The planar antennas built on PCBs are then discussed. For UWB applications, a directional antipodal Vivaldi antenna is also available. Last but not least, a UWB antenna for wearable applications is shown**.**

Ray (2008) gave the essential design calculations for obtaining the Ultra-Wide band antennas' lower-band edge frequency for all types of printed monopole antennas with various feed positions. The feed transmission line length is an important design element for monopole antennas. For all of these regular shaped monopoles, several design curves for the span of the feed transmission line for lower band-edge frequencies have been shown. The ultra-wide bandwidth attained by these antennas has been described in detail in a paper.

Ryu and Kishk (2009) With a substrate size of 24mm36mm, the UWB Fork shaped Antenna with band notched features is given. The UWB frequency runs from 3 to 12 GHz, including a notch at 5.15-5.35 GHz and a configurable strip from 5.725-5.825 GHz in the WLAN spectrum.

Karthik and Sharma (2011) presents Use dielectric properties of tissues due to their moisture content Because, malignant tumor have high moisture content than normal. The model with 2 antennas (one on either side of Breast tissue) and 6 antenna (3 as an array on either side of the tissue) are propose here. This satisfies the UWB spectrum of (3-10) GHz.

Banu *et al*. (2013) A circular patch antenna with a radius of 14.5 mm was created utilising a flexible FR-4 substrate. The proposed antenna is also integrated with the skin model to determine the body's cancer status. Both models are created using Ansoft HFSS software and operate at a frequency of 2.5GHz. The proposed antenna's findings are studied, including return loss, VSWR, gain, and directivity, which is around -21dB, 1.2, 4.404dB, and 4.48dB. Because it only talks about the malignancy level, the current density parameter plays a big role here. The cancer

becomes more visible as the current density parameter rises. It is approximately 127 A/m 2 here. To increase the system's performance, a downsizing technology called Defected Ground Structure was used in the ground for this suggested antenna.

Bahrami *et al.* (2014) Using a high frequency structure simulator (HFSS), a flexible, compact monopole antenna on a 100 m Kapton polyimide is constructed to be in contact with biological breast tissues over the 2-5GHz frequency range. The antenna characteristics are fine-tuned to achieve a satisfactory impedance match across the desired frequency range. The antenna is 18mm x 18mm in size. In addition, a flexible conformal 444 ultra-wideband antenna array in the shape of a bra was designed for a radar-based breast cancer detection system..

DeSantis *et al.* (2014) The American Cancer Society provides a summary of female breast cancer statistics in the United States, including incidence, death, survival, and screening information. In 2013, the United States is predicted to see 232,340 new cases of invasive breast cancer and 39,620 breast cancer fatalities. In the United States, one in every eight women will acquire breast cancer over her lifetime. From 2006 to 2010, breast cancer incidence rates in African American women grew slightly, fell in Hispanic women, and remained unchanged in whites, Asian Americans/Pacific Islanders, and American Indians/Alaska Natives.

Ul Haq and Khan (2014) On a FR-4 substrate, a Multi Ring Slots Ultra Wide-Band (MRS-UWB) patch antenna is developed, simulated, and built. The goal of this antenna design is to incorporate it into a bigger antenna array system for breast cancer diagnosis. The proposed antenna has dimensions of 28×24 mm^2, which are ideal for including into an array of more than 20 antennas that can be worn around the human breast as a wearable device.

Four round rings make up the main antenna. Because of their consistent radiation patterns, circular patch antennas are widely used in wireless transceiver applications. The greatest ring's outer and inner radii are 8.2 mm and 7.2 mm, respectively. For all of the rings, the difference between the outer and inner radius is kept constant, resulting in symmetry in the design and making it simple to build. Furthermore, the two subsequent rings are separated by 1 mm from one another. A

micro-strip feed line feeds all of the circular slots. The VSWR of the proposed antenna is also proven to be less than two over the whole working frequency range. This paper's next work includes expanding this single antenna into an antenna array and combining the array's broadcast and reception signals to create a tumor image.

Cahskan *et al.* (2015) Inset fed rectangular micro-strip antenna configurations are being examined for microwave imaging with the goal of detecting breast cancer early. Basic 3D breast construction is used to approximate the antenna structure operating at 2.45 GHz. Modifying the ground plane and slotting on the micro-strip patch allows several antenna configurations to be studied. In the case of the fourth antenna structure with tumor, the electric field, magnetic field, and current density values are 137.36 V/m, 0.786 A/m, and 54.946 A/m2, respectively, while the values in the case of the breast structure without tumor are 170.38 V/m, 0.84634 A/m, and 68.15 A/m2, respectively.

Kahar *et al*. (2015) On a heterogeneous breast model, an ultra-wide band (UWB) monopole antenna is built for microwave breast imaging. On the breast model, antenna characteristics are investigated for close and distance proximity of the antenna to the breast surface. High current density has been recorded in all placements and sizes of deep and superficial tumors, although the specific absorption rate (SAR) on surrounding tissues and skin has remained within limits. The antenna is ideal for its intended purpose due to its UWB features and safe tolerable SAR.

Kanjaa *et al.* (2015) A novel UWB antipodal Vivaldi antenna for breast cancer detection is presented in this paper. It has been discovered that by inserting exponential slots into both patches of the antipodal Vivaldi antenna, good matching can be accomplished, especially for the lower bandwidth limit, without sacrificing the proposed antenna's other characteristics. The features of this antenna were examined numerically using the CST microwave studio commercial simulator**.**

Kahwaji *et al.* (2016) Ultra Wide Band (UWB) wireless communications, being an emerging technology, takes a fundamentally different approach to antenna construction than narrow band systems, making it a particularly appealing candidate for medical antenna research. The design and simulation of a hexagonal micro-strip

antenna, as well as a breast phantom simulation, are presented in this study. The antenna is emulated by inserting a hexagon slot in the patch's centre, resulting in an impedance bandwidth of roughly 5 GHz. The presented antenna has been successfully designed and simulated. The HFSS programme is used to carry out the simulation study of the planned antenna. Because of the results produced with this antenna, it is a good choice for UWB systems and portable applications.

Karli *et al* (2016) presented the UWB microstrip antenna with FR4 substrate & feeding is performed by a micro-strip line with normalized impedance at 50Ω. The model was developed in the form of cone composed of skin with dimension L is 10cm, W is 5cm & H is 5cm . The design was simulated by placing the antenna at a distance of 15 cm from the breast (case I) then 5 cm from the breast (case II) and in contact with the skin (case III). The antenna gain varies from 2.25 dBi to 4.55 dBi over the operating band with 96% average radiation efficiency. As the signal transmitted by an object depend on the density of the induced current in that object, the current density in the tumor, in the breast skin & fatty tissue are compared. The current density in the tumor in the III case (787.86 A/m2) is higher than the current density in the II case (141.64 A/m2) & about eight time higher than the current density in the first case (98.78 A/m2).

The visibility of the tumor or the sensitivity for the detection of the tumor can be increased by placing an antenna in contact with the breast.

Kwon and Lee (2016) provides an overview of current advancements in microwave imaging for the detection of breast cancer. Finally, we will discuss new research on a microwave imaging system that uses time-domain measurement to achieve quick measurement times and inexpensive system costs. The scan time of the time-domain measuring method is less than 1 second, and it does not require expensive equipment like a VNA. When 1000 repeated signals are averaged with 16 antenna, a CMOS chip-based time-domain microwave system can minimise the scan time to less than 1 second. In the time domain, analogous time sampling with a 1.76 GHz sample clock takes 1.32 seconds as a single measurement. The development of such a microwave breast imaging system will assist young women with dense breasts

in receiving regular breast exams. The development of a microwave breast imaging system like this will allow young women with dense breasts to have regular breast cancer screenings while remaining safe.

Cicchetti *et al.* (2017) It is offered an overview of the geometry, manufacturing technology, and numerical methods used to examine and design wideband and ultra-wide band (UWB) antennas for wireless applications. Planar, printed, dielectric, and wearable antennas are available for consideration on laminate (rigid and flexible) and textile dielectric substrates.

Loktongbam and Solanki (2017) A flexible slot antenna working in the ISM band has been proposed by researchers. Their design is integrated in PDMS to make it biocompatible for implantation (Poly Dimethyl Siloxane). It was then evaluated by immersing it in a human phantom liquid, which mimicked the dielectric and electrical properties of human muscle tissue, and a study of the antenna performance sensitivity as a function of the dielectric parameters was conducted. To provide a brief summary of the issues faced and proposed solutions for implantable antennas for biomedical applications in terms of design, simulations, and limits. Implantable antennas are designed primarily for miniaturisation and biocompatibility, despite the fact that electrically tiny antennas have poor radiation performance and narrow bandwidths. Gain optimization is critical because it jeopardises the system's overall performance.

Naeem A. Jan *et al*. (2017) shows a UWB monopole antenna design that takes use of a ground structure flaw (DGS). The defective ground design is identified as a spiral staircase-shaped pattern, with a volume of 26 25 1.6 mm3 for the optimum antenna. The resulting antenna works across the whole UWB frequency range, from 3.1 GHz to 10.6 GHz, with anticipated gains ranging from 0.1dBi to 3.36dBi.

Shanwar and Othman (2017) proposes a concept for a high-performance ultra-wideband (UWB) transparent micro-strip patch antenna employing polyimide as a substrate and copper as conductors for use in medical applications. Based on the application, which is skin cancer diagnosis, the antenna is designed to resonate at lower frequency ranges as much as possible. Computer Simulation Technology (CST) software is used to study the antenna's characteristics throughout a frequency range of

100GHz to 20THz. Broad bandwidth (BW), high gain, and radiation efficiency are all features of the proposed antenna. The major objective of this study is to develop a THz antenna for medical purposes, including skin cancer detection. To achieve this goal, some strategies for improving THz performance have been developed. In order to achieve this goal, certain strategies for improving the performance of THz antennas were applied. The antenna was etched on polyimide with a permittivity of 3.5 and a copper (optical) conductor with an apparent compact size of 75 x 70 x 3 m^3.

Aliakbar Dastranj *et al.* (2018) Two open ended rounded inverted L-shaped slots are etched on the square ground plane to present a UWB antenna with a small size. Additionally, creating a bevel on the asymmetrical radiating patch improves bandwidth even more. The antenna is fed by a 50 micro-strip line and is only 28×28×1.6mm3 in size. The antenna can provide a wide impedance bandwidth of more than 129 percent from 2.7 to 12.55 GHz with a -10 dB reflection coefficient, according to the simulated and measured results. Furthermore, it was discovered that by introducing multiple antenna designs, the impedance bandwidth could be increased from 58 to 129 percent.

Alsharif and Kurnaz (2018) A unique design for a wearable micro-strip patch ultra-wide band (UWB) antenna with enhanced bandwidth for breast cancer detection is shown. The planned antenna's operating frequency runs from 1.6 to 11.2 GHz. A rectangular radiating patch is fed by a rectangular feed line in this antenna. This antenna will be used in a wearable device for early detection of breast cancer in women. To support wearability, a 100 percent cotton substrate with a dielectric constant of 1.6 was used, with copper as the conductive material for the transmitting component patch and ground planes. CST Microwave Studio was used to conduct the study of the antenna and breast models.

Ibtisam Amdaouch *et al* (2018) proposes a design that is characterized by UWB and frequency range of (3-12) GHz for the FCC band. This antenna has been implemented in a designed system model with dielectric properties of a human breast capable to detect strange objects. The maximum value of SAR is 1dentified in order to accurately detect different locations of tumor inside the breast. The principle of

microwave imaging for breast cancer detection is based on the large contrast of the dielectric constant and conductivity between the turns is printed on and other breast tissues. The antenna is printed on an FR-4 dielectric substrate, with a thickness of 1.6 mm and relative permittivity ϵr of 4.4. For the ISM band of central frequency of 5.8GHz the peak gain is equal to 5.2 dBi which proves that the proposed antenna is a good candidate for cancer detection.

Misilmani *et al*. (2020) This paper presents a comprehensive examination of the various array configurations proposed for microwave breast imaging, as well as a detailed examination of the antenna elements proposed to be used with these systems, which are classified by antenna type and by the improvements in operational bandwidth, antenna size, radiation characteristics, and the techniques used to achieve the improvement. At the conclusion of the inquiry, a qualitative evaluation of the antenna designs is offered, including a comparison of the investigated antennas and a determination of whether or not a design is suitable for use in microwave breast imaging antenna arrays based on its performance. The researched arrays are also evaluated, with the benefits and drawbacks of each array arrangement discussed.

Materials and Methods

Chapter 3 MATERIALS AND METHODS

The design considerations for the proposed antenna, as well as the methodology and materials used for simulation, manufacturing, and measurement, are detailed in this chapter. The first section covers the fundamentals of microstrip patch antennas, including feeding strategies and DGS. The monopole antenna and slotting are addressed in the second section. In the third portion, the breast phantom, as well as the SAR, current density, and electric field distribution, are addressed in depth. In the fourth section, the models used to analyse patch antennas are discussed. The simulation software utilized is Ansys HFSS, which is detailed in the fifth section of this chapter. Simulation and analysis of each parameter of the proposed antenna are aided by software. The sixth portion is further divided into four subsections, each of which discusses the design process for the proposed antenna. The specifications of a standard microstrip antenna, a planar monopole antenna with T-shaped slots in the patch, and the design of a breast phantom are all discussed. The method of manufacture is discussed in the concluding section of this chapter. The design steps involved in the development of the proposed antenna are thoroughly documented.

3.1 Microstrip Patch Antenna (Balanis 1997)

Patch and ground are separated by the dielectric in a microstrip antenna. As indicated in Fig. 3.1, the dielectric is referred to as the substrate. The substrate's height is assumed to be low (h 0), where 0 denotes the free space wavelength. The ground plane and the patch are largely made of the same metal. By using a high dielectric constant, the size of the microstrip antenna is minimized. Microstrip antennas have a low profile, tiny size, and light weight, which allows them to be integrated into modern communication devices. Microstrip antennas have some limitations, such as narrow bandwidth and limited strength. In the modern period, experts have focused on improving these traits.

A tiny microstrip antenna can meet this need since it can exhibit multiband behaviour, which can be enabled by modifying the patch or ground plane shape.

Because of its small size, MSA can easily be integrated into modern electronic devices.

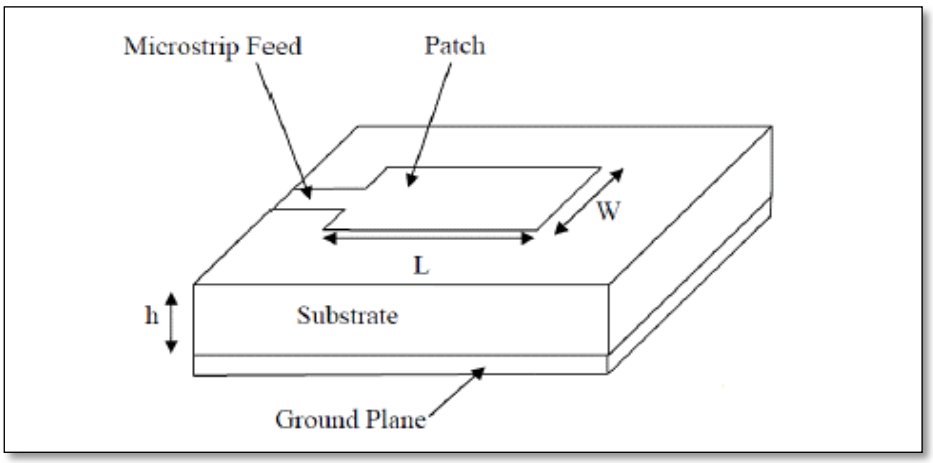

Fig. 3.1: Microstrip antenna

Microstrip line feed

To deliver power to the patch, a conducting strip with a significantly smaller width than the microstrip feed line is used. As shown in Fig. 3.2, the microstrip feed line is directly attached to the patch's border. Because the feed line and patch can both be positioned on the same substrate, this approach creates a planer structure. It is the simplest of all feeding techniques due to its ease of production and modelling. To correctly match the impedance, an inset cut is sometimes employed. This approach does not require any additional matching elements. Increasing the thickness of the substrate might result in spurious feed and surface wave radiation, reducing the antenna's bandwidth and lowering its performance.

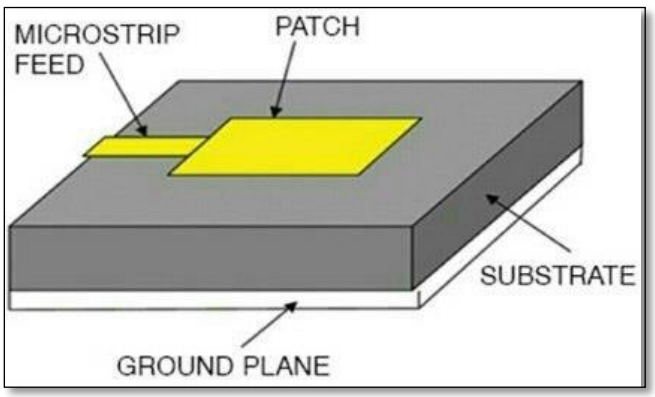

Fig. 3.2: Microstrip feed line

3.2 Printed Monopole Antenna (PMA) for UWB applications (Ray 2008)

The printed monopole antennas have a very wide bandwidth of impedance and a very good radiation pattern in the azimuthal plane, which may be defined and grouped into the two categories below.

(i) A printed monopole antenna is a type of microstrip antenna in which the ground plane backing is positioned at infinity. On the dielectric substrate, there is a patch (commonly FR4). It is possible that a very thick air dielectric substrate (r = 1) exists beyond the substrate. It allows MSA to be configured on a thick substrate with r close to unity, resulting in a huge bandwidth.

(ii) Vertical monopole antennas, such as printed monopole antennas, are a type of vertical monopole antenna. By and large, a monopole antenna is made up of a cylindrical vertical wire positioned above the ground plane, the diameter of which increases with the bandwidth. To put it another way, a printed monopole antenna is similar to a cylindrical monopole antenna with a high effective diameter. In the event of varied feed configurations, the second analogy has aided in establishing the lower band-edge frequency for each and every typical shape of printed monopole antenna.

(iii) There are many different varieties of printed monopole antennas with regular shape such as such as printed triangular monopole antenna (PTMA),printed square monopole antenna (PSMA),printed hexagonal monopole antenna (PHMA), printed rectangular monopole antenna (PRMA), printed circular monopole antenna (PCMA), and printed elliptical monopole antenna (PEMA).Figure 3.3 shows different planar antennas for different feed positions. The suffix 1 or 2, has been written for different feed positions as illustrated from the fig 3.3. These antennas are commonly made on FR4 substrate (εr=4.4, h = 0.16 cm, and tan δ = 0.01) with backing ground plane is removed. These antennas are fed by 50Ω microstrip line or by coplanar waveguide.

The standard formula for cylindrical monopole antenna has been given to estimate the lower band-edge frequency of PMAs. Ray also demonstrated reduced band edge equations for various PMAs for UWB applications.

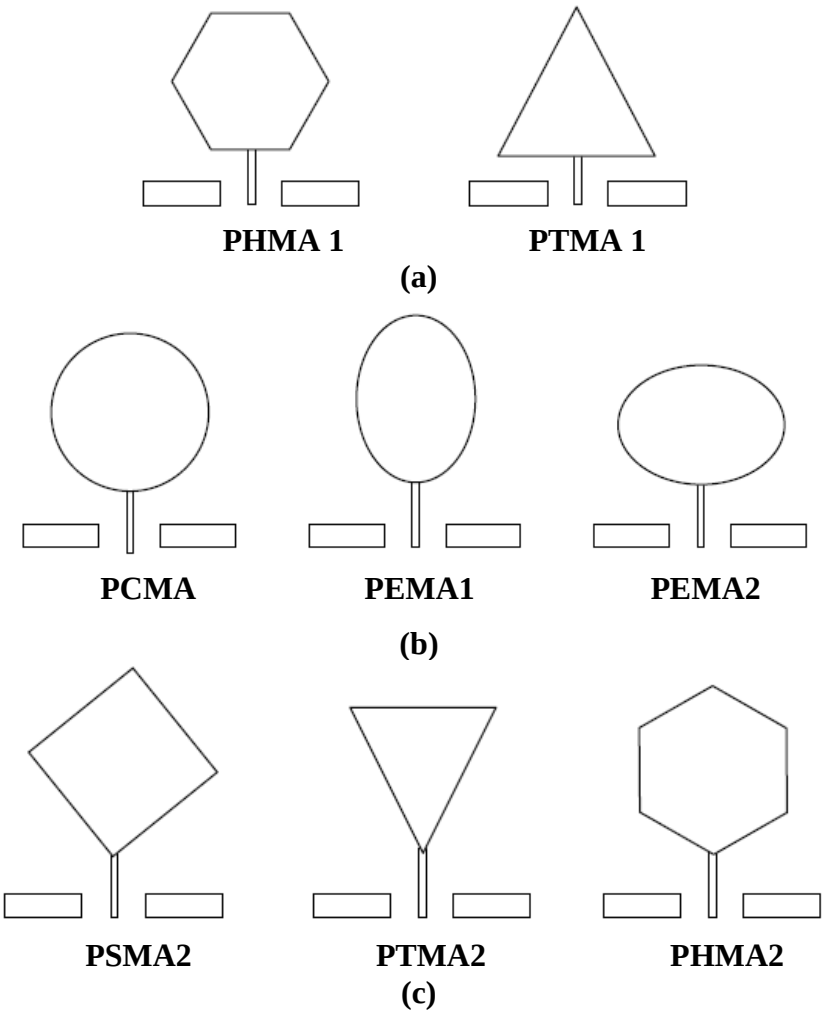

Fig 3.3: Various Regular shaped PMA for different feed configurations.

3.3 Methods of analysis

For analysis point of view, microstrip antenna may be categorized as a planer antenna due to its planar radiating patch and very thin substrate height. There are different methods for the analysis of microstrip antenna based on the electromagnetic wave propagation around the patch among them most popular are

- Transmission line model
- Cavity model
- Full wave method

Among above transmission line model is commonly used due to easy analysis and provide good physical insight. But then this model has less accuracy and model coupling is difficult. Cavity model is more accurate but more complex provides good physical insight and model coupling is difficult. Full wave model is most accurate and versatile model but most complex and gives less physical insight. Hence TLM is widely used for analysis purpose.

3.3.1 Transmission line model (Garg *et al.* 2002)

Transmission line model provides a good physical insight of the antenna and is very easy to model and realize. In this model MSA is represented by two slots of width 'W' and height 'h' separated by the distance 'L'. The antenna is considered as a non-homogeneous line of two dielectrics i.e. substrate and air.

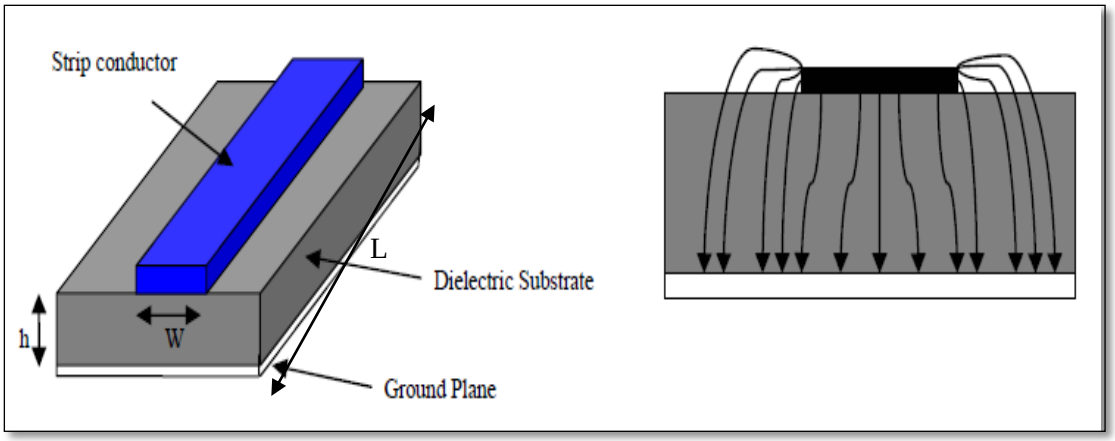

Fig. 3.4: Microstrip line and fringing phenomenon

The electric field line does not exist inside the substrate completely and some electric field lines reside in a small portion of air as shown in fig 3.4. As air and the dielectric substrate have different phase velocity this microstrip line doesn't support pure TEM (Transverse electromagnetic) mode of operation. The dominant mode of operation here would be quasi-TEM mode. This phenomenon is termed as 'Fringing'. After taking fringing effect into consideration the value of ε_r is modified to ε_{reff}.

Some equations which are used in calculation of the length and width of the patch are given below.

i) Width of the patch

$$W = \frac{c}{2f_0\sqrt{(\varepsilon_r + 1)/2}} \tag{3.1}$$

Where c is the velocity of light and f_0 is the operating frequency

ii) Effective dielectric constant of MSA

$$\varepsilon_{reff} = \frac{\varepsilon_r + 1}{2} + \frac{\varepsilon_r - 1}{2}\left(\frac{1}{\sqrt{1 + 12h/w}}\right) \tag{3.2}$$

iii) Increment in the electric length of the patch

$$\Delta L = 0.412h\frac{(\varepsilon_{reff} + 0.3)(w/h + 0.264)}{(\varepsilon_{reff} - 0.258)(w/h + 0.8)} \tag{3.3}$$

iv) Effective length

$$L = L_{eff} - 2\Delta L \tag{3.4}$$

v) Resonant frequency

$$f_0 = \frac{c}{2\sqrt{\varepsilon_{reff}}}\left[(m/L)^2 + (n/W)^2\right]^{1/2} \tag{3.5}$$

Where **m** and **n** are the modes along **L**and **W** respectively

3.5 HFSS Software

Various types of software are used to build and simulate antennas, one of which is the high frequency structure simulator (HFSS) programme. HFSS uses the finite element method (FEM) numerical methodology to aid in the investigation of the electromagnetic component. In aeronautical engineering, FEM m was designed to tackle structural analysis and elasticity problems.

A tetrahedron is the most basic mesh element in HFSS. Maxwell's equations are used to obtain the answer at each node of the tetrahedron. As a result, it can

readily solve any 3D shape in a short amount of time. ANSYS Gain, resonant frequency, fields, and S-parameters are only a few of the parameters that HFSS can determine. In HFSS, a 3D model can be created based on user needs, and different parameters can be obtained afterward. The main processes are to design the model and then obtain simulation results from that model

- Create 3D model
- Boundary assign
- Excitation assign
- Solution set up
- Validation and analysis of model
- Results

3.5.1 Create 3D model

The initial step in designing an antenna is to create a model based on the substrate, patch, and ground plane dimensions. A completely parametric 3D model allows you to change each geometrical dimension and material property. As a result, the best outcomes are obtained by adjusting the various factors. For different types of models, different solutions such as driven model, driven terminal, and eigen mode are utilised. The model-based S-parameter of passive and high frequency structures is obtained using the driven model. The terminal-based S-parameter of single and multi-conductor transmission line ports is obtained using the driven terminal. The structure's resonance is calculated in Eigen mode.

3.5.2 Boundary assign

Perfect E, perfect H, finite conductivity, and radiation boundaries are applied after the 3D model is created. Patch and ground planes are usually allocated perfect E or finite conductivity in MSAs, while the radiation box is usually assigned radiation. The assigned boundary has a direct impact on the HFSS solution.

3.5.3 Excitation assign

The type of excitation employed has a direct impact on the quality of the results. When designing an antenna, either a lumped port or a wave port is used for excitation. External boundaries are defined by wave ports, whereas inside boundaries are defined by lumped ports.

3.5.4 Solution setup

The desired frequency at which the user works is selected during the solution setup. Following that, the total number of adaptive passes and the frequency sweep for which results are required are chosen.

3.5.5 Validation and analysis of the model

Validation and analysis are essential to check for faults while developing the antenna. The amount of time it takes to analyse a model is mostly determined by its shape, solution frequency, sweep, and step size.

3.5.6 Results

After performing the above designing steps, one can get the antenna parameters like S parameters, VSWR, gain, directivity, radiation pattern etc.

3.6 Development of the proposed antenna

The general design consideration to design the UWB antennas are given below as:-

(i) The antenna's bandwidth should be between 3.1 and 10.6 GHz, with good omni-directional radiation patterns and high efficiency across the whole spectrum.

(ii) In the event of an ultra-wide bandwidth, a very low level of emission power must be ensured. Emission restrictions of 41.3 dBm /MHz have been established by the Federal Communications Commission (FCC).

(iii) Across the whole spectrum of UWB, the antenna must convey short-pulse signals with little distortion.

The first point denotes the requirement that the antenna have a 3.42:1 impedance bandwidth ratio with a VSWR of less than 2. Only multi resonance printed monopole antennas, which have strong pass impedance properties, can achieve such a wide impedance bandwidth. As a result, the above-mentioned aspect should be considered when dealing with UWB Technology.

As a result of the aforesaid considerations, the following antennas have been designed and manufactured: -

(i) For UWB applications, a small semi-circular Patch Monopole antenna with T-shaped Slotted and DGS ground.

(ii) For UWB applications, a small semi-circular Patch Monopole antenna with DGS ground and three T-shaped structures **(Proposed Antenna).**

(iii) A variation of the suggested antenna is also constructed for breast cancer diagnosis using SAR analysis.

(iv) An analysis based on the antenna's current density and electric field distribution, which are utilized to discriminate between normal skin, malignant cells, and fatty tissues

Primarily, in the first design stage a conventional semi-circular patch microstrip antenna is designed and miniaturized by using DGS ground Technique and thus obtaining the desired UWB antenna. In second design stage a T slot is designed for obtaining the desired frequency range. Later on, two small horizontal T slot structures are inserted at the patch for maintaining the lower frequency range of 4.5-7 GHz and ground for obtaining for second lower frequency range 3-5GHz (Proposed Antenna). Variant of proposed antenna is also designed to analysis the SAR, current density and electric field distribution characteristics for the detection of malignant tissues in the breast. The fabrication of the proposed antenna is carried out using PCB prototype machine (EP 2002) and measured through VNA.

Dielectric substrate used for the proposed antenna is FR4 epoxy of thickness 1.6 mm. The dielectric constant and loss tangent of substrate is 4.4 and 0.02, respectively. Following Subsection describe the design techniques.

3.6.1 Conventional patch antenna design and miniaturization.

The design of a circular microstrip patch antenna is simpler than other patch configurations since it only requires one design parameter, the patch radius. The process assumes the provided data comprises the substrate's dielectric constant (r), operating frequency (fr), and substrate height (h). We need to determine the patch's exact radius 'a'.

$$a = \frac{F}{\left\{1+\frac{2h}{\pi\varepsilon_r F}\left[\ln\left(\frac{\pi F}{2h}\right)+1.7726\right]\right\}^{1/2}} \tag{3.6}$$

Where F can be calculated as

$$F = \frac{8.791\times10^9}{f_r\sqrt{\varepsilon_r}} \tag{3.7}$$

In the above equations we should remember that the operating frequency fr should be taken in Hertz (Hz) and the height of the substrate h should be taken in Centimeters (cm).

The length of microstrip line feed line is calculated as: -

$$L_{ml} = \frac{c}{4f_r\sqrt{\varepsilon_{effml}}} \tag{3.8}$$

Where

$$\varepsilon_{effml} = \frac{\varepsilon_r+1}{2} + \frac{0.5(\varepsilon_r-1)}{\sqrt{1+12(h/W_{ml})}} \tag{3.9}$$

Where W_{ml}, C, ε_{eff}, and f_r are the width of the microstrip line, speed of light in free space, effective dielectric constant, and resonance frequency, respectively. Initially, the dimension of the substrate is L = 30 mm and Width =30 mm respectively.

Calculation of the dimension is carried out using Transmission Line Model. Variation for radius of patch and width of feed line is shown in fig 3.5(a) and (b) respectively.

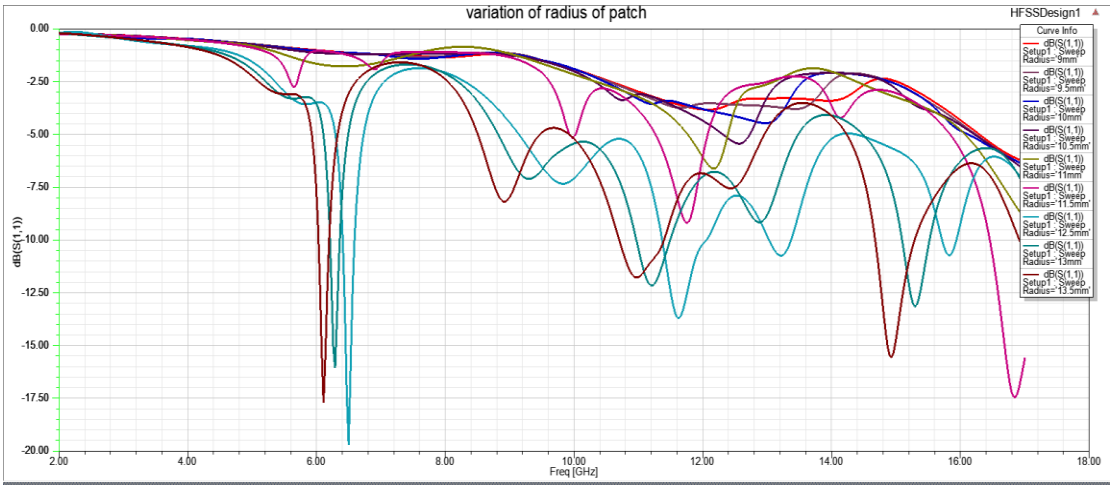

(a)

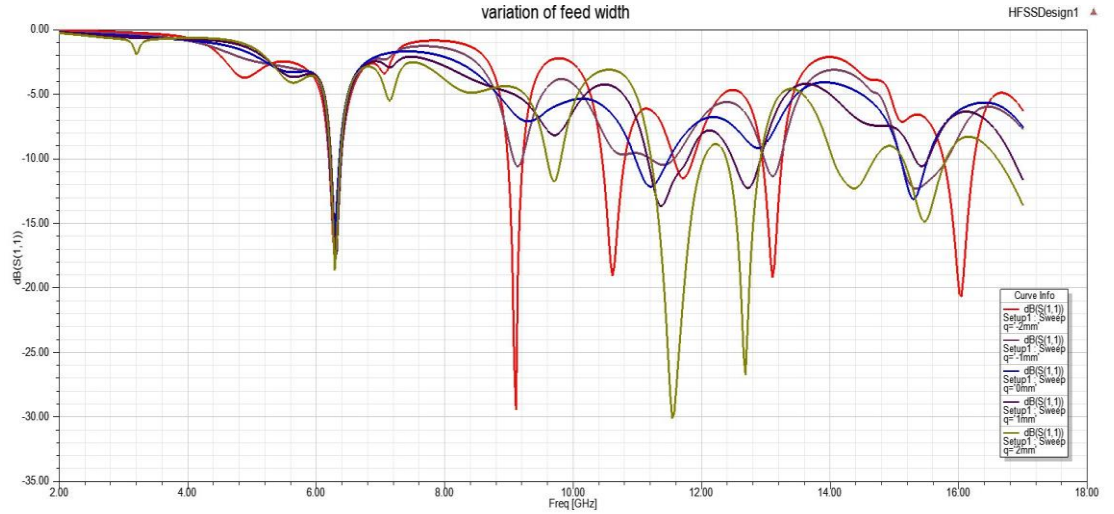

(b)

Fig. 3.5 (a) S parameter for parametric variation of radius of patch.
(b) S parameter for parametric variation of width of feed line.

The radius of the semi-circular patch is calculated as 11.5 mm which is optimized to be A = 13 mm. Microstrip line is used as feeding mechanism. The length and width of microstrip feed is $F_{L=}$13.08 mm and $F_{W=}$ 3 mm. The tapered feed line is done for proper impedance matching. S parameter for radius of semi-circular patch and optimized width of feed line is shown in fig 3.6(a) and (b) respectively.

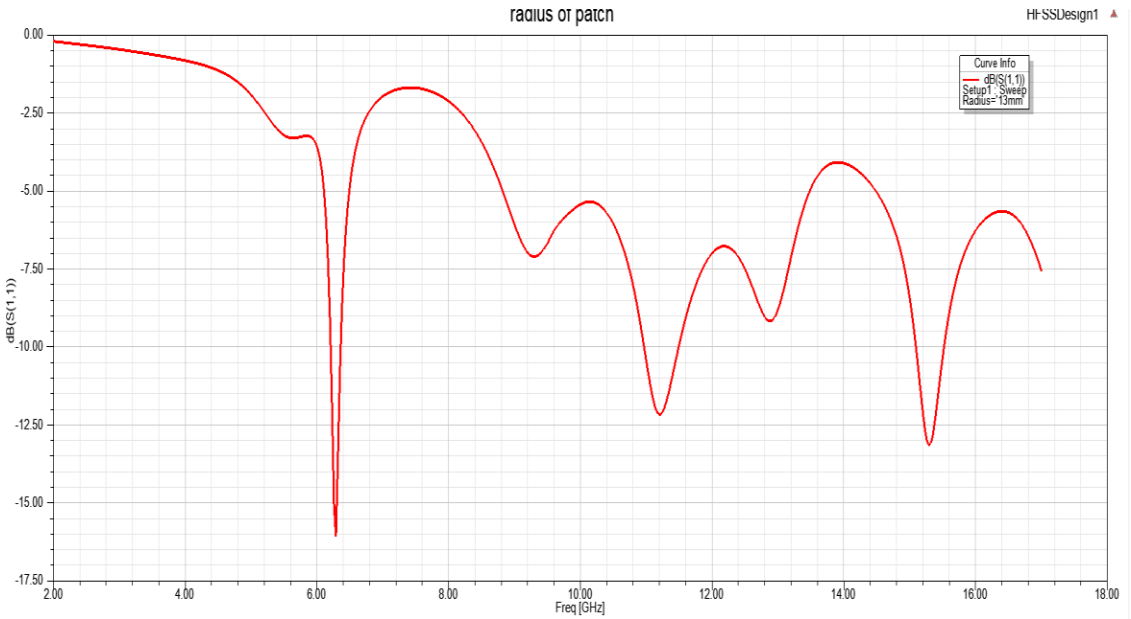

(a)

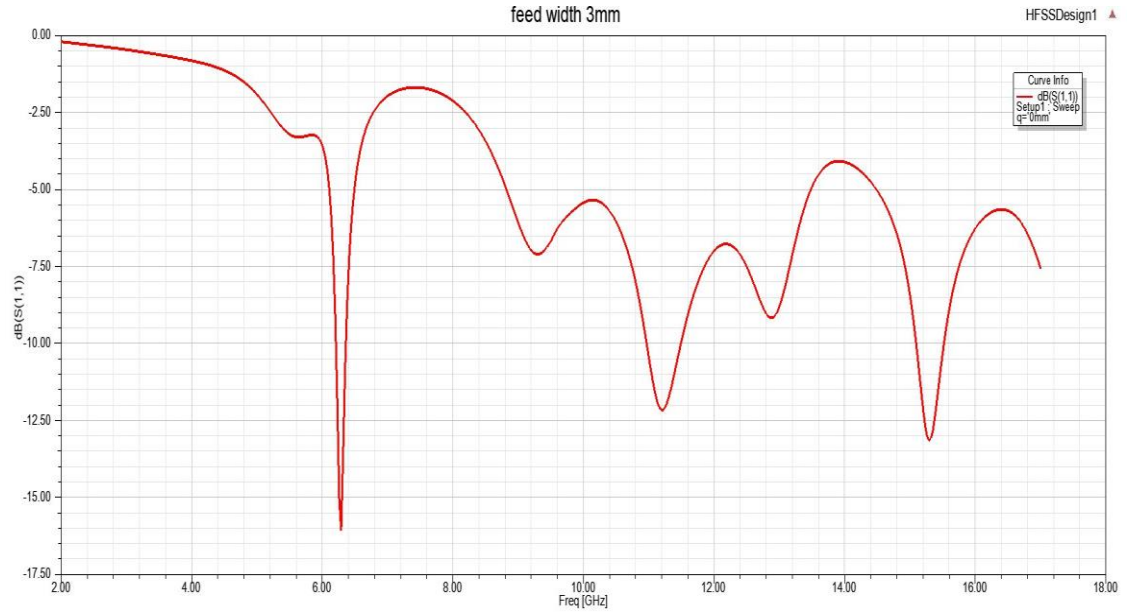

(b)

Fig 3.6(a) S-parameter for radius of patch at A=13mm
(b) S-parameter for width of feed line at F_W=3mm

The geometry of equilateral semi-circular patch antenna is shown in Fig. 3.7(a) and S parameters of semi-circular patch designed at 10.5 GHz is shown in fig 3.7(b).

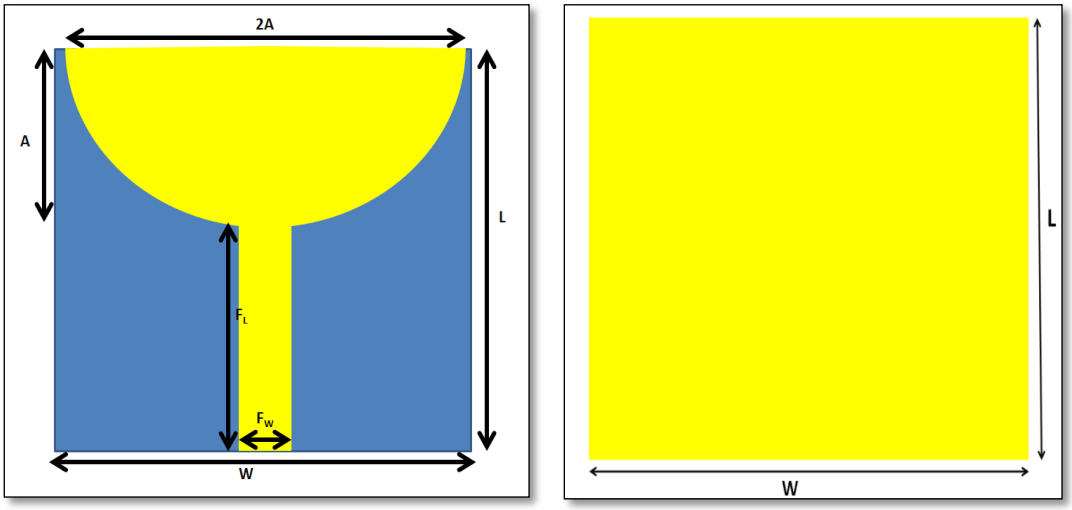

Top view Bottom view

(a)

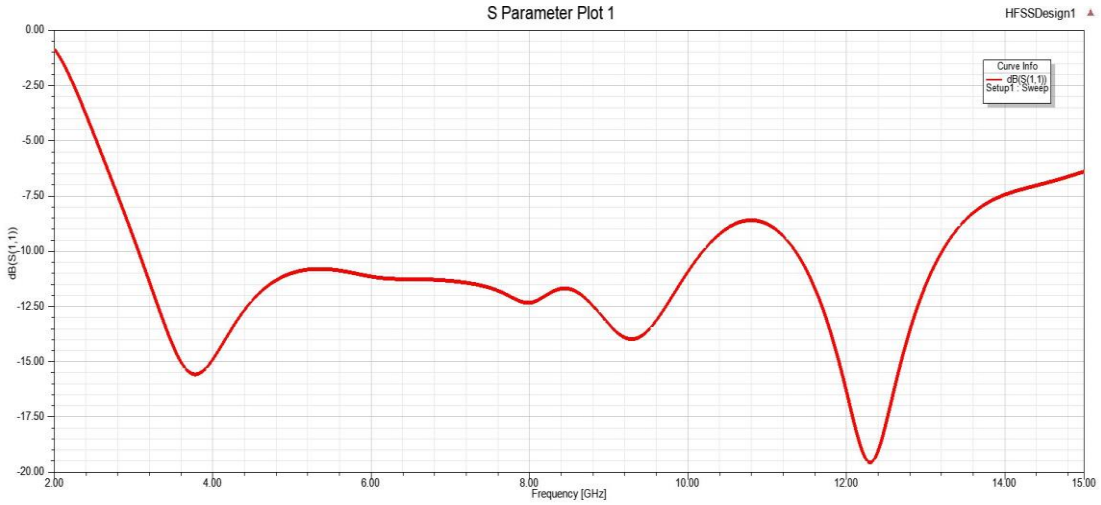

(b)

Fig. 3.7: (a) Geometry of conventional Microstrip Patch Antenna (b) Reflection Coefficient (dB) of the Antenna

3.6.2 Monopole UWB Antenna

After designing the conventional microstrip patch antenna. It is modified to monopole antenna by reducing the ground. The printed monopole antenna can be deemed as a particular structure of microstrip antenna, where the ground plane is positioned at infinity. A patch is directly above the dielectric substrate and moreover, further than the substrate, it can be expected to find that an extremely profuse air dielectric substrate (ε_r =

1) is present which leads to the creation of the microstrip antenna on a dense substrate with ε_r nearer to unity, generating substantial bandwidth. The lower band-edge frequency of printed monopole antennas is specified as (**Ray, 2007**).

$$f_L = \frac{7.2}{\{(L+r+p)\times k\}} GHz \quad (3.10)$$

For Printed circular Monopole Antenna (PCMA), the values of L and r of the equivalent cylindrical monopole antenna are given by.

$$L = 2A,\ r = A/4 \quad (3.11)$$

Here, A is the radius of the semi-circular patch. L, r, p should be taken in cm for equation (3.10). The value of k for commonly used FR-4 substrate with ε_r = 4.4 and h = 0.16 cm is 1.15 which estimates the lower band-edge frequency.

For the better compact structure, PCMA is chosen. The dimensions of the antenna are then miniaturized with the help of defective ground structure. The semi-circular patch which is resonating for 4 GHz, after reducing the ground the same structure is working for 3 GHz. Thus, miniaturization of antenna is done as per the resonating frequency. The semi-circular patch is inserted with the T-shaped slot structure to fit the overall patch in a compact substrate and tapered feed is used for impendence matching. The DGS properties are obtained by reducing the size of ground. The geometry of modified semi-circular patch and ground is shown in fig 3.8(a) and 3.8(b) respectively.

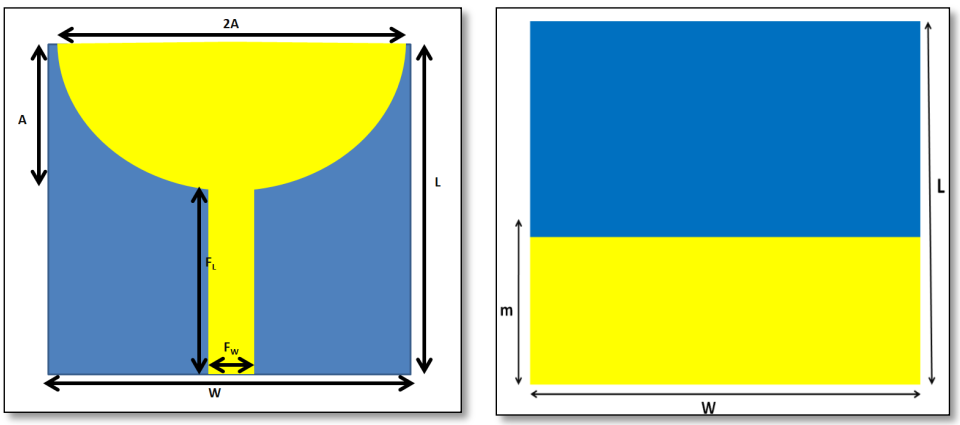

(a)Top View **(b) Bottom View**

Fig 3.8: Geometry of the Monopole Antenna

The optimized radius of semi-circular patch is 13 mm. After achieving the desired lower band-edge frequency the parametric study of ground structure is carried out to achieve the desire UWB characteristics as shown in fig 3.9.

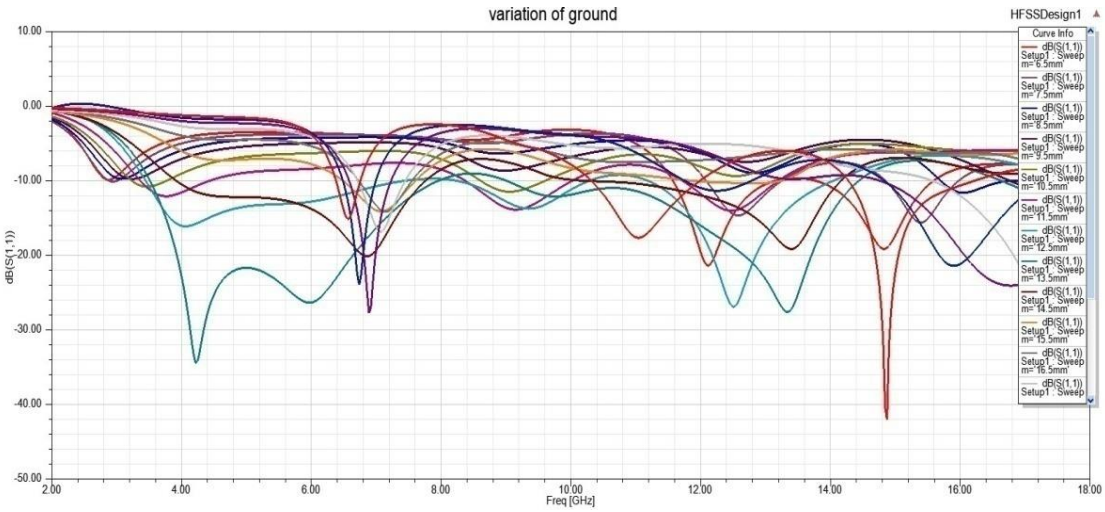

Fig. 3.9: S parameters for the parametric variation of the length of the ground

The result of parametric study shows as the length of the ground increases there is improvement in the lower band frequency from 3 to 7 GHz further increasing the length of the ground decreases the upper band from 7.2 to 12 GHz. Thus, an optimized value of ground structure around m= 11.5 mm is taken so that the UWB characteristics for the entire band can be achieved. At m= 11.5mm the return loss characteristics is below -10 dB from 3.2 to 7.3 GHz as shown in fig 3.10 but not in UWB band. The optimized dimensions of the Antenna are shown in the Table 3.1.

Table 3.1: Design parameters of the proposed Antenna

Parameters	Length(mm)
L	**27**
W	**27**
H	**1.6**
A	**13**
M	**11.5**
F_L	**13.08**
F_W	**3**

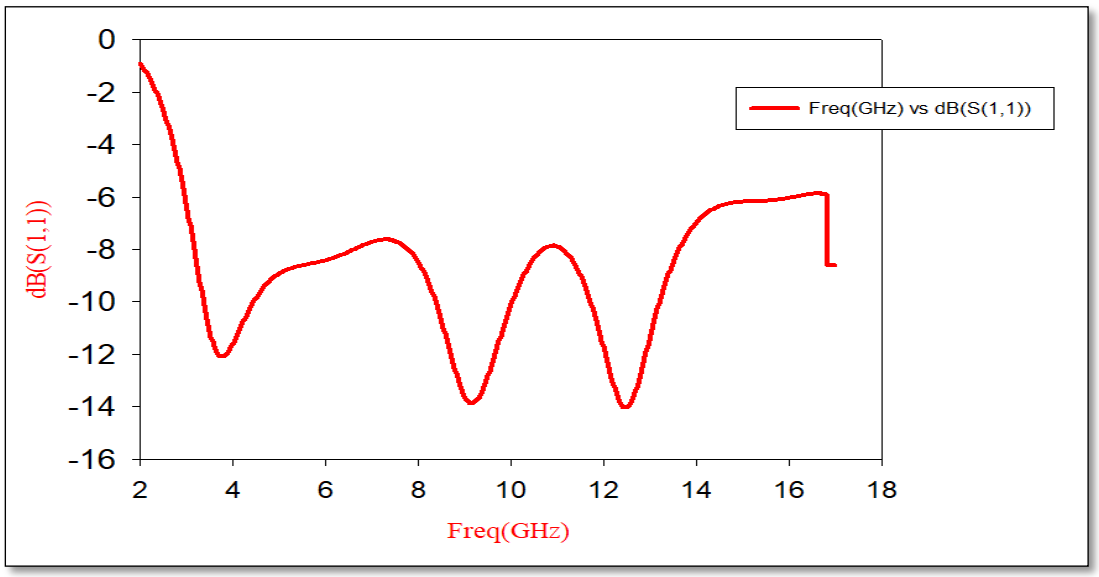

Fig 3.10: Reflection Coefficient of the Modified Antenna at m=11.5mm

To further improve the S_{11} parameter T shaped slots are cut horizontally in the patch to further improve the return loss characteristics. The 2 T-shaped slots at right and left side facing each other on the patch are cut to improve the S_{11} characteristics. The antenna structure with T-shaped slots is shown in the fig. 3.11. The optimization of the two T-shaped slots are done simultaneously to further improve the return loss characteristics and the study results of small T on right side is shown in fig 3.12 and the S-parameter for the modified T-structure is shown in fig 3.13.

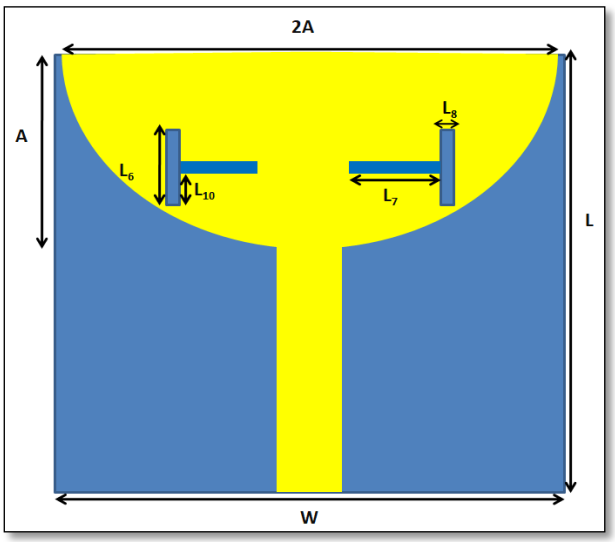

Fig 3.11: Modified Antenna with T-shaped slots at the patch

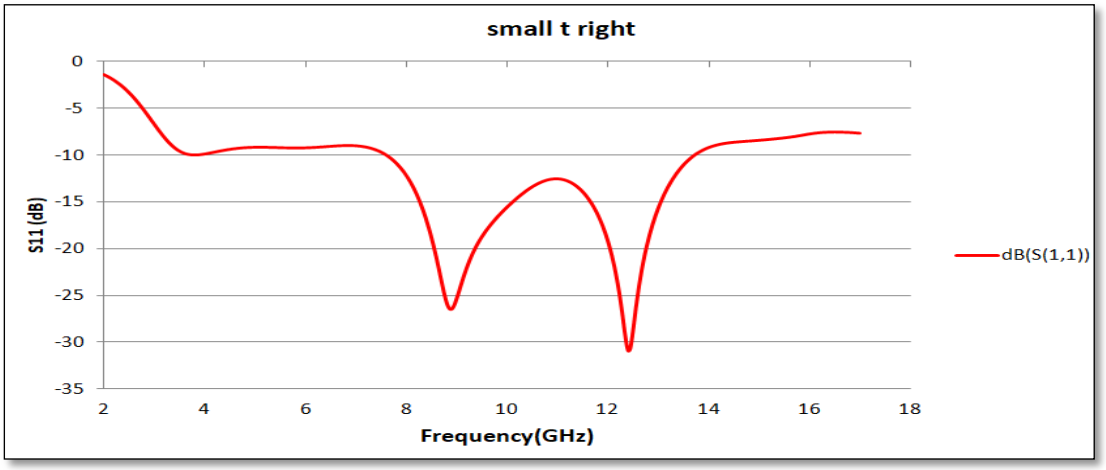

Fig 3.12 Effect of T-shaped structure on right side of patch

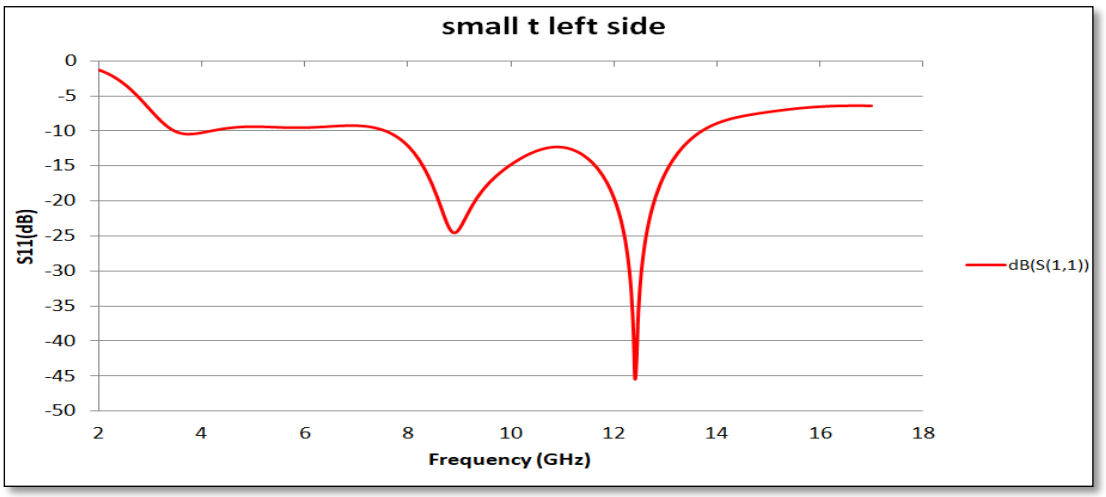

Fig 3.13: S parameters of modified antenna with T-shaped slots

The best result is obtained at 15.5 mm. The T-shaped slots increase the current path length of the antenna. Thus, improving the return loss characteristics of the antenna. The bandwidth is further improve the bandwidth from 3.08 to 10.16 GHz.

To further achieve the monopole UWB antenna characteristics a rectangular slot is cut at the ground. The DGS rectangular slot is cut in such a way as to achieve the desire monopole properties. The parametric study and analysis of rectangular slot has been carried out and length of the rectangular slot is found to be 3.5mm is shown in fig 3.14. After cutting the rectangular slot the desired antenna starts resonating in UWB region but the lower band frequency from 3.35 to 13.62 GHz is nearly touching the -10dB. The optimized size of rectangular slot is obtained as 3mm × 3.5mm and s-parameter for that is shown in fig.3.15 (a) and (b) respectively.

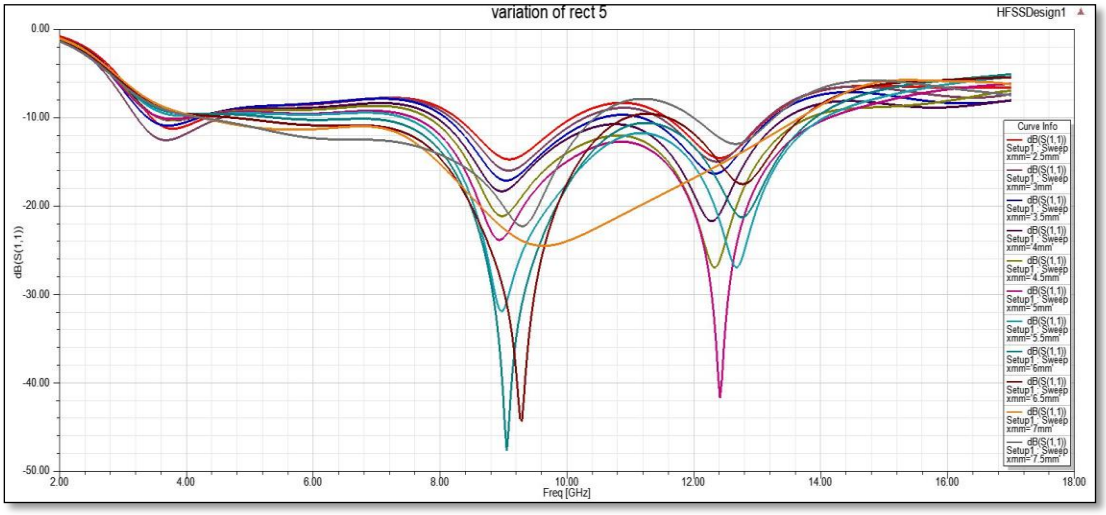

Fig 3.14 S-parameter variation for the rectangular slot

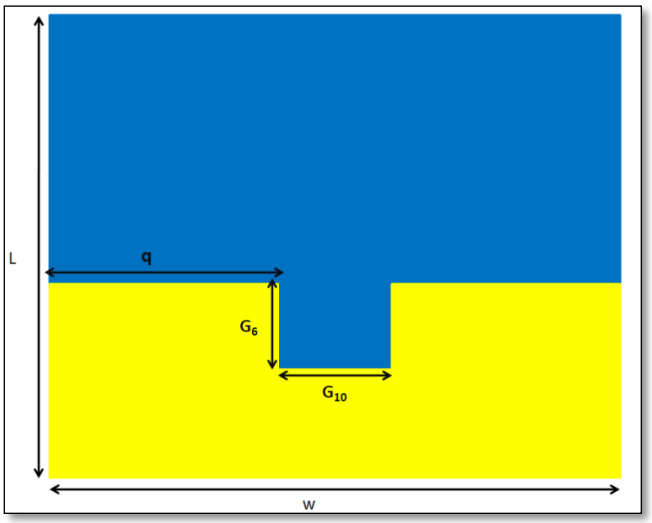

(a)

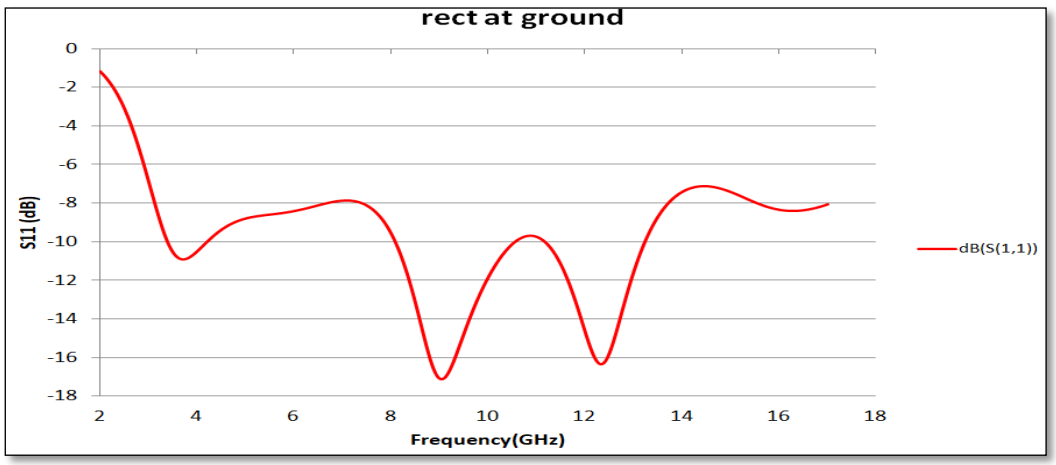

(b)

Fig. 3.15(a): modified antenna with rectangular slot at q=12mm
(b) S- parameter for the modified antenna with rectangular slot

To further improve the S_{11} parameter rectangular slots are cut along the corner of the ground to further improve the return loss characteristics. The pair of rectangular slots at right and left edge of the ground are cut to improve the S_{11} characteristics. The antenna structure after rectangular slots is shown in the fig. 3.16. The parametric study and optimization of all the rectangular slots are done simultaneously to further improve the return loss characteristics and the study results are shown in fig 3.17. The best result is obtained at 3.5 mm.

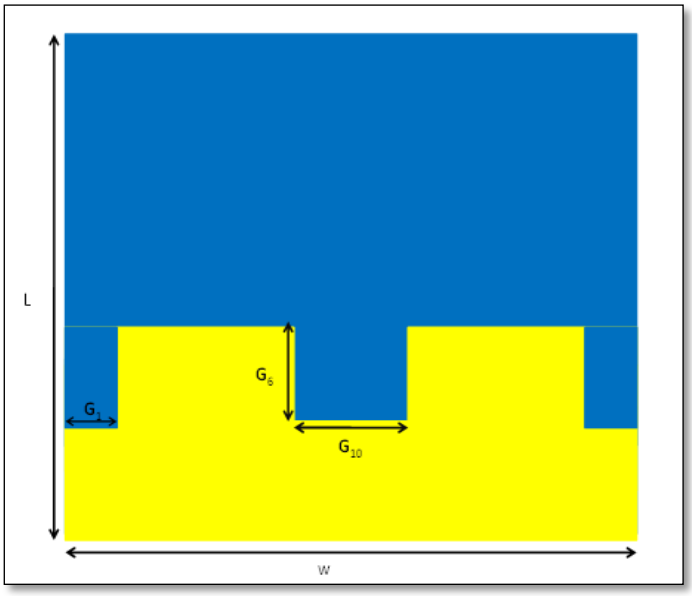

Fig 3.16: Antenna with pair of rectangular slots at the ground

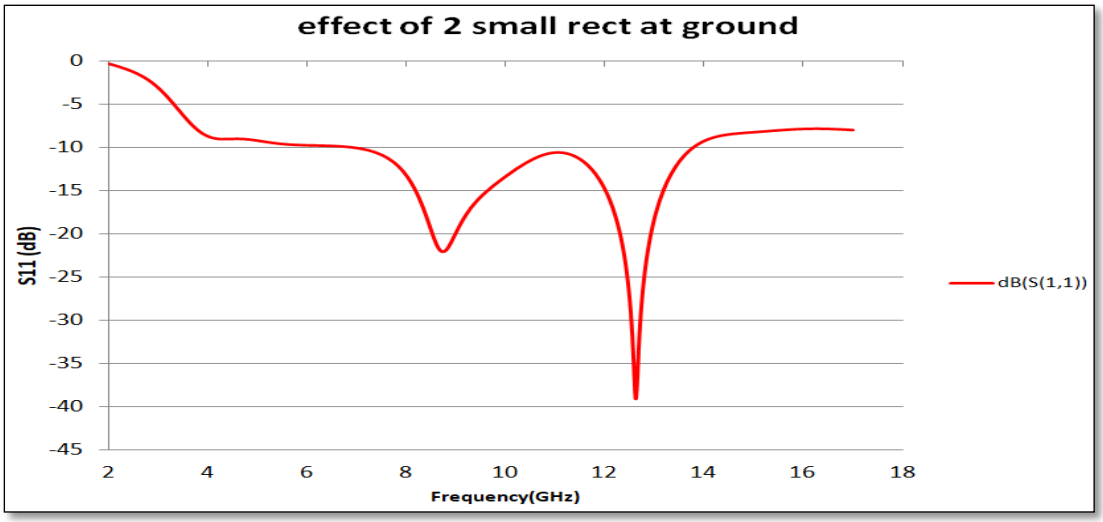

Fig 3.17: S parameters for pair of rectangular slots

To further increase the current path length of the antenna another pair of rectangular slot with dimension 1mm×2mm is added to the ground plane. Thus, improving the return loss characteristics of the antenna. The bandwidth is further improve the bandwidth from 3.7 to 13.5 GHz. The modified ground structure is shown in fig 3.18 and s-parameter for the same is shown in fig 3.19.

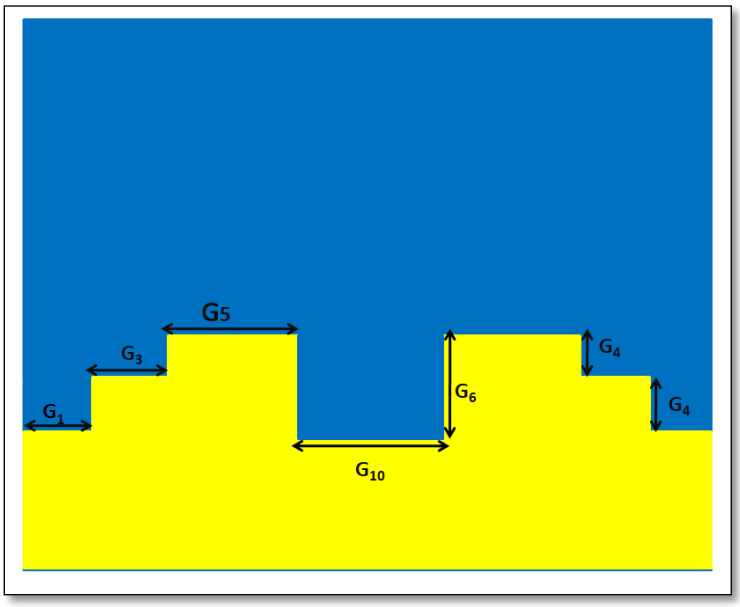

Fig. 3.18: Modified Antenna with rectangular slots at the ground

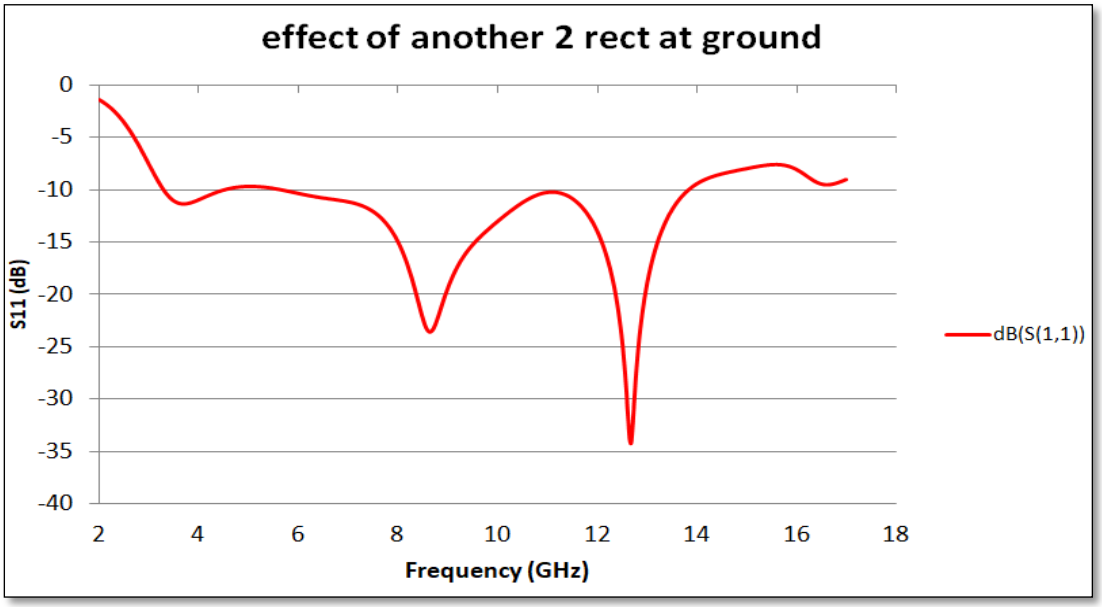

Fig. 3.19: S parameters for modified rectangular slots

To further achieve the monopole UWB antenna characteristics a T-shaped slot is added in the middle of the patch. The parametric analysis of length of T from 5 to 18mm is done to achieve the optimized value. The parametric variation of length is shown in fig 3.20.

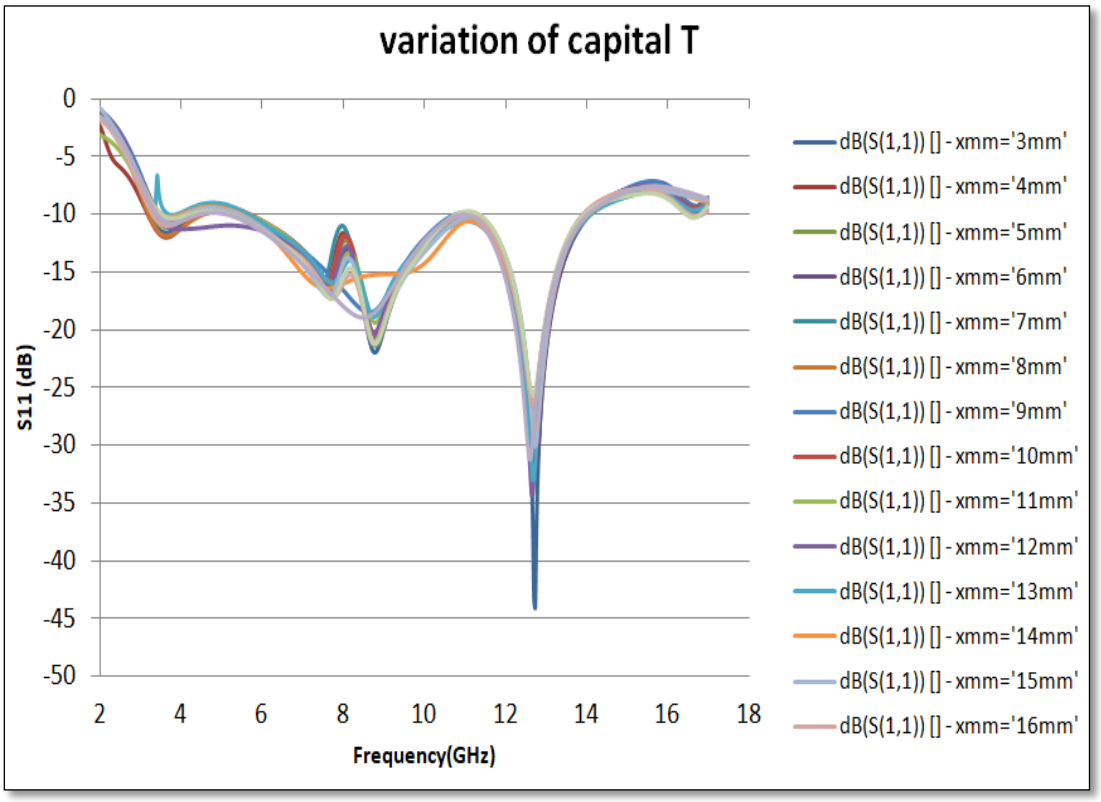

Fig 3.20 S- parameter for variation of length of T

The above result shows that the best value for the length of large T-shaped slot is obtained at x=16mm, the modified patch structure along with the reflection coefficient at x=16mm is shown in fig 3.21(a) and (b) respectively.

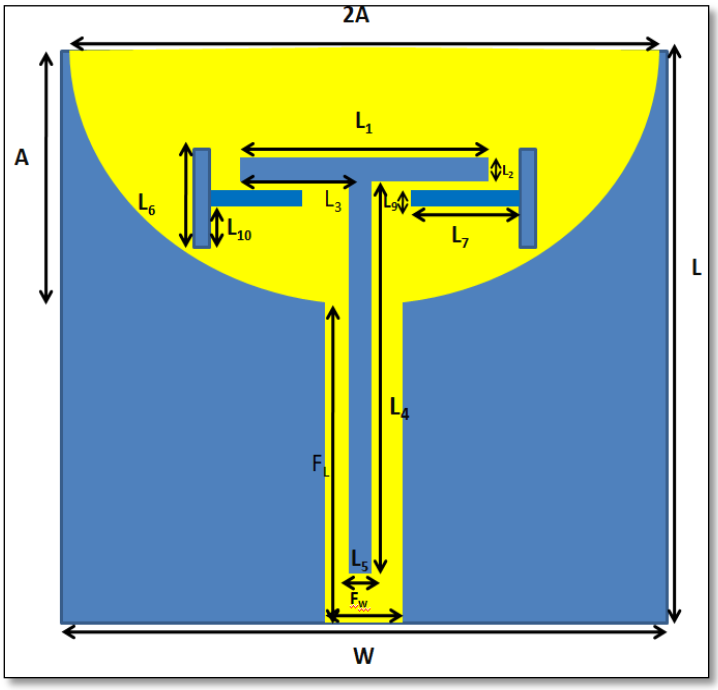

(a)

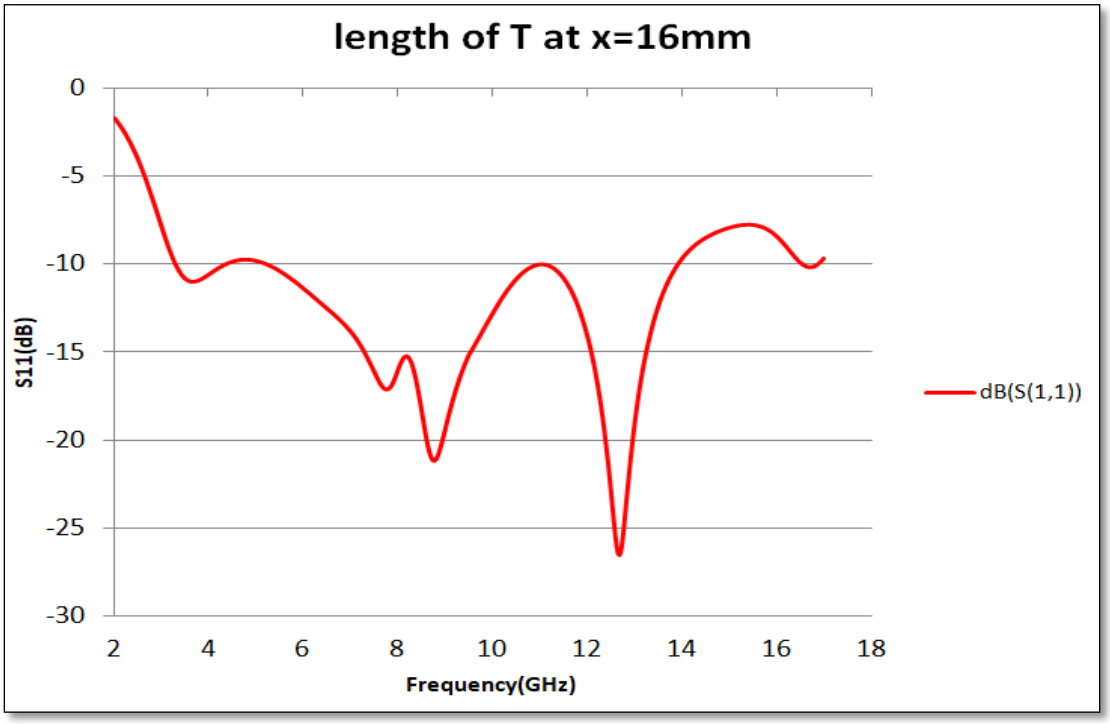

(b)

Fig 3.21(a) Modified patch structure with T- slot

(b) S-parameter for length of T at x= 16mm

To further achieve the monopole UWB antenna characteristics a rectangular slot is cut at the ground. The DGS rectangular slot is cut in such a way as to achieve the desire monopole properties. The parametric study and analysis of rectangular slot has been carried out and width of the rectangular slot is set to be 1mm while the variation of the length of the rectangular slot from 4 to 8 mm is carried out as show in fig.3.22.

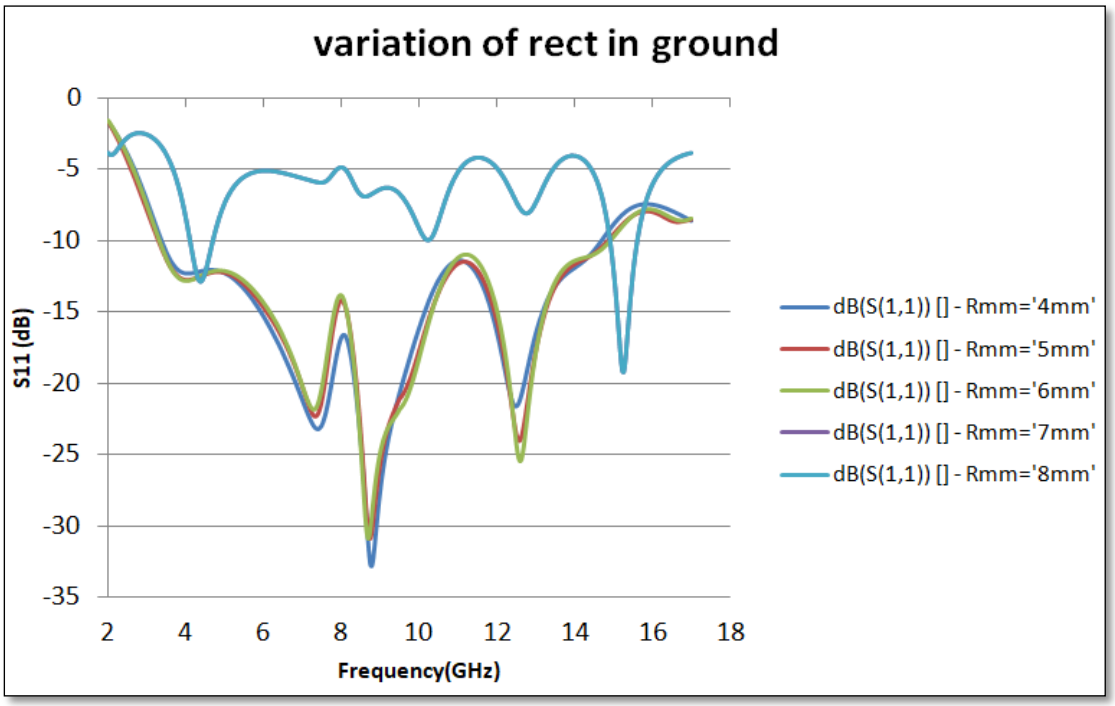

Fig. 3.22: Parametric variation of rectangular slot

The optimized value of the rectangular slot is then obtained is 6mm×1mm. The modified ground plane and reflection coefficient are shown in fig 3.23.

Thus, desired UWB characteristics are achieved. The optimized dimension of the substrate is 27×27 mm^2.The DGS structure not only improves the S_{11} parameters but also the gain of the antenna. The geometry of the proposed UWB antenna is shown in fig 3.24 (a) & (b). The dimension of antenna is shown in Table 3.2.

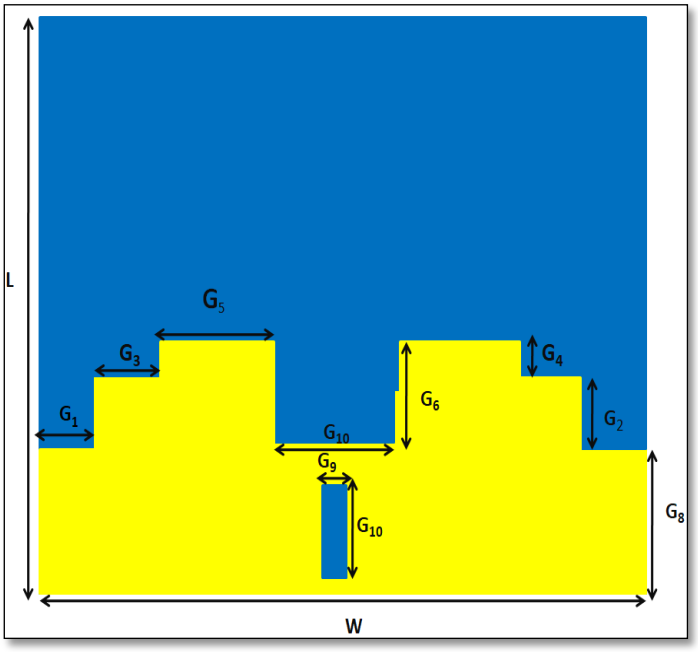

(a)

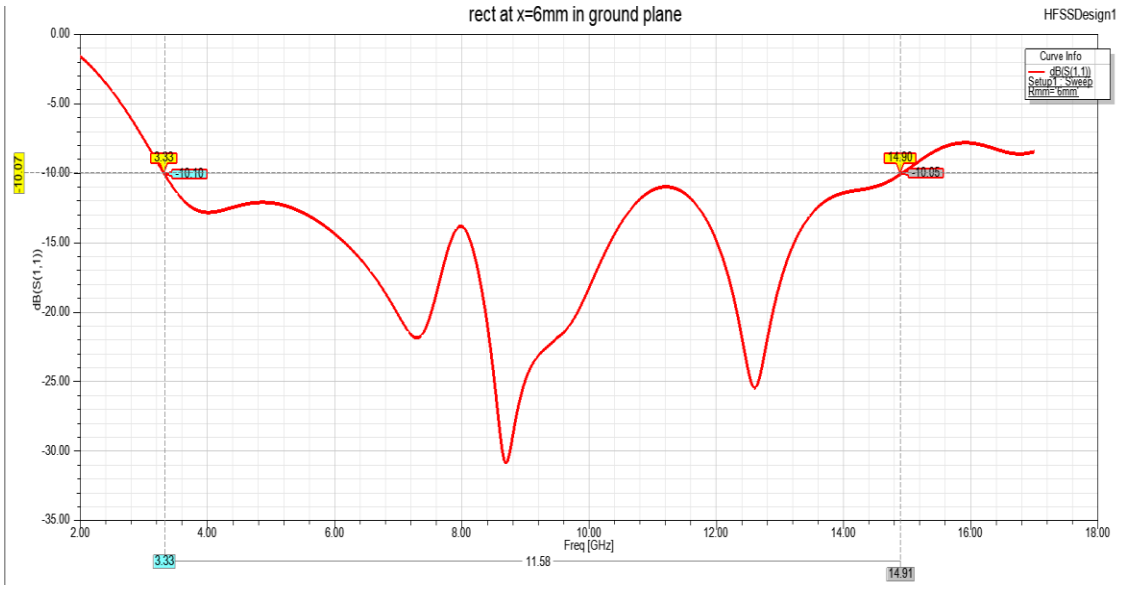

(b)

Fig 3.23: (a) modified ground plane with rectangular slot

(b) S-parameter with modified ground plane

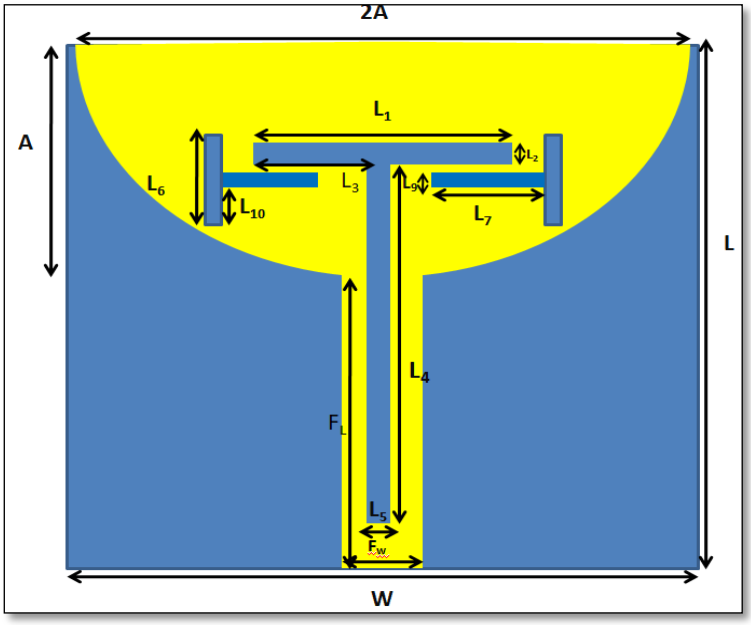

(a) Top View

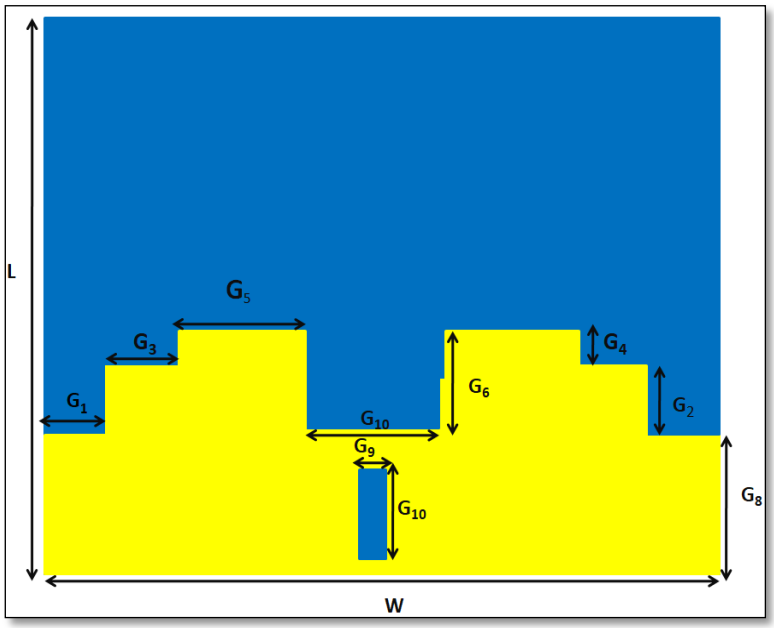

(b) Bottom View

Fig 3.24: Geometry of the Proposed UWB Antenna

Table 3.2: Design Consideration of the Proposed Antenna

Parameters	Length(mm)	Parameters	Length(mm)
L	27	L_8	1
W	27	L_9	2.25
A	13	L_{10}	0.5
M	11.5	G_1	1.5
Q	12	G_2	2.5
F_L	13.08	G_3	2
F_W	3	G_4	1
L_1	10	G_5	8.5
L_2	1	G_6	3.5
L_3	4.5	G_7	3
L_4	16	G_8	8
L_5	1	G_9	1
L_6	5	G_{10}	6
L_7	3	H	1.6

The UWB Antenna resonates from 3.32 to 14.92 GHz covering the entire UWB characteristics as shown by S parameters in Fig 3.25. The peak gain of the Antenna in the entire range is above 2.33 db. The peak gain vs Frequency curve is shown in fig 3.26. The VSWR is also below 5 in the entire range of the operation as shown in Fig. 3.27.

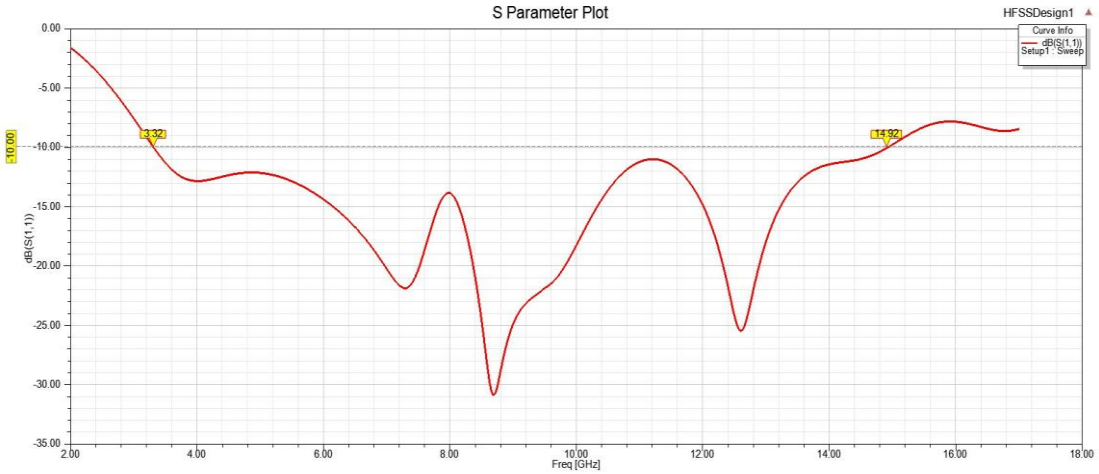

Fig 3.25: Return loss characteristics of Proposed UWB Antenna

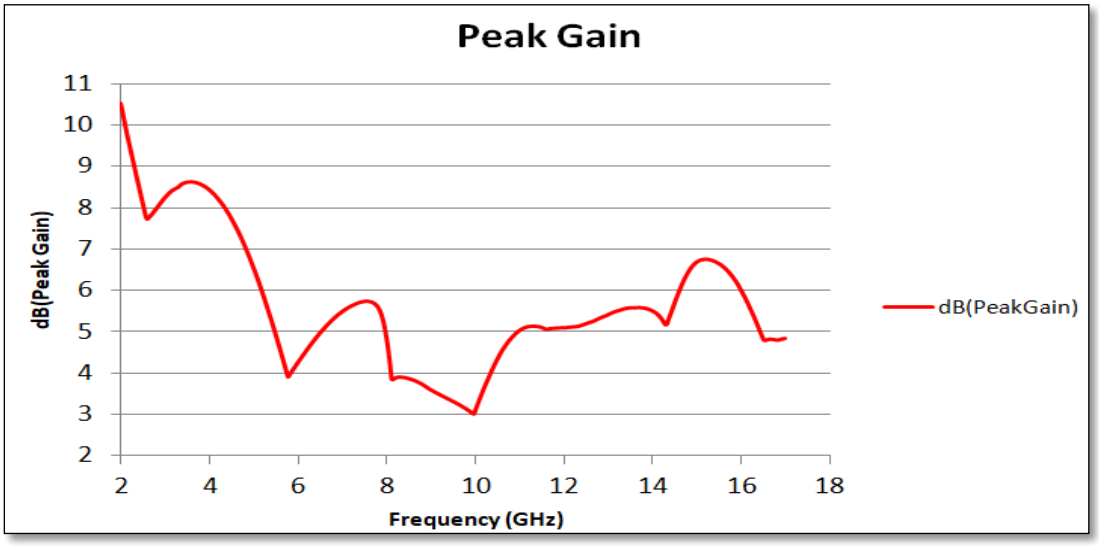

Fig 3.26: Simulated Peak Gain of Proposed UWB Antenna

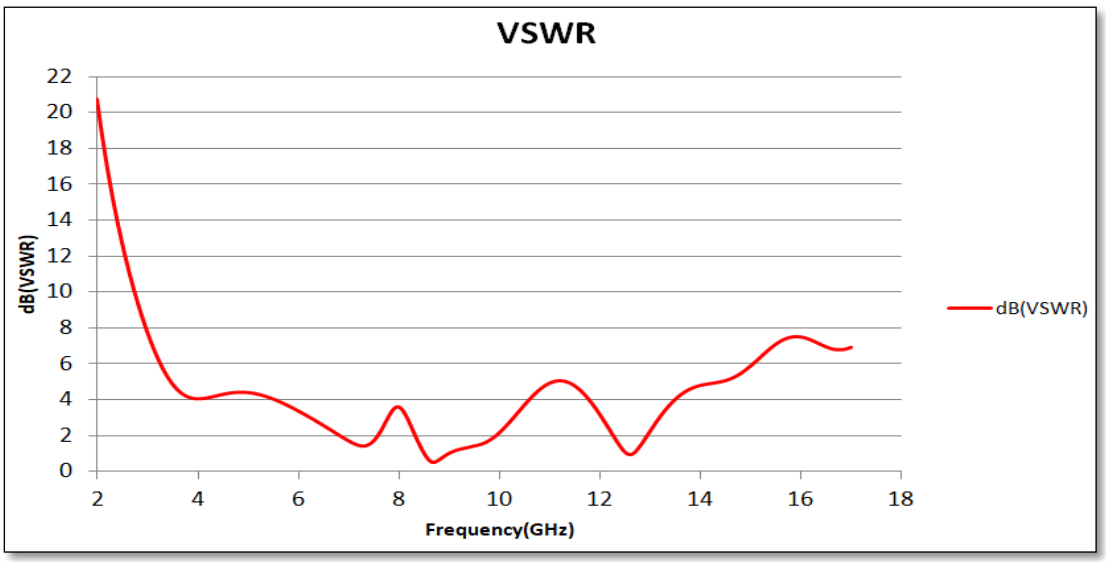

Fig 3.27: Simulated VSWR of Proposed UWB Antenna

3.7 SPECIFIC ABSORPTION RATE

The current basic safety limits applicable to the wireless device are defined in terms of specific absorption rate (SAR), which is defined as the rate at which a person absorbs Electromagnetic energy per unit mass; where SAR averaged over X grams of tissue can be denoted by X-g SAR. The SAR in a biological body exposed to a radio frequency (RF) field depends on a number of factors, including tissue geometry and

dielectric properties and the orientation of the body relative to the source **(Chou *et al.* 1996).**

There exist three different limits defined by: 1. Whole-body average SAR; 2. Local peak SAR; 3. Specific absorption (SA); which limits the power of short pulses. 1 and 2 must be averaged over a defined period of time.

Absorption occurs only in regions of the body that are close to the device while using wireless devices with frequencies above 300 MHz. As a result, the local peak SAR limit is the most essential value. The IEEE/ANSI/FCC recommends an upper safety limit of 2.0 W/kg for localised SAR averaged over 10-g and 1g of tissue, i.e. peak 10-g SAR and peak 1-g SAR not exceeding 2.0 W/kg and 1.6 W/kg, respectively **(Mahmud *et al.* 2013).**

Using measuring techniques or numerical models to evaluate the SAR distributions associated with electronic equipment is a difficult undertaking. Two experimental methods for evaluating compliance with specific SAR standards use anthropomorphic models of the human head or other parts to determine either the electric field (E-field) strength or the rate of temperature increase in a tissue-equivalent liquid.

The SAR, or specific absorption rate, is a measurement of how much RF radiation is absorbed by human tissue. SAR is a function of electrical conductivity (measured in Siemens per meter), induced E-field from radiated energy (measured in volts per meter), and tissue mass density (measured in kilogram per cubic meter). Averaging (or integrating) across a specified volume (usually a 1 gram or 10 gram area) yields the SAR:

$$\mathrm{SAR} = \int_{\mathrm{sample}} \frac{\sigma(\mathbf{r})|\mathbf{E}(\mathbf{r})|^2}{\rho(\mathbf{r})} d\mathbf{r} \tag{3.12}$$

The units of SAR are W/kg or mW/g, respectively. In the United States, the SAR limit for cell phones is 1.6 W/kg, averaged across 1 gram of tissue. SAR limits in Europe are 2.0 W/kg averaged over 10 gram of tissue.

The electric-field probe method and the thermographic method are the two methods now available for SAR measurements, which are used to estimate the SAR in human models exposed to microwave sources **(Wang *et al.* 2016)**

3.7.1 The Electric-field Probe Method

The electric-field probe method, as a rapid and non - invasive SAR measurement solution, is based on utilizing automatic positioning systems to move an E-Field measuring probe in a liquid phantom to assess SAR values. The specific absorption rate (SAR) is usually used as the primary dosimetric parameter of EM wave exposure for standardization, expressed as:

$$SAR=\frac{\sigma|E|^2}{\rho} \qquad [W/kg] \tag{3.13}$$

Where, σ[S/m] is the conductivity of the tissue, ρ [kg/m3] is the density of the tissue, and E [V/m] is the electric field intensity within the tissue.

Measurement System (DSAY-5):

Because of the FCC's adoption of safe exposure limits to radiofrequency (RF) energy, which are specified in terms of SAR. The latest SAR completely automated test system, DSAY-5, is depicted in fig 3.28. It has the ability to perform SAR tests and measurements faster and more accurately than earlier test systems.

Fig 3.28 The schematic of DASY-5 (Wang *et al.*2016)

Measurement Setup:

As illustrated in Figure 3.29, the DASY-5 system includes a PC, data acquisition unit (DAE), E-field probe, robot controller, phantom shell with tissue, equipment under test (EUT), and device holder.

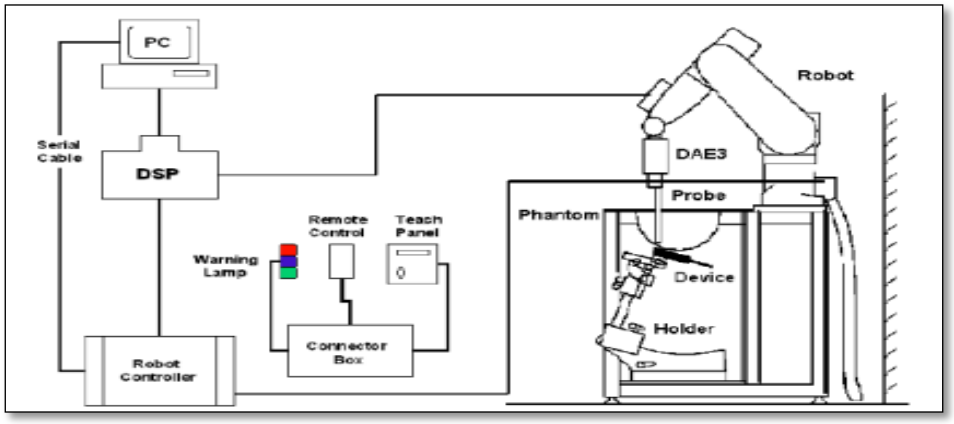

Fig 3.29: The structure of SAR measurement system by using DASY-5 (Wang *et al.*2016)

The SAR measurement setup is shown in Fig 3.30

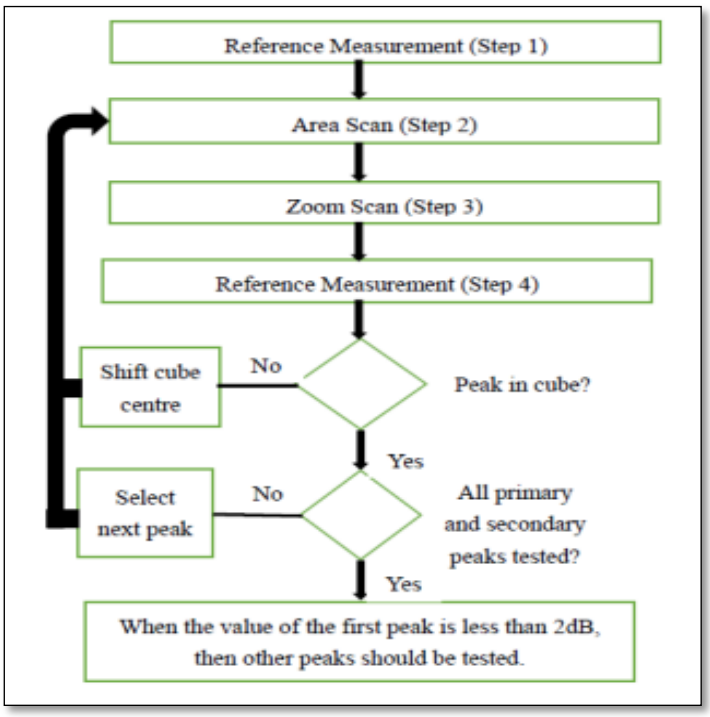

Fig 3.30: The flow chart of SAR measurement setup (Keshvari and Kivento 2013)

The SAR reference measurement is the first. Local SAR must be measured at a stationary reference point where the SAR exceeds the measuring system's lower detection limit prior to the SAR test.

The Area scan comes in second. The goal of the area scan is to find peak SAR spots. To locate the approximate location(s) of SAR peak, an E-field probe passes through tissue-equivalent liquid in a SAM or a flat phantom (s). To find peak positions, the measured values are interpolated.

The Zoom scan comes in third. The zoom scan's purpose is to calculate cube averaged SAR. The peak spatial-average SAR value is then determined by doing zoom scans around one or more of these peak locations. It employs 5×5×7 points in a 3×3×3 cm3 cube when the frequency is less than 3 GHz. When the frequency ranges between 3 and 6 GHz, more than 7×7×7 points should be used, and interpolations to a finer resolution should be made between all measured and extrapolated points.

The SAR drift measurement is the final step. At the same place as in Step 1, the local SAR (or conducted power) is measured. The absolute value of the measurement drift (the difference between the SAR measured in Step 4 and Step 1) is then recorded, and the drift should be kept to less than 5% to ensure appropriate accuracy. After each zoom scan, SAR drift measurements are taken to check accuracy and consistency, with drift constantly being compared to the starting measurement.

3.7.2 The Thermographic Method

The thermographic method of producing SAR over a two-dimensional internal plane within an exposed model is more efficient. This strategy works for fields in both the far and close zones. It entails recording temperature distributions caused by energy absorption in phantom models after exposure to radiating fields with a thermographic camera. The model is dismantled along the plane where SAR is to be calculated, and a thermograph-temperature scan is performed over the plane. The model is then reconstructed and briefly subjected to a high power density signal, before being disassembled and undergoing another thermographic scan.

To determine the SAR distribution in human heads, thermographic investigations **(Balzano *et al.* 1978; Guy and Chou 1986)** are carried out utilising brain and skull-equivalent solid phantom models. The SAR at an arbitrary place is given by if heat diffusion is negligibly tiny during the exposure duration.

$$\mathrm{SAR}=c\frac{\Delta T}{\Delta t} \quad [W/kg] \tag{3.14}$$

where, c [J/kg·K] is the specific heat of the phantom, ΔT [K] is the temperature rise at the point, and Δt [second] is the exposure time.

Measurement System:

A thermographic camera, a phantom, an antenna, a radio anechoic chamber, oscillator, power amplifier, and a computer are the components of the thermographic SAR measuring system, as shown in Fig.3.31.

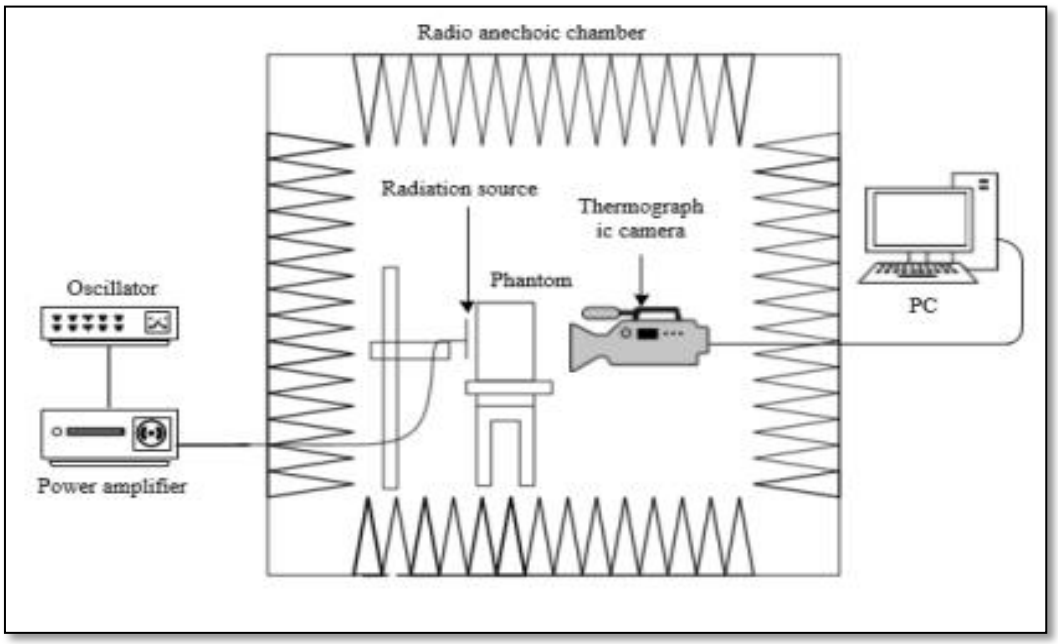

Fig 3.31. SAR measurement system (Wang *et al.* 2016)

Measurement Procedure:

Figure 3.32 depicts the measurement technique. A uniformly heated phantom is initially placed in a radio anechoic chamber and exposed to UHF radio waves from a nearby source for about 2 minutes. The exposure time must result in a temperature

increase of at least 1 K. Before the exposure, the phantom is split open to examine the inside. The phantom is instantly reopened in front of a thermographic camera after the exposure interval. To trace the temperature rise profile on a segment or surface of the phantom, a thermographic image is taken right away. SAR measurements in the vicinity of the phantom boundary are difficult to achieve with the E-field probe method, but they are doable with the thermographic method outlined. The thermographic method's use of a solid phantom has the advantage of being able to quantify SAR in materials with complex geometries. The thermographic method has a number of drawbacks, including the impossibility to test genuine mobile phones due to the high power required for the experiment; SAR images are confined to two-dimensional cuts **(Okano *et al.* 2000).** As a result, the thermographic approach is ineffective for evaluating genuine RF devices.

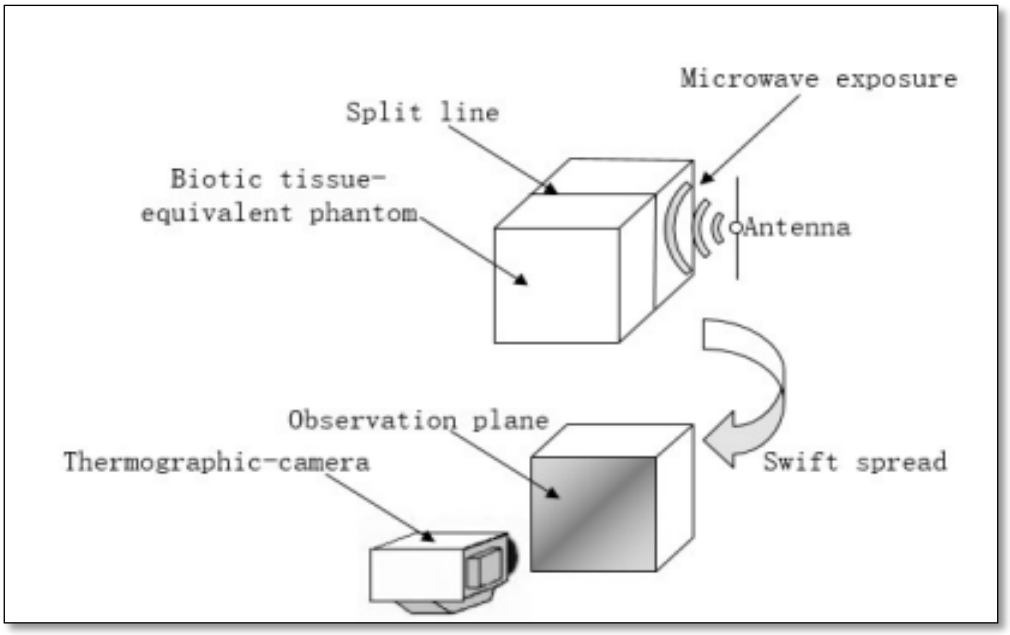

Fig. 3.32 SAR measurement procedure (Kobayashi *et al.*1993)

3.8 CURRENT DENSITY

In electromagnetism, current density is the amount of charge per unit time that flows through a unit area of a chosen cross section. The current density vector is defined as a vector whose magnitude is the electric current per cross-sectional area at a given point in space, its direction being that of the motion of the positive charges at

this point. In SI base units, the electric current density is measured in amperes per square meter.

A common approximation to the current density assumes the current simply is proportional to the electric field, as expressed by:

$$j = \sigma E \tag{3.14}$$

where **E** is the electric field and σ is the electrical conductivity.

Conductivity σ is the reciprocal (inverse) of electrical resistivity and has the SI units of siemens per metre ($S \cdot m^{-1}$), and **E** has the SI units of newton per coulomb ($N \cdot C^{-1}$) or, equivalently, volts per metre ($V \cdot m^{-1}$).

Importance of current density

- The design of electrical and electronic systems is influenced by current density.
- The specified current level has a big impact on circuit performance, and the current density is governed by the dimensions of the conducting parts. For example, despite the lower current demands of smaller devices, there is a tendency toward increasing current densities to achieve higher device counts on ever smaller chip areas as integrated circuits shrink in size. Moore's law is one example of this.
- The conducting zone of a wire gets concentrated near its surface at high frequencies, increasing the current density in this region. This is referred to as the skin effect.
- Current densities that are too high have unfavourable implications. Because most electrical conductors have a limited, positive resistance, power is dissipated as heat. To avoid the conductor from melting or burning, the insulating material from failing, or the desirable electrical qualities from altering, the current density must be kept low. The material making the linkages actually moves at high current densities, a phenomenon known as electro-migration. Excessive current density in superconductors can provide a

strong enough magnetic field to cause the superconductive property to be lost spontaneously.

- Current density analysis and observation are also used to investigate the physics underlying the nature of solids, such as metals, semiconductors, and insulators. Many fundamental findings have been explained using a complex theoretical framework.
- In Ampere's circuital law (one of Maxwell's equations), which ties current density to magnetic field, current density is an important quantity.
- Charge and current are merged into a 4-vector in special relativity theory.

3.9 BREAST PHANTOM MODEL AND TUMOR MODEL

Several models of the breasts have been used by researchers (**Wang *et al.* 2008)** .We used a model of semi-circular shaped with the most common sizes, as presented in Fig.3.33.

The dielectric properties that were used are shown in Table 3.3, where σ is the conductivity of tissue and or is the dielectric permittivity. We used a spherical tumor with a radius of 0.2cm, **(Shrestha *et al.* 2010)** to compare our results with other more common work in the literature.

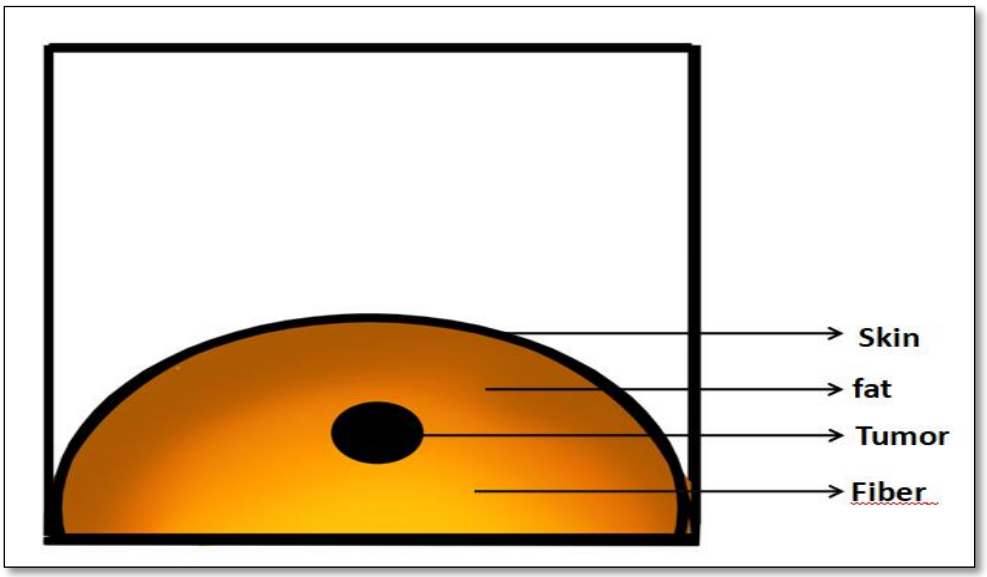

Fig 3.33: Breast Phantom Model

Table 3.3: Dielectric Properties of the Model

	Permittivity	Conductivity	Loss tangent
Skin	30	1.4	0.93
Fiber	16	0.4	0.94
Fat	3.4	0.6	0.16
Tumor	50	4	1.5

The model was developed in the form of semi-circle composed of outer-most layer with radius 30mm named as skin. The second layer after skin is fat layer with dimension breast radius – 5mm. The innermost layer is fiber layer having dimension breast radius -1mm. As shown in Fig 3.34, the designed breast model was simulated by placing the antenna at a distance.

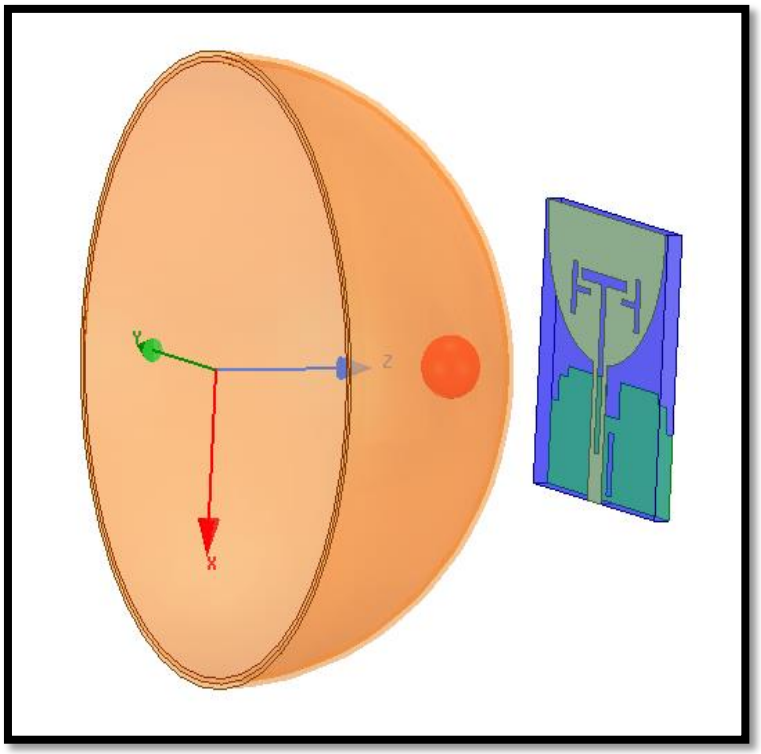

Fig 3.34: Antenna Placed at a Distance from the Breast Phantom

3.9 Fabrication methodology

The complete designing and simulation of proposed antenna is carried out in in HFSS software. After completion of the designing and simulation of the antenna, next step is to fabricate the antenna. The simulated results of the antenna are kept for further calculation and evaluation with respect to the measured results. The Fabrication of simulated antenna is carried out in Printed Circuited Board (PCB) prototype machine EP 2002 which is operated through the PCB prototype software. The PCB machine is a computerized machine that is software controlled in which different drill bits are used at different interval of time for completion of the fabrication process. The first step is to generate the drawing exchange format (*.dxf*) file from the HFSS software. The PCB designing machine require Gerber file format. To convert the *.dxf* file into Gerber file PCB prototype software is used. After conversion of *.dxf* file to Gerber file the complete steps of fabrication process are followed sequentially. The fabrication process consist selection of the counter line. Surface inspect, fixed point drilling, engraving and routing. Every step is carried out with different bits. These bits are changed manually. The substrate level is inspected with the yellow (0.2 mm) drill bit and the process is called surface inspect. The fixed-point drilling is done with the black (1.25mm) drill bit. The sheet is rotated upside down through the fixed positions. Fixed positions are drilled to find proper location while turning the substrate sheet around. Engraving is the procedure of designing of the patch and ground on either side of the copper coated FR4 substrate sheet. The engraving is done with yellow (0.2mm), blue (0.5mm) and red (1.5mm) drill bits. After completion of the designing of patch and ground, the routing path is given to the outer boundary of engraved design. The PCB machine then routes the antenna from the substrate sheet with white (3mm) drill bit. Routing is principally a procedure of cutting the antenna from the substrate sheet. After the completion of fabrication process the SMA connector is soldered to the feed position from where the power is delivered to the antenna. The connection of the connector should be done very sensibly as it should not disturb the impedance matching of feed.

The measurement of the antenna is done through the Vector Network Analyzer. The antenna parameters like reflection coefficient S_{11} (dB) and VSWR are measured with the help of VNA. While operating VNA, first step to calibrate the machine for desired range of frequency of the proposed antenna. Then VNA is calibrated in order to nullify the cable loss and other environmental losses through the calibration kit. The calibration kit manually calibrates the device via open, short load and load condition to remove the undesired losses. After that the fabricated antenna is tested via cable to measure the parameters i.e. reflection coefficient S_{11} (dB) and VSWR. The flow chart of simulation, fabrication and measurement is shown in Fig. 3.35.

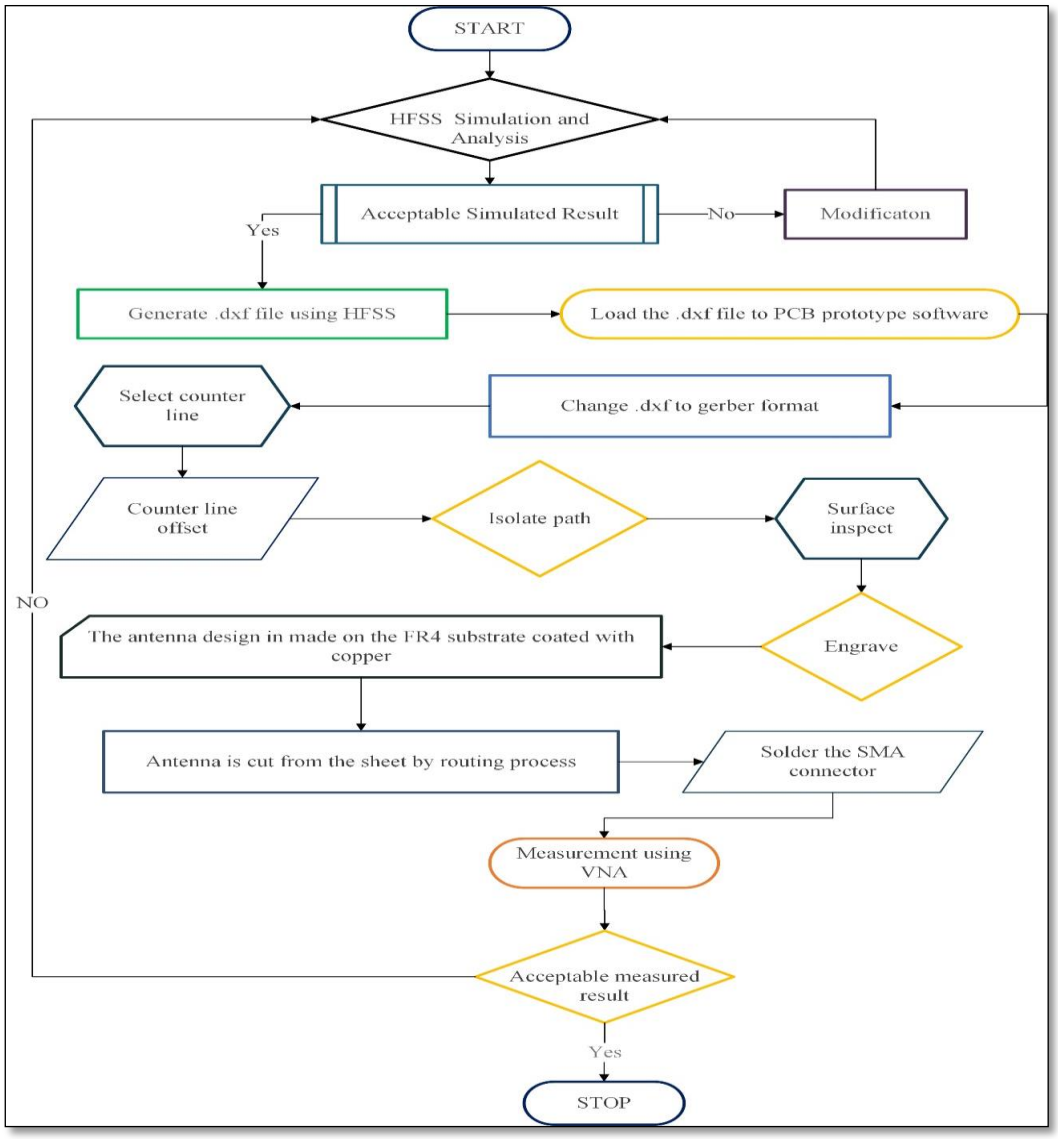

Fig 3.35: Designing and Fabrication Methodology with the help of flow chart

3.9.1 Fabrication of the proposed antenna

The fabrication of the proposed antennas is done by generation of the *.dxf* file from HFSS software. The *.dxf* file of the antenna is imported to PCB prototype software. Fabrication of the antenna is carried out with the help of PCB prototype machine (EP 2002). The fabricated prototype of the proposed UWB antenna is shown in the fig 3.36.

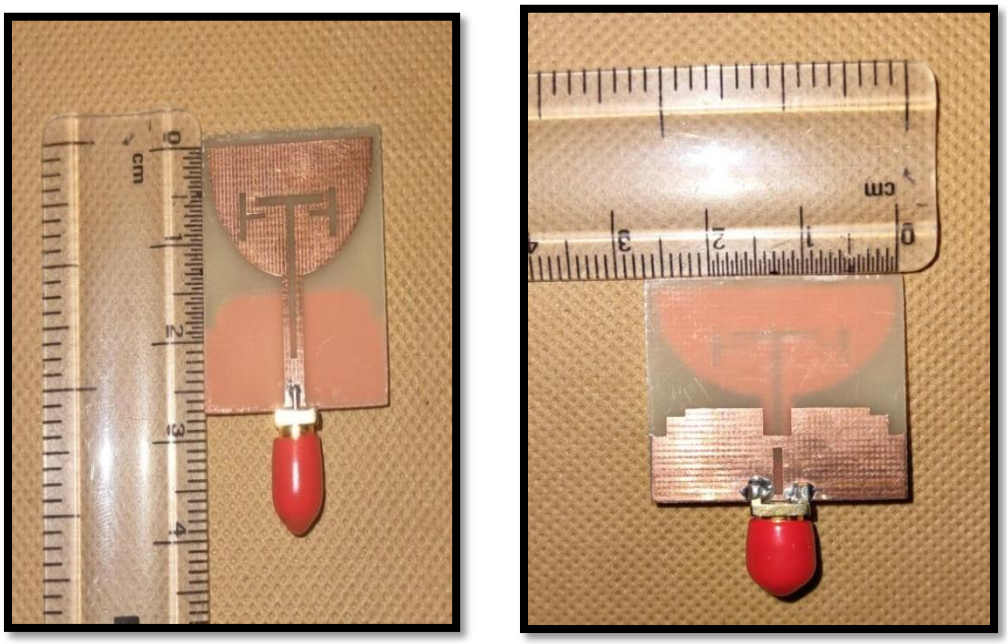

(a)Top view **(b) Bottom view**

Fig. 3.36: Fabricated antenna

3.9.2 Testing of Antenna

After the fabrication process the antenna parameters are measured. The parameters must match the results obtained by simulation of the proposed antenna. The return loss and VSWR is measured with the help of VNA. It works in the frequency range from 1MHz to 20 GHz, the measurement in VNA includes loss which influences the simulated result, so the calibration process is done manually using cable to avoid losses.

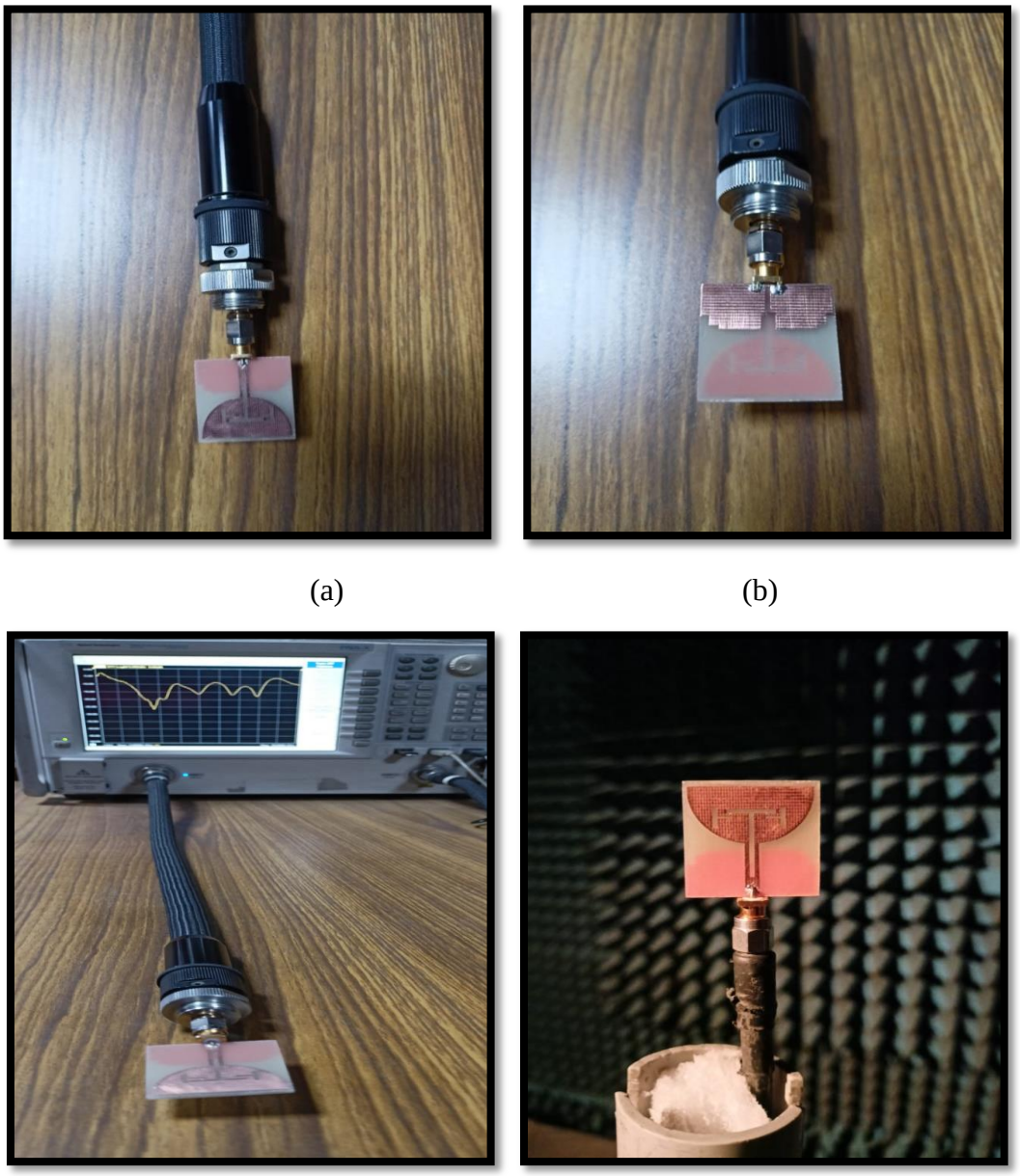

(a) (b)

(c) (d)

Fig 3.37 Testing of Fabricated Antenna

Fig 3.37 shows the testing setup of the proposed Antenna. The measurement procedure is kept same as stated for both the antennas. The discussion upon the measured results is stated in the following chapter.

Results and Discussion

Chapter 4 RESULTS AND DISCUSSION

Previous chapter is dedicated for the development of a proposed UWB Antenna, breast phantom and tumor. The designing of the antenna which has been proposed contains calculation of the patch dimension using TLM and simulation using HFSS software. After the fabrication and simulation of the proposed antenna, the next step is to measure its different performance parameters i.e. reflection coefficient S_{11} (dB), VSWR, Gain and Radiation Pattern. In this chapter the measured and simulated results are compared. The comparison is presented as well, along with the results from previous literature.

4.1 Measured results for the Proposed Antennas

The fabrication of this antenna has been done using PCB prototype machine EP 2002. The fabrication of the proposed UWB antenna is presented in the fig 4.1(a). The parameters of proposed antennas i.e. coefficient of reflection (S_{11}) and VSWR are measured with the assistance of VNA (Anritsu MS46322A). The calculated coefficient of reflection and VSWR of the proposed UWB antenna is presented in Fig.4.1(b) and 4.1(c) respectively. The antenna resonates from 3.06 GHz to 15.21 GHz and VSWR is not more than 2, within the entire range of the operation satisfying the condition of UWB.

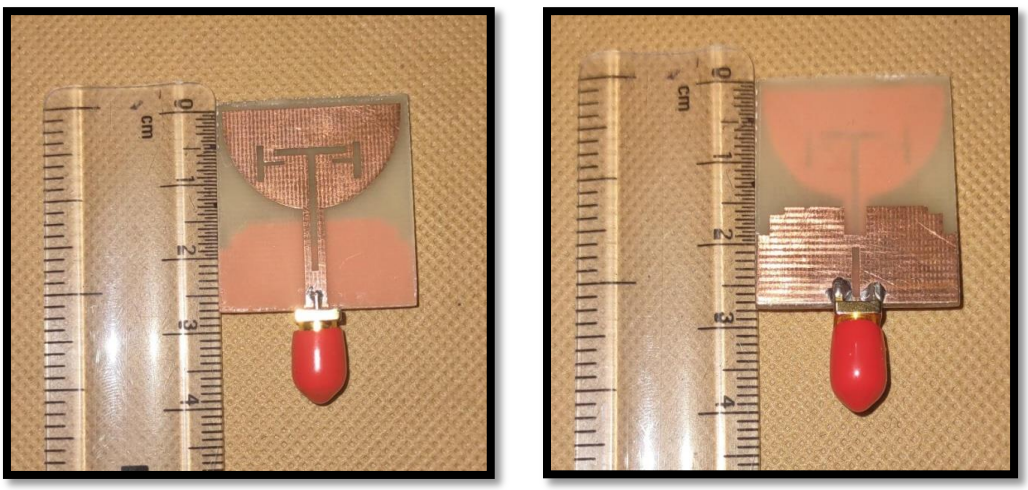

Fig 4.1(a): Fabricated UWB Antenna (Patch on the right and Ground on the left)

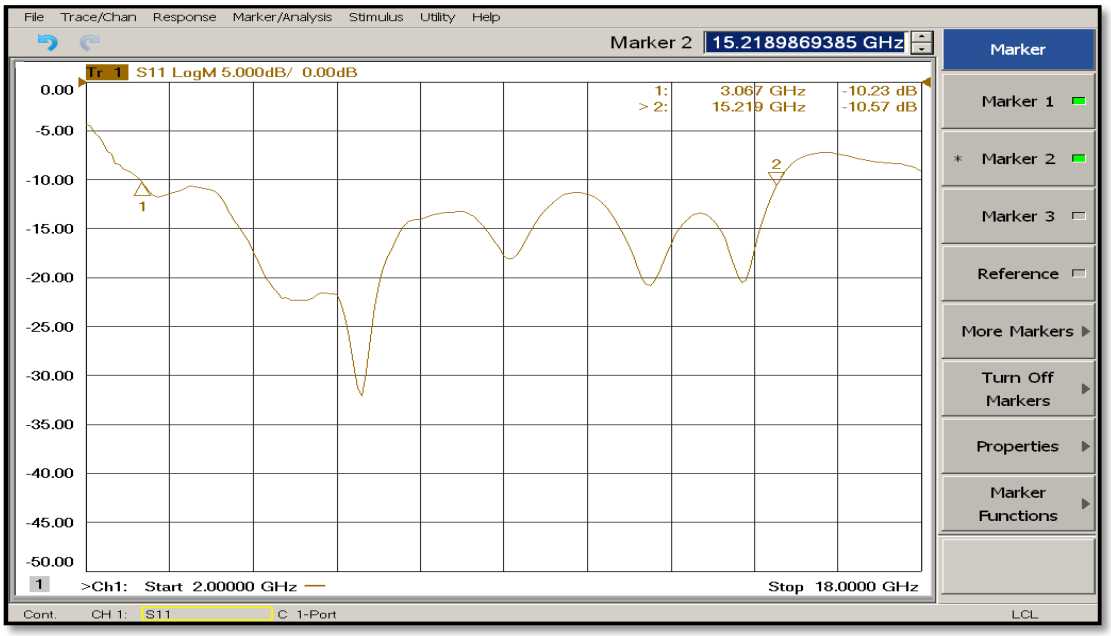

Freq (GHz)

Fig. 4.1(b): Measured reflection coefficient (S_{11}) of UWB Antenna

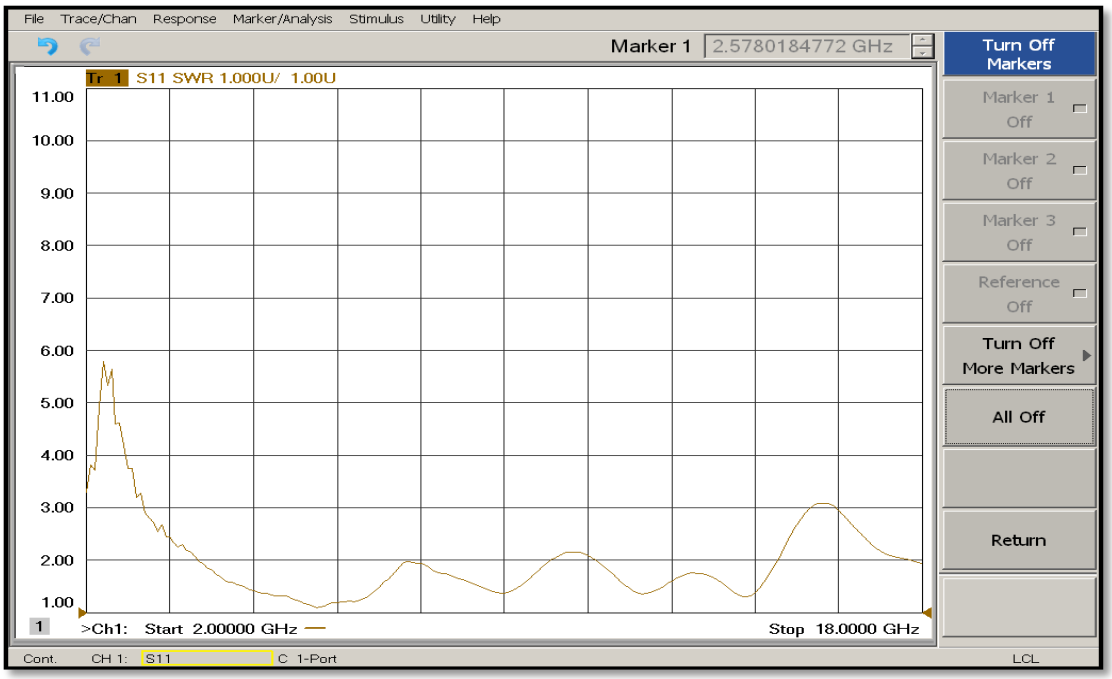

Freq (GHz)

Fig. 4.1(c): Measured VSWR of UWB Antenna

4.2. Comparison of the Measured and Simulated results of the Proposed Antennas

Measured results have been compared with simulated results in terms of different parameters like VSWR, and S parameters. The measured and simulated results are in good agreement but show some discrepancy because of the imperfections within the fabrication process.

i. *S parameters:* - The measured and simulated results for coefficient of reflection (S_{11}) for the proposed antennas are compared in Fig. 4.2. By analyzing the results, it is observed that the measured and the simulated results are in good agreement.

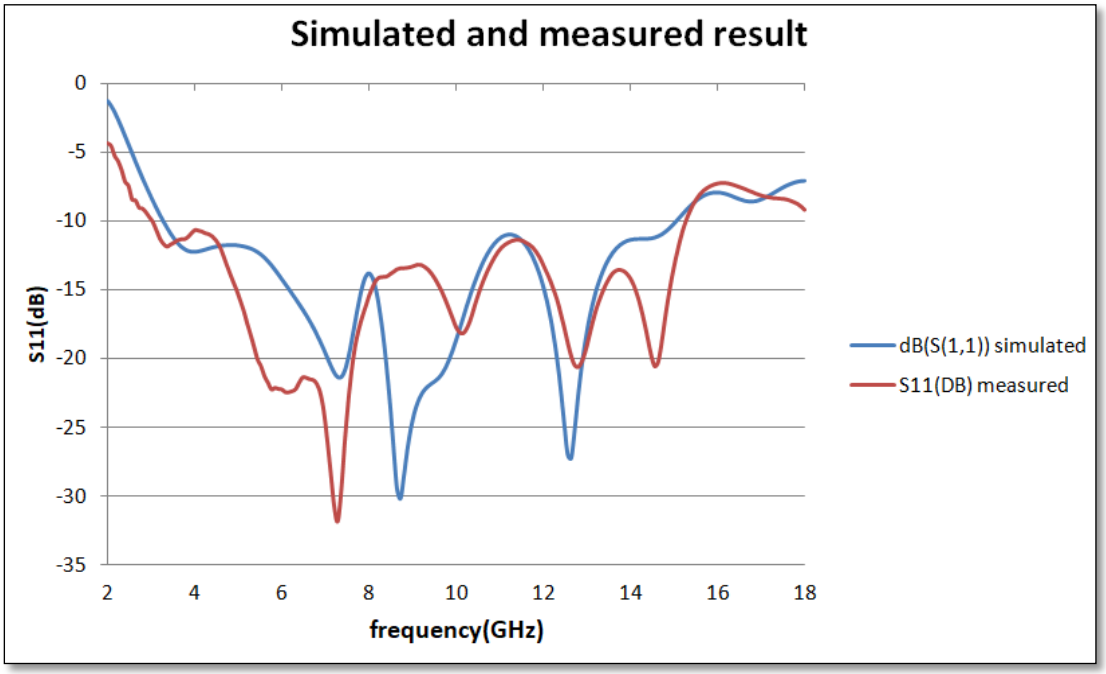

Fig. 4.2: Simulated and Measured S_{11} of Proposed Antenna

ii. *VSWR* :- The measured VSWR has also been compared with simulated VSWR for the UWB antenna, proposed antenna & variant of proposed Antenna II . Ideal value of VSWR at the operating range of frequency is unity hence for practical purpose the values ranging from 1 to 2 are acceptable for which return loss is not more than -10 dB. The compared results of the measured VSWR with simulated VSWR is presented in Fig. 4.3 for the antenna.

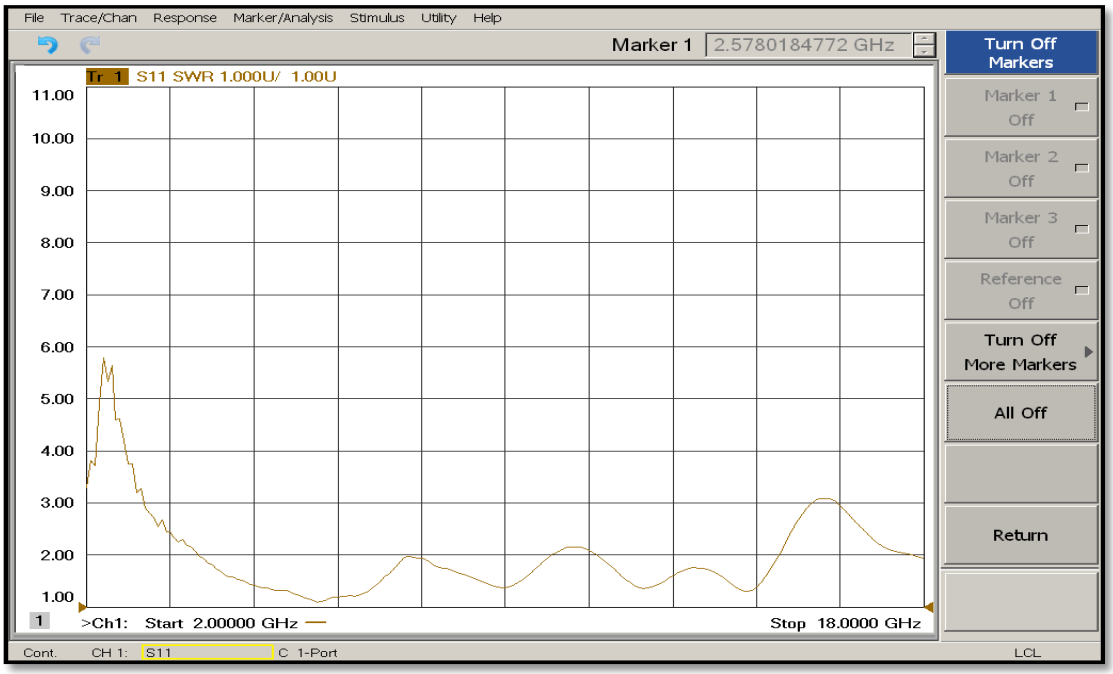

(a)

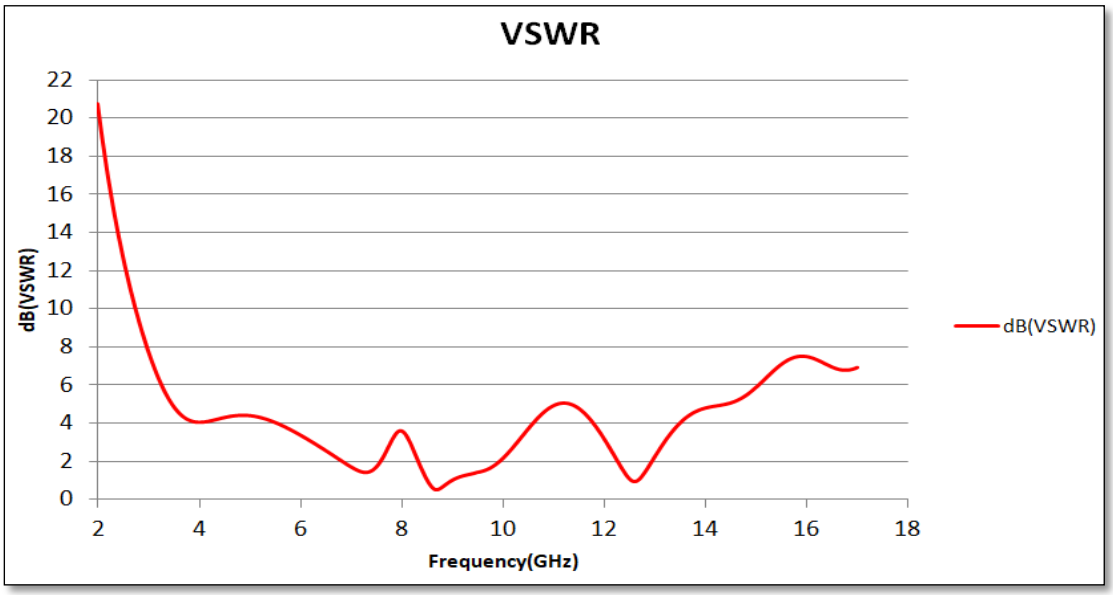

(b)

Fig. 4.3: Measured and Simulated VSWR of variant of Proposed Antenna

iii. *Peak Gain* :- The variation of simulated peak gain is presented in fig 4.4 for the proposed antennas.

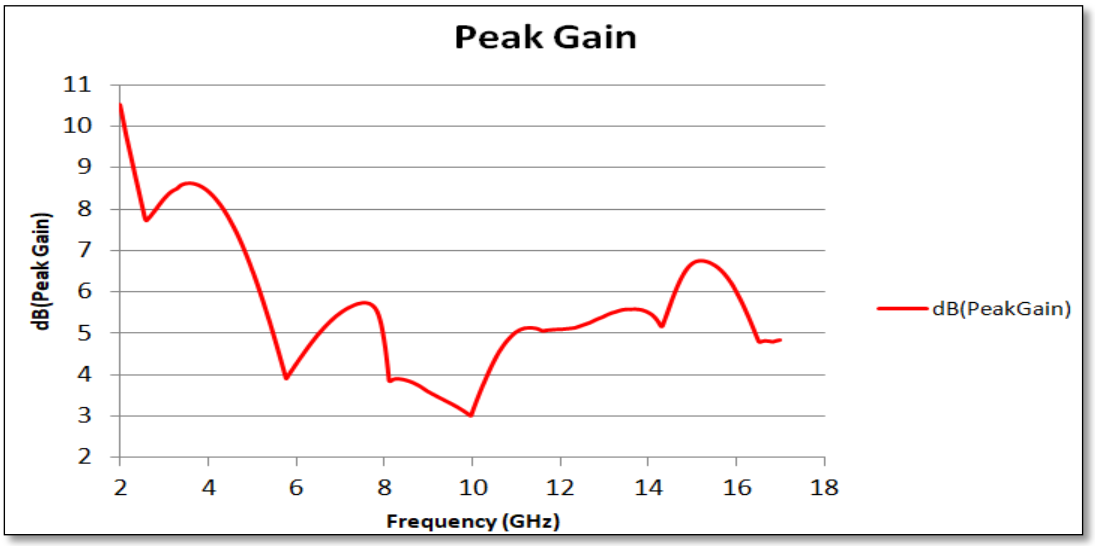

Fig. 4.4: Simulated Peak gains of the proposed Antennas

4.3 Simulated results for tumor detection

For detection of the tumor in the breast phantom the proposed antenna is placed in front of the phantom. The distance minimum between the phantom and antenna is taken as 3mm. Fig 4.5 shows the simulation setup of the stated antenna surrounding the breast phantom. The s-parameter for the phantom without tumor is shown in fig 4.6.

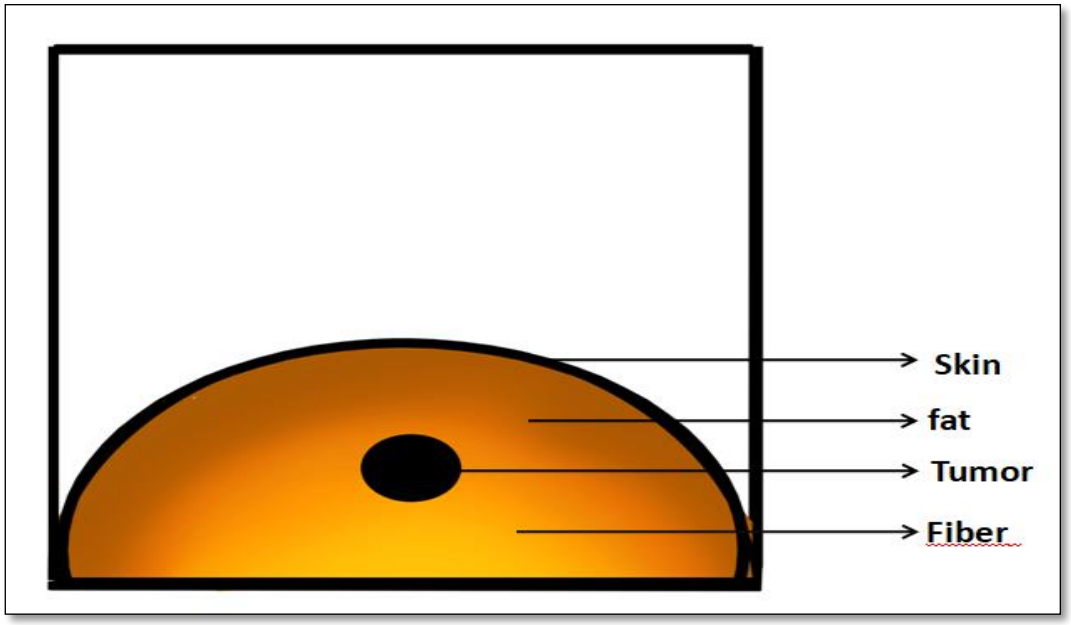

Fig 4.5: Breast Model for Simulation

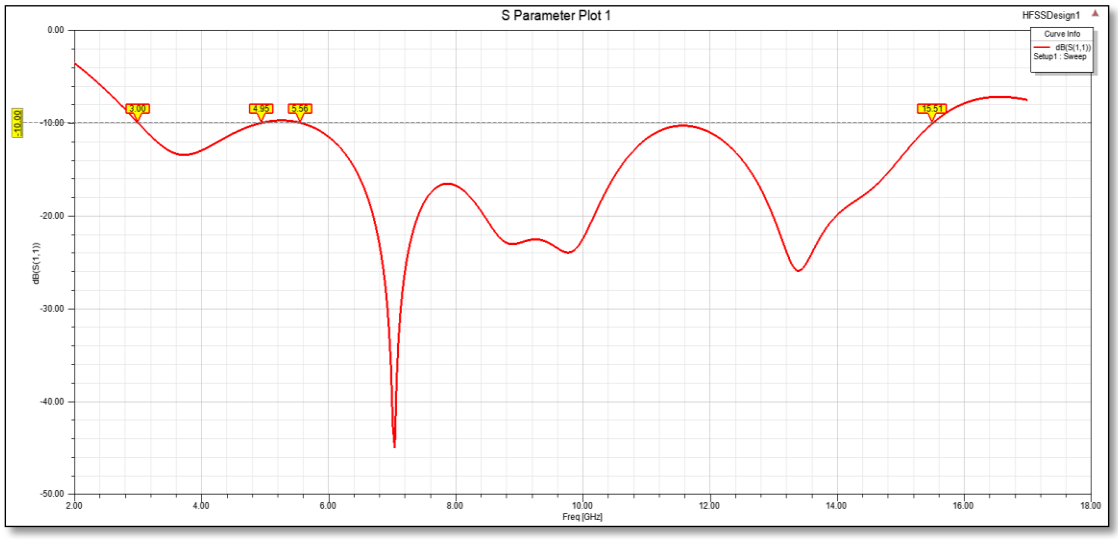

Fig 4.6: Simulated S-Parameter for the Phantom Structure Without-Tumor

For detection of tumor the analysis are made in two ways- first, fixed the tumor value i.e. size and location while varying the position of the antenna. Secondly, by fixing the antenna position and radius of the tumor while varying the position of the tumor in the breast phantom.

The s- parameter for the variable antenna distance from 32mm to 50mm for tumor radius T_r =2mm and position at (0,0,3) is shown in fig 4.7.

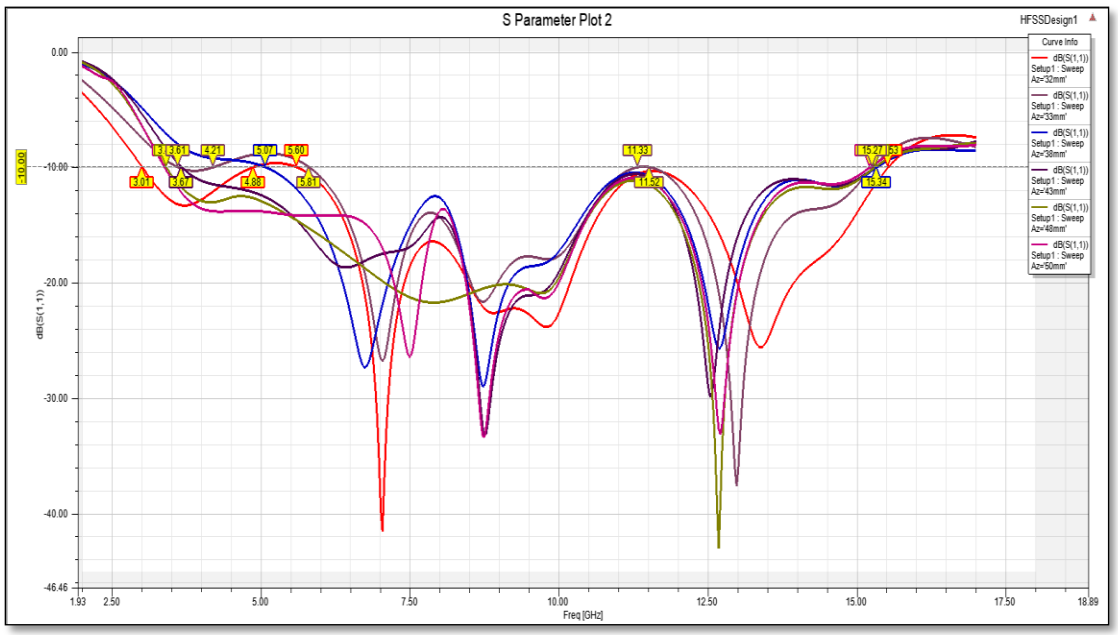

Fig 4.7 (a): S-Parameter for Variable Antenna Distance for T_r=2mm

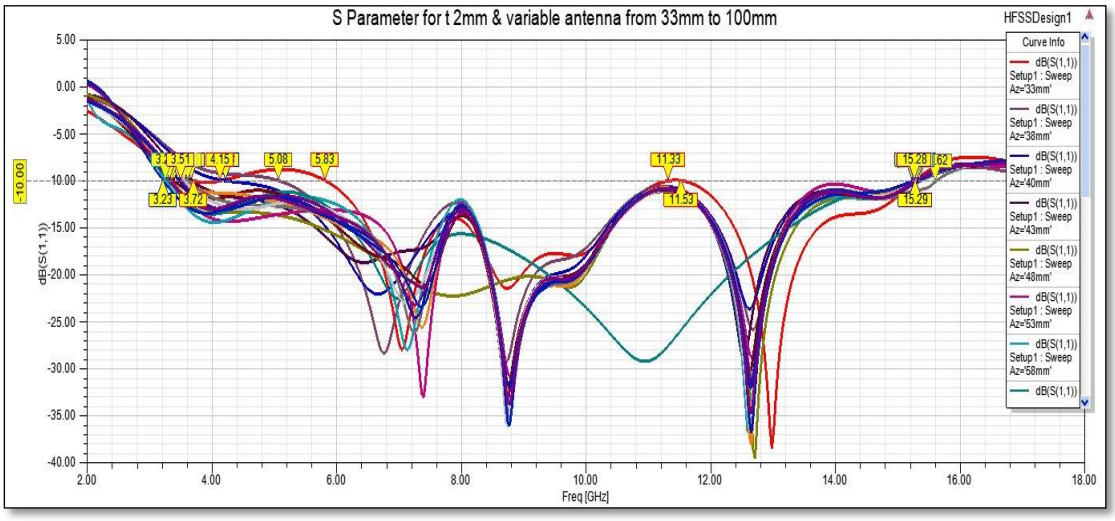

Fig. 4.7 (b): S-parameter for T_r= 2mm and variation of antenna from 33mm to 100mm.

The variation of tumor with radius 2mm and fixed antenna distance at 40mm is shown in fig 4.8.

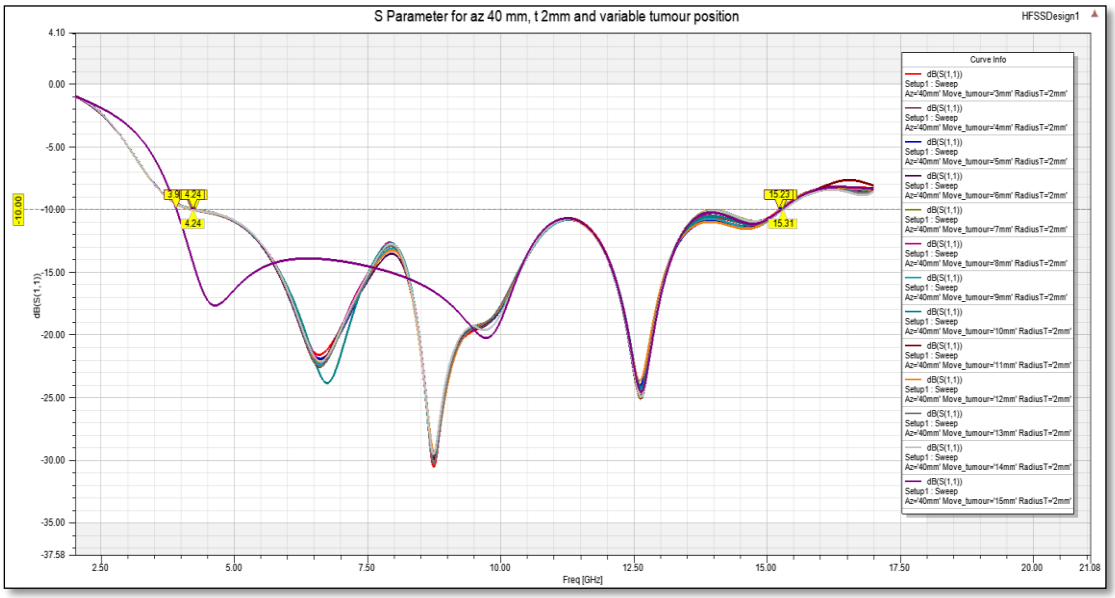

Fig 4.8: S- Parameter for Variable Tumor Position at T_r=2mm and Antenna Position at 40mm.

To define the value of the tumor the SAR analysis, current density and electric field intensity are analyzed for fixed tumor value and variable antenna as well as variable tumor position and fixed antenna location. The estimated values are organized in the form of tables below.

Table 4.1: For tumor radius 2mm and tumor location (0, 0, 3)

Antenna position from origin (mm)	SAR (W/kg)	Current density (A/m^2)	H-Field (A/m)	E – Field (V/m)
40	11.4	2141	0.8	27.49
45	8.14	2075	1.06	26.00
47	7.90	3251	1.195	41.749
50	7.02	2259	1.441	29.006
70	3.627	1604	0.75	20.60
80	2.921	1570	0.77	23.23
90	2.03	1250	0.43	19.14
100	1.76	662	0.32	8.51

Table 4.2: For tumor radius 2mm and tumor location (0,0,5)

Antenna position from origin (mm)	SAR (W/kg)	Current density (A/m^2)	H-Field (A/m)	E – Field (V/m)
33	58.8	1541	0.6606	19.79
40	10.84	2104	0.8702	27.014
50	7.89	2501	0.8678	32.1149
60	6.10	1159	0.5648	14.8779
70	3.54	1243	0.6497	15.9600
80	2.86	804	0.3111	10.3332
90	1.99	943	0.4750	12.1185
100	1.73	746	0.1924	9.5908

Table 4.3: For tumor radius 3mm and tumor location (0, 0, 15)

Antenna position from origin (mm)	SAR (W/kg)	Current density (A/m^2)	H-Field (A/m)	E – Field (V/m)
33	1.6122	377.7392	0.1178	4.8499
40	0.466	188.69	0.1323	2.4224
45	0.3548	198.2711	0.1276	2.5457
50	0.3354	264.97	0.1422	3.4022
80	0.1240	161.020	0.0424	2.06
100	0.0756	131.47	0.0445	1.6881

Table 4.4: For tumor radius 3mm and antenna distance is 45 mm from origin and t_z is 3mm

Tumor location (x,y,z) mm	SAR (W/kg)	E – Field (V/m)	H-Field (A/m)	Current density (A/m^2)
(0,0,3)	2.99	13.84	0.36	604.37
(0,2,3)	3.81	9.86	0.33	430.29
(0,4,3)	3.87	13.06	0.30	570.14
(2,0,3)	3.504	7.93	0.24	346.76
(4,0,3)	3.507	12.14	0.214	529.76
(0,-2,3)	3.98	9.98	0.323	435
(0,-4,3)	4.057	15.43	0.366	673.57

Table 4.5: For tumor radius 3mm and antenna distance is 45 mm from origin and t_z is 5mm

Tumor location (x,y,z)mm	SAR (W/kg)	E – Field (V/m)	H-Field (A/m)	Current density (A/m^2)
(0,0,5)	3.462	10.86	0.308	473
(0,3,5)	3.89	10.47	0.288	457.20
(0,6,5)	4.26	14.73	0.330	643.21
(0,8,5)	4.313	21.77	0.501	950.13
(3,0,5)	3.813	7.121	0.189	310.77
(6,0,5)	3.797	10.01	0.234	436.85
(8,0,5)	3.819	16.39	0.302	715.47
(-3,0,5)	2.92	16.37	0.458	714.70
(0,-6,5)	4.45	17.50	0.376	763.47

Table 4.6: For tumor radius 3mm and antenna distance is 45 mm from origin and t_z is 10mm

Tumor location (x,y,z)mm	SAR (W/kg)	E – Field (V/m)	H-Field (A/m)	Current density (A/m^2)
(0,0,10)	0.51	2.24	0.043	97.85
(0,3,10)	0.842	2.83	0.053	123.50
(0,6,10)	1.60	2.74	0.080	119.92
(0,10,10)	2.53	7.48	0.114	326.66
(0,14,10)	4.36	10.63	0.256	463.87
(0,-10,10)	2.66	6.701	0.119	292.43
(0,-14,10)	4.46	11.94	0.270	521.27
(3,0,10)	0.76	1.88	0.051	82.24
(10,0,10)	1.74	3.48	0.081	152.08
(-14,0,10)	2.88	10.03	0.254	437.98

Table 4.7: For tumor radius 3mm and antenna distance is 45 mm from origin and t_z is 15mm

Tumor location (x,y,z)mm	SAR (W/kg)	E – Field (V/m)	H-Field (A/m)	Current density (A/m^2)
(0,0,15)	0.024	0.440	0.0143	19.216
(0,6,15)	0.097	0.760	0.020	33.185
(0,10,15)	0.268	1.122	0.033	48.992
(0,14,15)	0.656	2.817	0.046	122.632
(0,17,15)	2.611	3.498	0.109	152.64
(6,0,15)	0.072	0.612	0.0147	26.70
(10,0,15)	0.162	0.816	0.0236	35.63
(14,0,15)	0.393	1.637	0.0315	71.45
(17,0,15)	1.633	3.502	0.201	152.82
(-17,0,15)	2.124	8.719	0.0979	380.52
(-10,0,15)	0.302	2.320	0.056	101.242
(0,-17,15)	2.606	3.594	0.110	156.87

Table 4.8: For tumor radius 3mm and antenna distance is 45 mm from origin and t_z is 25mm

Tumor location (x,y,z)mm	SAR (W/kg)	E – Field (V/m)	H-Field (A/m)	Current density (A/m^2)
(0,0,25)	0.025	1.573	0.0568	68.665
(5,0,25)	0.023	1.760	0.0357	76.826
(10,0,25)	0.037	1.685	0.0467	73.530
(15,0,25)	0.195	1.189	0.0393	51.901
(20,0,25)	0.233	1.539	0.0466	67.169
(25,0,25)	0.330	6.920	0.1458	302.014
(0,5,25)	0.025	1.382	0.0472	60.349
(0,10,25)	0.063	1.150	0.0345	50.211
(0,15,25)	0.379	1.261	0.0426	55.032
(0,20,25)	0.495	2.453	0.0627	107.072
(0,25,25)	0.603	5.417	0.1366	236.414

The above tabular data signifies that the value of SAR, current density and electric-field distribution is maximum when the distance between the tumor and antenna is minimum while it became minimum as soon as the distance between the antenna and tumor became maximum. Secondly, these values become maximum for tumor of greater radius while it is minimum for the tumor having small radius.

The dimensions of the projected antenna have been diminished in terms of substrate area when compared to reference antenna. The performance of the projected antenna is improved in terms of peak gain, size. The complete size of the projected antenna has been obtained as 27×27×1.6 mm^3. It was observed that the measured and simulated results are in good agreement with each other. It is to be concluded that the semi-circular patch monopole antenna with three T-shaped slot along with DGS ground having two pair of rectangular slots works well in UWB applications. It is also concluded that by measuring the current density, SAR and electric field distribution along tumor, the value of tumor and its value is defined.

The summary and conclusion of this work along with the future scope is described in the next chapter.

Table 4.9: Comparison of the Proposed Antenna

References	**Size (mm^2)**	**Bandwidth (GHz) for s_{11}<-10dB**	**Reflection coefficient (dB)**	**Average gain (dBi)**	**Average efficiency (%)**
Mahmud *et al.* (2018)	76×78	5	-20	11	80
Aziz *et al*. (2019)	42×48	0.9	-8.5	6.7	NR
Karli *et al.* (2016)	25×16	0.9	NR	3.5	NR
Aldhaeebi *et al.* (2019)	125×51	0.002	-12	NR	NR
Alibakhshikenari *et al.*	22×22	10	-20	11	74
Rokunuzzaman *et al.* (2019)	25×25	0.26	-20	6.6	NR
Proposed antenna	27×27	11.6	-30.8	8	79

Summary and Conclusions

Chapter 5 SUMMARY AND CONCLUSION

This chapter highlights the work done in developing and fabricating the proposed UWB antenna, which will be employed in biomedical applications to identify breast tumor tissues. Microstrip antennas can be thought of as a type of Printed Monopole Antenna in which the ground plane is at infinity. When a patch is placed directly above and beyond the dielectric substrate, it is predicted to encounter an exceptionally dense air dielectric substrate (r = 1), resulting in the development of a micro strip antenna on a dense substrate with r closer to unity, creating significant bandwidth. The main emphasis of using monopole configuration and DGS in this work is to achieve a large bandwidth with acceptable gain i.e. Ultra-wide band (3.1-10.6 GHz) antenna. The main concern regarding UWB antennas lies in their sensitive towards electromagnetic interferences along with the present wireless narrowband communication systems, thus it is essential to design antennae having characteristics of multiband filtering to evade interferences.

In the first chapter, a brief introduction about the microstrip antenna, printed monopole antenna is discussed. Introduction of different printed monopole structures and their role in enhancing the bandwidth is also described.

The objectives which are decided to achieve are also mentioned and the process which is followed to accomplish the wanted aims is also specified in this chapter. A detailed assessment of previous literature is discussed in second chapter. The research work done by previous scientist and researchers on the same work and technology is cited. The third chapter is dedicated to the materials and methods helpful in the designing the proposed antenna.

Details about microstrip antenna basics, method of analysis and the software used for simulation i.e. HFSS are described. Method of fabrication and techniques used for measurement of the planned antenna are also mentioned. In the final section of this chapter, different steps which are followed during process of designing of the projected antenna, have been described in detail. Dimensions and the effects of

each design step on the simulation results have also been also depicted. The optimized design parameters for the proposedantenna which are obtained with the support of parametric study are also mentioned. In fourth chapter, various outcomes attained during the progression of simulation and measurement, aredepicted.

The performance characteristics of the proposed antenna are likened to the reference antenna and previously reported antennas. The proposed work contains a designed antenna i.e.Proposed UWB Antenna resonates in the UWB range from 3.1-14.7 GHz with peak gain of 8 dB for UWB antenna.

A breast model is designed with 30 mm radius and it consists of three layers such as skin layer, fatty tissue layer and fiber tissue layer. Here the malignant tumor is introduced in fiber tissue and fatty tissue layers with various size and different location. Here a UWB antenna is used to detect the tumor based on the SAR1g. The breast model is simulated without tumor using a UWB antenna. The distance between antenna and breast model is variable from 10 mm to 70 mm. The relative permittivity of tumor is high when it is compared with skin, fatty tissue and fiber tissue layers. Due to its permittivity SAR1g value of tumor is high when it is compared with other layers. While introducing tumor with relative permittivity (εr) of 50 and conductivity of 4 S/m in different sizes and varies locations in glandular tissue and fatty tissue layer in the breast model, the local and average SAR1g value of skin, fatty tissue, and fiber tissue layer is changed, not only every layer, SAR1g value of entire breast model is changed. From this it is possible to identify the tumor in the breast model when the local and average SAR1g value of entire breast model is above 30.959 W/Kg and 6.5007 W/kg respectively in almost all cases. The designed antennas are applied for breast cancer detection after being subjected to various parameters. Though the antenna is used for detecting breast cancer, considering the antenna size and bandwidth, is concluded as the best antenna for breast cancer detection.

Future Scope

The proposed antenna has a gain that can be enhanced by using unique meta-surfaces as a superstrate or reflector in conjunction with the current design. The

antenna's performance can be improved even more with a change in feeding technique. For example, for better impedance matching, use a coaxial probe feeding approach, or use proximity coupled feeding for a wider bandwidth. With the help of diodes, the desired antenna might be employed as an application-based reconfigurable antenna. The array structure of the proposed UWB antenna improves the antenna's efficiency and the accuracy of identifying the tumor in the breast phantom. It can have a minimum of 4 antennas and a maximum of 64 antennas, where it can be used as set of transmitting and receiving antenna.

1. To test tumor detection systems on real patients using an actual UWB antenna array.
2. Create an experimental set-up for a real-life breast.
3. To repeat the same studies using alternative methodologies that has been established, as well as to confirm tumor detection.

Literature Cited

LITERATURE CITED

Adnan, S., Abd-Alhammed, R. A., See, C. H., Hraga, H. I., Elfergani, I. T. E., and Zhou, D. 2010. 'A Compact UWB Antenna Design for Breast Cancer Detection', *PIERS* online., 6(2): 129-132.

Aldhaeebi, M. A., Almoneef, T. S., Attia, H., and Ramahi, O. M. 2019. Near-field microwave loop array sensor for breast tumor detection. *IEEE Sensors J.*, *19*(24): 11867-11872.

Alibakhshikenari, M., Virdee, B. S., Shukla, P., Parchin, N. O., Azpilicueta, L., See, C. H., and Limiti, E. 2020. Metamaterial-inspired antenna array for application in microwave breast imaging systems for tumor detection. *IEEE Access.*, *8*: 174667-174678.

Alsharif, F., and Kurnaz, Ç. 2018. Wearable microstrip patch ultra-wide band antenna for breast cancer detection. *In:* 2018 41st Int. Conf. on Telecommunications and Signal Processing (TSP): pp.1-5.

Amdaouch, I., Aghzout, O., Naghar, A., Alejos, A. V., and Falcone, F. J. 2018. Breast tumor detection system based on a compact UWB antenna design. *Progress In Electromag. Res.* M, 64: 123-133.

Ashehri, S. A., and Khatun, S. 2009. 'UWB imaging for breast cancer detection using neural network', *Progress In Electromag. Res.* C, 7: 79-93.

Aziz, A., Ahmad, D., Shila, T. A., Rana, S., Hasan, R. R., and Rahman, M. A. 2019. On-body circular patch antenna for breast cancer detection. In: *2019 IEEE Int. Electromag. and Antenna Conf. (IEM ANTENNA),* pp. 29-34.

Bahrami, H., Porter, E., Santorelli, A., Gosselin, B., Popovic, M., and Rusch, L. A. 2014. Flexible sixteen monopole antenna array for microwave breast cancer detection. *In*: 2014 36th Annual Int. Conf. of the IEEE Engg. in Medicine and Bio. Society (pp. 3775-3778).

Balzano, Q., Garay, O., and Steel, F. R. 1978. Energy deposition in simulated human operators of 800-MHz portable transmitters. *IEEE Trans. on Vehicular Tech., 27*(4): 174-181.

Banu, S., Vishwapriya, A., and Yogamathi, R. 2013. Performance analysis of circular patch antenna for breast cancer detection. *In:* 2013 4th Int. Conf. on Computing, Comm. and Netw. Tech. (ICCCNT)., pp. 1-7 IEEE.

Baskaran Kasi, Lee Chia Ping and Chandan Kumar Chakrabarty 2011. 'A Compact Microstrip Antenna for Ultra Wideband Applications', *European J. of Scientific Res.*, 67(1): 45-51.

Bindu, G., Lonappan, A., Thomas, V., Anandan, C. K., Mathew, K. T., and Abraham S. J. 2006. 'Active Microwave Imaging for Breast Cancer Detection' *Progress in Electromag. Res., PIER.,* 58: 149-169.

Calıskan, R., Gültekin, S. S., Uzer, D., and Dundar, O. 2015. A microstrip patch antenna design for breast cancer detection. *Procedia-Social and Behavioral Sciences*, 195: 2905- 2911.

Chen, Z. N., Ammann, M. J., Qing, X., Wu, X. H., See, T. S., and Cai, A. 2006. Planar antennas. *IEEE microwave magazine, 7*(6): 63-73.

Chou, C. K., Bassen, H., Osepchuk, J., Balzano, Q., Petersen, R., Meltz, M., and Heynick, L. 1996. Radio frequency electromagnetic exposure: Tutorial review on experimental dosimetry. *J. of the Bioelectromag. Society, The Society for Physical Regulation in Biology and Medicine, The European Bioelectromag. Assoc., 17*(3): 195-208.

Cicchetti, R., Miozzi, E., and Testa, O. 2017. Wideband and UWB antennas for wireless applications: A comprehensive review. *Int. J. of Antennas and Propag., 2017*.

Dastranj, A., and Bahmanzadeh, F. 2018. A compact UWB antenna design using rounded inverted L-shaped slots and beveled asymmetrical patch. *Progress In Electromag. Res. C,* 80: 131-140.

DeSantis, C., Ma, J., Bryan, L., and Jemal, A. 2014. Breast cancer statistics, 2013. CA: *A Cancer J. For Clinicians*, 64(1): 52-62.

Eesuola, A., Chen, Y., and Tian, G. Y. 2011. Novel ultra-wideband directional antennas for microwave breast cancer detection. *In:* 2011 IEEE Int. Symp. on Antennas and Propag. (APSURSI), pp. 90-93.

El Misilmani, H. M., Naous, T., Al Khatib, S. K., and Kabalan, K. Y. 2020. A survey on antenna designs for breast cancer detection using microwave imaging. *IEEE Access.,* 8: 102570-102594.

Fear, E. C., and Stuchly, M. A. 2000. Microwave detection of breast cancer. *IEEE Trans. on Microwave Theory and Tech..,* 48(11): 1854-1863.

Gautam, A. K., Richa Chandel and Binod Kr Kanaujia 2013, 'A CPW Fed Hexagonal shape monopole-like UWB antenna', Microwave Optical Tech. Letters., 55(11): 2528-2587.

Guy, A. W., and Chou, C. K. 1986. Specific absorption rates of energy in man models exposed to cellular UHF mobile-antenna fields. *IEEE Trans. on Microwave Theory and Tech., 34*(6): 671-680.

Huo, Y., Bansal, R., and Zhu, Q. 2003. 'Breast tumor characterization via Complex Resonances', Proceedings of the IEEE MTT-S Int. Microwave Symp., ed. IEEE, Philadephia, PA,USA, pp. 387-390.

Huynh, P.T., Jarolimek, A.M., and Daye, S. 1998 'The false-negative mammogram', Radiograph., 18: 1137-1154.

Jan, N. A., Kiani, S. H., Muhammad, F., Sehrai, A., Iqbal, A., Tufail, M., and Kim, S. 2020. V-shaped monopole antenna with chichena itzia inspired defected ground structure for UWB applications. *CMC Comput. Mater. Contin., 65*: 19-32.

Kahar, M., Ray, A., Sarkar, D., and Sarkar, P. P. 2015. An UWB microstrip monopole antenna for breast tumor detection. Microwave and Optical Tech. Letters, 57(1): 49-54.

Kahwaji, A., Arshad, H., Sahran, S., Garba, A. G., and Hussain, R. I. 2016. Hexagonal microstrip antenna simulation for breast cancer detection. *In* 2016 IEEE Int. Conf. on Indus. Info. and Computer Systems (CIICS) pp. 1-4.

Kanjaa, M., El Mrabet, O., Khalladi, M., and Essaaidi, M. 2015. Exponentially tapered antipodal Vivaldi antenna for breast cancer detection. *In*: 2015 IEEE 15th Mediterranean Microwave Symp. (MMS) pp. 1-3.

Karli, R., Ammor, H., Shubair, R. M., AlHajri, M. I., Alkurd, R., and Hakam, A. 2016. Miniature planar ultra-wide-band microstrip antenna for breast cancer detection. *In:* 2016 IEEE 16th Mediterranean Microwave Symp. (MMS), pp. 1-4.

Keshvari, J., and Kivento, M. 2013. Hand effect on head specific absorption rate (SAR) exposed by two realistic phone models. *In:* IOP Conf. Series: Materials Sci. and Engg., 44(1) :012017.

Kobayashi, T., Nojima, T., Yamada, K., and Uebayashi, S. 1993. Dry phantom composed of ceramics and its application to SAR estimation. *IEEE trans. on Microwave Theory and Tech.., 41*(1): 136-140.

Kornguth, P. J., Keefe, F. J., Wright, K. R., and Delong, D. M. 2000. Mammography pain in women treated conservatively for breast cancer. *The J. of Pain,* 1(4): 268-274.

Kwon, S., and Lee, S. 2016. Recent advances in microwave imaging for breast cancer detection. *Int. j. of biomed. imaging*, 2016.

Lai, J. C. Y., Soh, C.B., Gunawan, E., and Low, K. S. 2011. 'UWB Microwave Imaging for Breast Cancer Detection – Experiments with Heterogeneous Breast Phantoms', *Progress In Electromag. Res,* M., 16: 19-29.

Loktongbam, P., and Solanki, L. S. 2017. A brief review on implantable antennas for biomedical applications. *Int. J. of Advance Res. in Sci. and Engg.,* 6(5): 821-851.

Mahmud, M. S., Jabri, F. J. J., and Mahjabeen, B. 2013. Compact UWB Wearable antenna on leather material for wireless applications. *In*: *2013 IEEE Antennas and Propag. Society Int. Sym. (APSURSI)* (pp. 2191-2192).

Mahmud, M. Z., Islam, M. T., Misran, N., Kibria, S., and Samsuzzaman, M. **2018.** Microwave imaging for breast tumor detection using uniplanar AMC based CPW-fed microstrip antenna. *IEEE Access.*, *6*: 44763-44775.

Mazhar, W., Tarar, M. A., Tahir, F. A., Shan Ullah and Bhatti, F. A. 2013. 'Compact Microstrip Patch Antenna for Ultra-wideband Applications', PIERS Proceedings, Stockholm, Sweden, pp. 12-15.

Mieke Kriege., Cecile TM Brekelmans., Carla Boetes., Peter E Besnard., Harmine M Zonderland., Inge Marie Obdeijn., Radu A Manoliu., Theo Kok., Hans Peterse., Madeleine M. A. Tilanus-Linthorst., Sara H Muller., Sybren Meijer., Jan C Oosterwijk., Louk VAM Beex., Rob AEM Tollenaar., Harry J de Koning., Emiel J. T. Rutgers and Jan G. M. Klijn 2004. 'Efficiency of MRI and Mammography for Breast-cancer screening in Women with a familial or Genetic Predisposition' *The New Eng. J. of Medi.*, 351(5): 427-437.

Nahalingam, K., and Sharma, S. K. 2011. An investigation on microwave breast cancer detection by ultra-wide bandwidth (UWB) microstrip slot antennas. *In:* 2011 IEEE Int. Symp. on Antennas and Propag. (APSURSI), pp. 3385-3388

Okano, Y., Ito, K., Ida, I., and Takahashi, M. 2000. The SAR evaluation method by a combination of thermographic experiments and biological tissue-equivalent phantoms. *IEEE Trans. on Microwave Theory and Tech.*, *48*(11): 2094-2103.

Ray, K. P. 2008. Design aspects of printed monopole antennas for ultra-wide band applications. *Int. j. of antennas and propag., 2008.*

Rokunuzzaman, M., Samsuzzaman, M., and Islam, M. T. 2016. Unidirectional wideband 3-D antenna for human head-imaging application. *IEEE Antennas and Wireless Propag. Letters.*, *16*: 169-172.

Santanu Mondal and Partha P Sarkar 2013. 'A Novel Design of Compact Wideband Hexagonal Antenna', Microwave Optical Tech. Letters., 55(1): 1-4.

Schantz, H. G. 2004. A brief history of UWB antennas. *IEEE Aerospace and Electronic Systems Magazine., 19*(4): 22-26.

Shahira Banu., M. A., Vanaja, S., and Poonguzhali, S. 2003 'UWB Microwave Detection of Breast Cancer Using SAR', Proceedings of the Int. Conf. on Energy Efficient Technol. for Sustainability ICEETS ed. IEEE, pp. 113-118.

Shanwar, A. R., and Othman, N. S. 2017. UWB printed antenna for medical applications. *In:* TENCON 2017-2017 IEEE Region 10 Conf., pp. 2931-2936

Shao, W and Zhou, B 2005. 'UWB microwave imaging for breast tumor detection in inhomogeneous tissue', Proceedings of the 2005 IEEE Engg. in Medicine and Biology, 27th Annual Conf., shanghai, China, pp. 1496-1499.

Shrestha, S., Agarwal, M., Reid, J., and Varahramyan, K. 2010. Microstrip antennas for direct human skin placement for biomedical applications. In: *PIERS Proceedings*.

Sill, J. M., and Fear, E. C. 2005. 'Tissue sensing adaptive radar for breast cancer detection–experimental investigation of simple tumor models', *IEEE Trans. on Microwave Theory and Tech.*, 53: 3312-3319.

Tapan Mandal and Santanu Das 2012. 'Ultra wide band-printed Hexagonal monopole Antennas with WLAN Band Rejection', Microwave Optical Technol. Letters., 54(6): 1520-1525.

Ul Haq, M. A., and Khan, M. A. 2014. A Multiple Ring Slots Ultra-Wide Band Antenna (MRS-UWB) for Biomedical Applications. *In*: 17th IEEE Int. Multi Topic Conf. 2014, pp. 56-60.

Wang, J. C., Lim, E. G., Leach, M., Wang, Z., Man, K. L., and Huang, Y. 2016. Two methods of SAR measurement for wearable electronic devices. *In*: Proceedings of the Int. Multi Conf. of Engineers and Computer Scientists (Vol. 2).

Wang, J., Chen, H., Wu, X., and Tang, L. 2015. 'Comparison of diagnostic efficiency of breast cancer imaging in Chinese women: Digital mammography, ultrasound, MRI and combinations of these modalities', *J. of Med. Imag. and Health Info.*, 5(7): 1488-1493.

Wang, M., Yang, S., Wu, S., and Luo, F. 2008. A RBFNN approach for DoA estimation of ultra wideband antenna array. *Neurocomputing*, *71*(4-6): 631-640.

Wenyi Shao and Ryan S. Adams 2011. 'UWB Microwave Imaging for Early Breast Cancer Detection: A Novel Confocal Imaging Algorithm'., pp. 707-709, AP-S/URSI.

Xia Xiao and Takamaro Kikkawa 2008. 'Study on the Breast Cancer Detection by UWB Microwave Imaging', Proceedings of the ICMMT.

CURRICULUM VITAE

Name	**:**	Rekha Kandpal	**Phone No**	**:**	9758650505
Mailing Address	**:**	Ward no 1, Nainital Road, Dakbungla Kaladhungi Nainital	**Permanent Address**	**:**	Same as mailing address
E-mail	**:**	Kandpalrekha115@gmail.com			
Career objectives	**:**	To secure a challenging position in a reputable organization to expand my learning, knowledge and skills.			

Educational Qualification

Sr. No.	Examination Passed	Institution	Year	Percentage/ CGPA
1.	M.Tech (E&CE)	G.B.P.U.A&T, Pantnagar	2021	Pursuing
2.	B.Tech (E&CE)	B.T.K.I.T, Dwarahat, Uttarakhand	2019	65%
3.	Diploma(Electronics)	Govt. Poly. Kotabagh, Nainital	2016	79.84%
4.	Intermediate	CBSE Board	2013	60%
5.	High School	CBSE Board	2011	74.1%

Specialization : Major: Electronics and Communication Engineering **Minor:** Nil

Thesis Title : A Compact Defected-Ground UWB Antenna for Breast Tumor Detection Using SAR Analysis

Publication: Nil

Papers published from thesis: Nil

Papers published other than thesis : Nil

Conference/ Seminar/ Workshops/ Training Attended:

(i) One week workshop on "Antenna :Design, Fabrication and Measurement Techniques" from Govind Ballabh Pant Institute Of Engineering And Technology Pauri Garhwal.

(ii) One week international workshop on "Metamaterial and its Application" organized by IEEE Delhi Section Antenna & Propagation Society (APS) chapter- Jaipur.

(iii) Three days national training program on "Design, Simulation & Measurement of Different Types of Antenna for 5G Application Using HFSS" by Meerut institute of engineering & technology in online mode.

(iv) Attended workshop on "Design & Fabrication of Planar Microwave Circuits" conducted by IEEE Microwave Theory & Techniques Society Student Branch Chapter IIT Jammu.

(v) One week workshop on "Modern Antennas for Present & Future Wireless communication Technology" conducted by department of ECE, National Institute of Technology Sikkim.

(vi) Attended workshop on "Advanced Antenna for Space & Industrial Applications: Design, Modeling Hardware & Test" jointly organized by IEEE MTT-S Kerala Section, IEEE IIST SBC and Government engineering college, Barton hill, Thiruvananthapuram.

(vii) Attended "CST workshop on Simulation and Co-Simulations of RF Modules" organised by IEEE MTT-S student branch chapter, IIT Delhi and IEEE MTT-S delhi chapter in association with M/S Jyoti Electronics, Ahemedabad.

(viii) One week online short term training program on "Innovative & Inventive Problem Solving" organised by department of production engineering AISSMS COE, Pune.

(ix) Attended a webinar on "Innovation in Technology Adoption and Development of High Precision Slipring: A Case Study" organised by department of production Engineering and Institution of Engineers (India), Kolkata student chapter, AISSMS COE, Pune.

(x) One week online short term course on "Microwave Material Processing : Opportunities and Challenges" organized by department of Mechanical Engineering, NIT Uttarakhand, Srinagar (Garhwal).

(xi) Summer internship from "Bharat Sanchar Nigam Limited" Haldwani.

(xii) Summer internship from "Bharat Heavy Electrical Limited" Rudurapur.

(xiii) One month course on "PLC Programming (Siemens)" from Electronics service & Training Center Kaniya Ramnagar.

Software Skills : HFSS, CST

Professional Skills : Data Presentation, Problem Solving, Research and Analytical skill, Leadership

Professional Affiliations: Nil

Awards / Honours/Achievements: Awarded third prize in Extempore Competition on "Role of Professionals in the Development of Uttarakhand" by Hon. Chief Minister Uttarakhand Shree Harish Rawat ji organized by Professional Wing of Uttarakhand Congress.

Place: Pantnagar

Date: February, 2022

(Rekha Kandpal)

Name	**:**	Rekha Kandpal	**Id. No.**	**:**	**55621**
Sem. & Year of Admission: First, 2019-20			**Degree**	**:**	M.Tech. (E&CE)
Department	**:**	Electronics & Communication Engineering			
Major	**:**	Electronics & Communication Engineering			
Thesis title	**:**	**A Compact Defected-Ground UWB Antenna for Breast Tumor Detection Using SAR Analysis**			
No. of pages	**:**	76	**Advisor**	**:**	Dr. Paras

ABSTRACT

Tumor is the world's most serious health issue. There are various methods for detecting a tumor in any region of the human body. Breast cancer is one of the most frequent cancers worldwide. Tumor generated by improper tissue growth. It is classified based on its size and location within the body. Magnetic Resonance Imaging (MRI), Biopsy Test, Computerized Tomography (CT) scan, Positron Emission Tomography (PET) scan, mammography, Electro Encephalogram (EEG), and other tests are available for early diagnosis of breast tumors. Existing approaches are noninvasive, but they are constrained by cost and reliability concerns. These diagnostic approaches are insufficient to detect tumors that are deeper than 20% and cause major problems.

In the dissertation, an ultra wideband antenna has designed with variable size (i.e. radius) of the tumor and breast phantom models, and the tumor is detected with the help of antenna. An ultra wide band planer antenna with T-shape slot in the front plane and the modified defected ground plane has been designed.

A 3-D three layer simulated breast phantom model with radius 30mm is designed and interfaced with the proposed antenna with and without tumor. The three layer breast phantom model consists of skin, fat and fiber layer. The tumor is detected by observing changes in antenna performance parameters viz. electric field distribution, return loss, current density, SAR (specific absorption rate). Sphere shaped tumor is detected by observing variation in the antenna performance parameter.

The tumor detection is applied on the semi-hemispherical breast phantom on the HFSS software. The result shows that the change in the radius of tumor, location of tumor and the position of the UWB antenna changes the antenna performance parameters because of the electrical properties of tumor and breast phantom. The value of SAR decreases on increasing the distance between the antenna and phantom as well as increases on increasing the radius of the tumor. The current density, electric field and magnetic field distribution also decreases on moving the tumor tissue deep inside the cell. Thus, SAR is best choice for detection of the malignant tissue inside the phantom and the antenna therefore be used in bio-medical applications.

(Paras)
Advisor

(Rekha Kandpal)
Authoress

नाम	: रेखा कांडपाल	परिचयांक सं.	: ५५६२१
सत्र और प्रवेश का वर्ष	: प्रथम, २०१९-२०	उपाधि	: एम.टेक.
विभाग	: इलेक्ट्रॉनिक्स एंड संचार इंजीनियरिंग		
मुख्य विषय	: इलेक्ट्रॉनिक्स एंड संचार इंजीनियरिंग		
शोध शीर्षक	: एसएआर विश्लेषण का उपयोग करके स्तन ट्यूमर का पता लगाने के लिए एक कॉम्पैक्ट डिफेक्टेड-ग्राउंड यूडब्ल्यूबी एंटीना		
पृष्ठ संख्या	: ७६	सलाहकार	: डॉ. पारस

सारांश

ट्यूमर दुनिया की सबसे गंभीर स्वास्थ्य समस्या है। मानव शरीर के किसी भी क्षेत्र में ट्यूमर का पता लगाने के लिए विभिन्न तरीके हैं। स्तन कैंसर दुनिया भर में सबसे अधिक होने वाले कैंसर में से एक है। ट्यूमर अनुचित ऊतक वृद्धि से उत्पन्न होता है । इसे इसके आकार और शरीर के भीतर स्थान के आधार पर वर्गीकृत किया जाता है। चुंबकीय अनुनाद इमेजिंग (एमआरआई), बायोप्सी टेस्ट, कम्प्यूटरीकृत टोमोग्राफी (सीटी) स्कैन, पॉज़िट्रॉन एमिशन टोमोग्राफी (पीईटी) स्कैन, मैमोग्राफी, इलेक्ट्रो एन्सेफेलोग्राम (ईईजी), और अन्य परीक्षण स्तन ट्यूमर के शुरुआती निदान के लिए उपलब्ध हैं। मौजूदा दृष्टिकोण गैर-आक्रामक हैं, लेकिन वे लागत और विश्वसनीयता की चिंताओं से विवश हैं। ये नैदानिक दृष्टिकोण उन ट्यूमर का पता लगाने के लिए अपर्याप्त हैं जो २० % से अधिक गहरे हैं और बड़ी समस्याएं पैदा करते हैं।

शोध प्रबंध में, एक अल्ट्रा वाइडबैंड एंटीना को ट्यूमर और स्तन फैंटम मॉडल के चर आकार (यानी त्रिज्या) के साथ डिजाइन किया गया है, और एंटीना की मदद से ट्यूमर का पता लगाया जाता है। फ्रंट प्लेन में टी-शेप स्लॉट के साथ एक अल्ट्रा वाइड बैंड प्लानर एंटीना और संशोधित डिफेक्टेड ग्राउंड प्लेन को डिजाइन किया गया है।

३० मिमी त्रिज्या के साथ एक ३-डी तीन परत सिम्युलेटेड ब्रेस्ट फैंटम मॉडल को ट्यूमर के साथ और ट्यूमर के बिना, प्रस्तावित एंटीना के साथ डिजाइन और इंटरफेस किया गया है। थ्री लेयर ब्रेस्ट फैंटम मॉडल में त्वचा, वसा और फाइबर परत होती है। एंटेना के प्रदर्शन मापदंडों में बदलाव देखकर ट्यूमर का पता लगाया जाता है। विद्युत क्षेत्र वितरण, वापसी हानि, विद्युत प्रवाह घनत्व, एसएआर (विशिष्ट अवशोषण दर) जैसे ऐन्टेना प्रदर्शन पैरामीटर में भिन्नता देखकर गोलाकार आकार के ट्यूमर का पता लगाया जाता है।

ट्यूमर का पता लगाने को एचएफएसएस सॉफ्टवेयर पर अर्ध-गोलार्द्ध स्तन फैंटम पर लागू किया जाता है। परिणाम से पता चलता है कि ट्यूमर की त्रिज्या में परिवर्तन, ट्यूमर का स्थान और यूडब्ल्यूबी एंटीना की स्थिति, ट्यूमर और स्तन फैंटम के विद्युत गुणों के कारण एंटीना प्रदर्शन मापदंडों को बदल देती है। एंटीना और फैंटम के बीच की दूरी बढ़ने पर एसएआर का मान घटता है और ट्यूमर की त्रिज्या बढ़ने पर एसएआर का मान बढ़ता है।विद्युत प्रवाह घनत्व, विद्युत क्षेत्र और चुंबकीय क्षेत्र वितरण भी कोशिका के अंदर ट्यूमर ऊतक को गहराई तक ले जाने पर कम हो जाता है। इस प्रकार एसएआर, फैंटम के अंदर घातक ऊतक का पता लगाने के लिए सबसे अच्छा विकल्प है और इसलिए एंटेना का उपयोग जैव-चिकित्सा अनुप्रयोगों में किया जाता है।

(पारस)
सलाहकार

(रेखा कांडपाल)
लेखिका